UNIVERSITY OF THESSALY

SCHOOL OF ENGINEERING

DEPARTMENT OF MECHANICAL ENGINEERING

Ph.D. Dissertation

STRUCTURAL INTEGRITY OF STEEL HYDROCARBON PIPELINES WITH LOCAL WALL DISTORTIONS

AGLAIA-EVGENIA POURNARA

Diploma in Civil Engineering, University of Thessaly, 2008

M.Sc. in Mechanical Engineering, University of Thessaly, 2011

Supervisor: Spyros A. Karamanos

Submitted to the Department of Mechanical Engineering

in Partial Fulfillment of the Requirements

for the Degree of Doctor of Philosophy

University of Thessaly, July 2015

Εγκρίθηκε από τα Μέλη της Επταμελούς Εξεταστικής Επιτροπής:

Πρώτος Εξεταστής (Επιβλέπων)	Δρ. Σπύρος Α. Καραμάνος, Καθηγητής, Τμήμα Μηχανολόγων Μηχανικών, Πανεπιστήμιο Θεσσαλίας
Δεύτερος Εξεταστής	Δρ. Αλέξης Θ. Κερμανίδης, Επίκουρος Καθηγητής, Τμήμα Μηχανολόγων Μηχανικών, Πανεπιστήμιο Θεσσαλίας
Τρίτος Εξεταστής	Dr. Ali Limam, Professor, INSA, Institut National Des Sciences Appliquées, Lyon
Τέταρτος Εξεταστής	Δρ. Φίλιππος Κ. Περδικάρης, Καθηγητής, Τμήμα Πολιτικών Μηχανικών, Πανεπιστήμιο Θεσσαλίας
Πέμπτος Εξεταστής	Δρ. Γρηγόρης Ν. Χαϊδεμενόπουλος, Καθηγητής, Τμήμα Μηχανολόγων Μηχανικών, Πανεπιστήμιο Θεσσαλίας
Έκτος Εξεταστής	Δρ. Αντώνιος Ε. Γιαννακόπουλος, Καθηγητής, Τμήμα Πολιτικών Μηχανικών, Πανεπιστήμιο Θεσσαλίας
Έβδομος Εξεταστής	Δρ. Μιχάλης Αγόρας, Λέκτορας, Τμήμα Μηχανολόγων Μηχανικών, Πανεπιστήμιο Θεσσαλίας

Ευχαριστίες

Πρώτα απ' όλα, θέλω να ευχαριστήσω τον επιβλέποντα της διατριβής μου, Καθηγητή κ. Σπύρο Καραμάνο, για την πολύτιμη βοήθεια και καθοδήγησή του κατά τη διάρκεια της διδακτορικής μου δουλειάς. Επίσης, είμαι ευγνώμων στα υπόλοιπα μέλη της εξεταστικής επιτροπής της διατριβής μου, κ. Αλέξη Κερμανίδη, Ali Limam, Φίλιππο Περδικάρη, Γρηγόρη Χαϊδεμενόπουλο, Αντώνιο Γιαννακόπουλο και Μιχάλη Αγόρα για την προσεκτική ανάγνωση της εργασίας μου και για τις πολύτιμες υποδείξεις τους. Οφείλω επιπλέον ευχαριστίες στον Καθηγητή κ. Φίλιππο Περδικάρη, υπέυθυνο του Εργαστηρίου «Τεχνολογίας Οπλισμένου Σκυροδέματος και Κατασκευών» του Τμ. Πολιτικών Μηχανικών του Πανεπιστημίου Θεσσαλίας που διέθεσε, εκτός από τον χώρο και τον εξοπλισμό του εργαστηρίου, και μεγάλο μέρος του χρόνου του συμβάλοντας σημαντικά στην διεξαγωγή των πειραμάτων μεγάλης κλίμακας τα οποία περιγράφονται στο Κεφάλαιο 3. Επίσης, οφείλω ειδικές ευχαριστίες στον Επίκουρο Καθηγητή κ. Αλέξη Κερμανίδη, υπεύθυνο του Εργαστηρίου «Μηχανικής και Αντοχής των Υλικών» του Τμ. Μηχανολόγων Μηχανικών του Πανεπιστημίου Θεσσαλίας, για την διάθεση του χώρου του εργαστηρίου και του εργαστηριακού εξοπλισμού καθώς και για τις υποδείξεις του στην διεξαγωγή των πειραμάτων μικρής κλίμακας. Επίσης ένα μεγάλο ευχαριστώ στον Θεοχάρη Παπαθεοχάρη για την πολύτιμη βοήθειά του, την τεχνική στήριξη και τις συμβουλές που μου προσέφερε κατά τη διάρκεια της συνολικής πειραματικής διαδικασίας. Επιπροσθέτως, θα ήθελα να ευχαριστήσω τον Αντρέα Τζαμτζή για την βοήθειά του στα πειράματα μικρής κλίμακας. Μεγάλες ευχαριστίες οφείλω στην ΕΒΕΤΑΜ Α.Ε. και κυρίως στην Καλλιόπη Διαμαντή για την παροχή του συστήματος παχυμέτρησης αλλά και στον Καργάκη Γενναιόδωρο για την βοήθειά του στην διεξαγωγή των πειραμάτων πίεσης στα εργαστήρια της ΕΒΕΤΑΜ Α.Ε. Μεγάλες ευχαριστίες επίσης οφείλω στο Πανεπιστήμιο του Porto (FEUP) και ιδιαίτερα στον Abílio M.P. de Jesus, για την παροχή των αποτελεσμάτων των πειραμάτων υλικού. Ευχαριστώ, επίσης, τους συναδέλφους και φίλους μου, Δανιήλ Βασιλική, Γιαννούλα Χατζοπούλου, Γρηγόρη Σαρβάνη, Γιώργο Βαρέλη, Μαρία Βάθη και Πατρίτσια Παππά για την πολύτιμη βοήθειά τους στις προσομοιώσεις του Κεφαλαίου 4 και για την ηθική στήριξή τους τα τελευταία χρόνια. Επίσης, ευχαριστώ την οικογένειά μου, τους συγγενείς και τους φίλους(ες) μου για την κατανόησή και την στήριξή τους, ιδιαίτερα κατά τη διάρκεια των τελευταίων μηνών της προσπάθειάς μου. Πάνω απ' όλα, είμαι ευγνώμων στους γονείς μου, Νικόλαο Πουρνάρα και Θεοδώρα Πορλίγκη και στην αδερφή μου Αθανασία

Πουρνάρα για την ολόψυχη αγάπη και υποστήριξή τους όλα αυτά τα χρόνια. Αφιερώνω αυτή την διατριβή στην οικογένειά μου.

Τέλος, ιδιαίτερες ευχαριστίες οφείλω στο πρόγραμμα Διδακτορικών Υποτροφιών "Ηράκλειτος ΙΙ" το οποίο υλοποιείται στα πλαίσια του Επιχειρησιακού Προγράμματος «Εκπαίδευση και Δια Βίου Μάθηση» για την χορήγηση υποτροφίας ώστε να πραγματοποιηθεί η παρούσα έρευνα με συγχρηματοδότηση από την Ευρωπαϊκή Ένωση (Ευρωπαϊκό Κοινωνικό Ταμείο) και από εθνικούς πόρους.

Αγλαΐα-Ευγενία Πουρνάρα

STRUCTURAL INTEGRITY OF STEEL HYDROCARBON PIPELINES WITH LOCAL WALL DISTORTIONS

AGLAIA-EVGENIA POURNARA

University of Thessaly, Department of Mechanical Engineering, 2015

Supervisor: Dr. Spyros A. Karamanos, Professor

Department of Mechanical Engineering, University of Thessaly

Short Summary

Local distortions in the form of dents or buckles on the wall of steel hydrocarbon pipelines may constitute a threat for the structural integrity of the pipeline. In the present study, experimental research supported by numerical simulations has been conducted to investigate the structural integrity of smoothly dented and buckled steel pipes. A series of sixteen (16) full-scale experiments on 6-inch-diameter X52 pipes has been carried out, and numerical simulations have also been conducted. At first, the pipe specimens are dented or buckled. Subsequently, the dented/buckled steel pipes are subjected mainly to cyclic loading (bending or pressure) in order to estimate their residual strength and remaining fatigue life. Some specimens are also monotonically pressurized to burst. The finite element analyses simulate the experimental procedure for each specimen and loading case, in order to calculate the local stress and strain distributions at the dented region. Small-scale tests in bent strips are also conducted, and correlate very well with the experimental and numerical results. Based on the numerical results, a damage factor is computed and the fatigue life is predicted and compared successfully with the experimental results. The results of the present study are aimed at evaluating existing guidelines and methodologies towards proposing a simple and efficient assessment of local wall distortions in steel pipelines.

ΔΟΜΙΚΗ ΑΚΕΡΑΙΟΤΗΤΑ ΑΓΩΓΩΝ ΥΔΡΟΓΟΝΑΝΘΡΑΚΩΝ ΜΕ ΤΟΠΙΚΕΣ ΠΑΡΑΜΟΡΦΩΣΕΙΣ ΤΟΙΧΩΜΑΤΟΣ

ΑΓΛΑΙΑ-ΕΥΓΕΝΙΑ ΠΟΥΡΝΑΡΑ

Πανεπιστήμιο Θεσσαλίας, Τμήμα Μηχανολόγων Μηχανικών, 2015

Επιβλέπων: Δρ. Σπύρος Α. Καραμάνος, Καθηγητής

Τμήμα Μηχανολόγων Μηχανικών, Πανεπιστήμιο Θεσσαλίας

Σύντομη Περίληψη

Τοπικές παραμορφώσεις στα τοιχώματα των αγωγών με τη μορφή υβώσεων ή εγκολπωμάτων συνιστούν απειλή για τη δομική ακεραιότητά και τη λειτουργία τους. Στην παρούσα έρευνα, πειραματική και αναλυτική διερεύνηση έχει πραγματοποιηθεί για την μελέτη της δομικής ακεραιότητας αγωγών που έχουν υποστεί ομαλές οδοντώσεις και υβώσεις στα τοιχώματά τους. Δεκάξι (16) πειράματα μεγάλης κλίμακας σε δοκίμια σωλήνων X52 6-ιντσών έχει πραγματοποιηθεί, και αριθμητικές προσομοιώσεις έχουν επίσης διεξαχθεί.

Τα δοκίμια, αφού έχουν πρώτα υποστεί εγκολπώματα ή υβώσεις, υποβάλλονται σε κυκλική φόρτιση (κάμψη ή πίεση), προκειμένου να εκτιμηθεί απομένουσα αντοχή τους και η υπολειπόμενη διάρκεια ζωής. Παράλληλα πραγματοποιήθηκε ανάλυση πεπερασμένων στοιχείων για την προσομοίωση της πειραματικής διαδικασίας για κάθε τύπο παραμόρφωσης και κάθε περίπτωση φόρτισης, προκειμένου να υπολογιστεί η κατανομή των τάσεων και η συγκέντρωση παραμορφώσεων στην κρίσιμη περιοχή. Με βάση τα αριθμητικά αποτελέσματα, εκτιμάται η αντοχή σε κόπωση σε σύγκριση με τα πειραματικά δεδομένα. Ο απώτερος στόχος της παρούσας έρευνας είναι η χρήση των πειραματικών και αριθμητικών αποτελεσμάτων για την ανάπτυξη αξιόπιστων μεθοδολογιών οι οποίες μπορούν να χρησιμοποιηθούν για τον έλεγχο αγωγών και την αξιολόγηση τοπικών παραμορφώσεων μορφής εγκολπώματος ή ύβωσης με στόχο την πιθανή επισκευή τους στο πλαίσιο μίας βέλτιστης διαδικασίας συντήρησης και της διατήρησης ενός αξιόπιστου επιπέδου λειτουργίας και ασφάλειας.

Table of Contents

Chapter 1 EXTENDED SUMMARY

Local deformations on pipeline wall in the form of dents or buckles may constitute a threat for the structural integrity of the steel pipeline. In the event of pipe wall damage, caused mainly by external interference, the pipeline may appear to fulfill its transportation function, however, the damaged area is associated with significant strain concentrations and, in the case of repeated loading cracks may develop, leading to fatigue failure. The evaluation of the remaining life of oil and gas transmission steel pipelines with local wall distortions has been considered a crucial issue for maintaining a reliable level of pipeline operation condition, and has triggered significant amount of research.

In the first part of the dissertation, an extensive literature survey is conducted on previous experimental and numerical work related to the structural response of dented and buckled steel tubular members and pipes. In particular, existing work on the analysis and assessment of dents and buckles on steel tubular members and pipes has been reviewed extensively. The literature review and the evaluation of current pipeline assessment guidelines indicated that significant information exists on dented steel pipes, but limited research has been conducted on the structural assessment of buckled pipes. Furthermore, the review indicates that the structural response of both buckled and dented steel pipes under cyclic structural loading (e.g. bending) is an open issue.

The main part of the present research refers to experimental testing. First, tensile and cyclic fatigue tests on coupon specimens extracted from the steel pipe material have been performed elsewhere [University of Porto (FEUP)], in order to obtain the monotonic stress-strain curve and the fatigue curve for the X52 steel. The experimental work consists mainly of sixteen (16) full-scale experiments on 6-inch-

diameter steel pipe specimens with nominal diameter D=168.3mm performed in the Laboratory of "Reinforced Concrete Technology and Structures" of the Department of Civil Engineering at the University of Thessaly located in Volos, Greece. The specimens thickness is either t=5mm (D/t ratio equal to 35) or t=3mm, (D/t ratio equal to 65). The latter specimens have been machined, so that the reduced thickness is obtained. Specimen thickness is measured via an ultrasonic device at several points around the circumference of the piped and along their length. Special attention is devoted to the machined pipe specimens, so that thickness measurements at various locations are obtained. Subsequently, strain gages are installed at critical locations.

Following material characterization, initial measurements and instrumentation, the first stage of loading is performed: the specimens are either dented or buckled. More specifically, the first group of six (6) specimens (D/t=35) are dented via a steel special-purpose wedge-form denting tool. Dent depths are equal to (a) 6% of the pipe diameter, corresponding to the geometrical limit of dents in ASME B31.8 provisions, and (b) 12% of the pipe diameter. Subsequently, four (4) of the dented specimens are subjected to cyclic bending, whereas the other two (2) specimens are tested under internal cyclic pressure. All six specimens failed because of fatigue cracking.

The mechanical behavior of the thinner (machined) 3-mm-thick pipes has also been examined. Ten (10) 6-inch-diameter thin-walled specimens are tested under various loading conditions. Four (4) of the specimens are also dented and subsequently subjected to either cyclic four point bending (2 specimens) or cyclic pressure (2 specimens). The remaining six (6) thin-walled specimens are buckled and subjected to either cyclic four point bending (4 specimens) or cyclic and monotonic pressure until burst (2 specimens). Denting, buckling and cyclic bending of the specimens have been performed at the laboratory of Civil Engineering Department, while pressure tests (cyclic and burst) have been conducted at EBETAM S.A. laboratories in Volos Greece.

Using the instrumentation set-up of the specimens, global load-displacement curves, and local strains have been obtained from the full-scale tests in each loading stage (denting/buckling process and cyclic loading). In addition, the fatigue life of the pipe specimens (i.e. the number of cycles to failure) is measured, and crack

development is detected and recorded during cyclic bending by means of a micro-camera placed manually at critical locations.

Small-scale tests are also performed on ten (10) 300-mm-long and 40-mm-wide strip specimens extracted longitudinally from the X52 6-inch-diameter pipe specimens (D/t=35). First, the longitudinal strips are bent monotonically at mid-length at 45 and 90 degrees, representing the shape of a dented pipe generator at the compression side, as obtained in the full-scale tests at the critical region of the dent. Secondly, cyclic load is applied through a special set-up until fatigue crack failure, simulating the local conditions in a dented or buckled region of a pipe subjected to cyclic bending, as in the case of the full scale tests. The local strain values were recorded at the crest of the strip during the first five loading cycles due to the limitation of the recording equipment. Nevertheless, the predicted values of local strain obtained from finite element analysis correlated very well with the X52 steel material fatigue data. Using the predicted values of local strain, the small-scale results correlate very well with the X52 steel material fatigue data.

Finite element analyses have also been conducted in order to simulate approximately the full-scale tests during dent/buckle development simulating the full-scale tests under cyclic bending and pressure loading. The detailed finite element models are developed in ABAQUS/Standard using reduced-integration four-node shell elements (S4R), and material behavior is simulated through a von Mises (J_2) plasticity model with isotropic hardening. Furthermore, the small-scale tests are also simulated numerically in ABAQUS/Standard using eight-node reduced integration solid elements (C3D8R) and J_2 flow plasticity model with isotropic hardening for the material inelastic behavior.

The main objective of the finite element simulations is the estimation of the maximum local strain variation ($\Delta\varepsilon_{max}$) developed at the critical region of both full-scale and small-scale experiments during pipe cyclic loading. The value of this local strain is also compared with the "nominal" $\Delta\varepsilon_{nom}$ value, which can be readily computed from elementary Mechanics of Materials. Having obtained the local strain variation, a simplified fatigue assessment methodology is developed for the prediction of the fatigue life of dented and buckled pipes. This methodology provides the fatigue life of the cyclic-loaded dent/buckled specimen, employing (a) the so-called damage

factor D, which is based on Miner's rule for fatigue accumulation under variable cyclic loading conditions, and (b) a strain-based fatigue curve for the parent material.

The calculated values of the damage factor for the specimens under consideration are quite close to 1, showing a very good correlation between material testing, full-scale experiments and numerical simulations. This good correlation motivates the proposal of a simple and efficient assessment methodology, which can be considered as a reliable tool for the fatigue life prediction of damaged pipelines, towards efficient pipeline operational management and safeguarding the unhindered flow of energy (hydrocarbon) resources.

Chapter 2 INTRODUCTION

Oil and gas transmission pipeline systems have been significantly developed and expanded during the last decades. They are widely recognized as a safe and efficient means of transportation of hydrocarbons and energy resources. Due to their good functionality, many of these pipeline systems have been in-service for more than 4 decades, which exceeds their initial lifetime. During their operational life, pipelines are subjected to several types of external actions causing mechanical damage, which could threaten their structural integrity. Although, pipeline structural safety is based on safe design and construction process, potential failure of the pipeline may occur due to external interference during its operation. Ground- induced displacements, discontinuous frozen soil, or intersection with seismic faults are considered some of the common types of external interference that could be imposed on onshore buried pipeline systems and cause mechanical damage in the form of local buckling. Furthermore, significant damage can be caused by external interference of sharp objects that could accidentally crush on the pipe wall such as digging (excavation) tools. As far as offshore pipelines are concerned, seabed motions and landslips, striking by ship anchors or hawks or trawl gears are, also, considered to be the most common types of external interference. As pipelines are constantly exposed to the above external forces, defects, mechanical damage and corrosion are likely to occur during their operational stage [1], [2], [3]. More specifically, mechanical damage on pipeline wall may occur such as dents, gouges, cracks, buckles and weld defects [1]. In the present research work, the severity of mechanical defects in the form of plain (non-gouged) dents and buckles and their influence on the structural integrity of the pipelines are investigated

A pipe wall dent may occur, mainly, due to accidental impact by digging tools or ship anchors. Similarly, pipe wall wrinkling, referred to as local buckle, may be

developed during field cold bending, permanent ground motion in geohazard areas or local drifting by fishing nets. At the event of pipe wall dent or buckle occurrence the pipeline may appear to fulfill its transportation function, provided that the steel material is adequately ductile and no cracks occur. However, the damaged area is associated with significant strain concentrations and, in the case of repeated loading such as high pressure cycles or temperature and displacement variation, cracks may develop, leading to fatigue cracking and failure. Therefore, the damaged critical area and the associated strain concentrations may constitute a possible threat for the structural integrity of steel pipelines.

The United States Department of Transportation‘s database has published several reports of failure incidents caused by external damage from 1970 to 1984, and from 1984 to 1997 [4]. Pipeline accidents have been, also, reported by the Office of Pipeline Safety, USA, from 2002 to 2003 [5]. Furthermore, according to the report prepared by Alberta Energy and Utilities Board [6], it has been calculated that after internal and external corrosion, external damage constitutes the third common cause of pipeline failures from 1990 to 2005 in Alberta. More specifically, as shown in Figure 2-1**,** a large proportion of pipeline incidents were caused due to third-party interference with a proportion of about 22% and 14% referring to crude oil and natural gas pipelines, respectively. Moreover, Figure 2-2 shows the annual number of pipeline damage due to external impact and whether those impacts (“hits”) resulted in leak or rupture of the pipeline. Since the beginning of recording these “hits”(from 1994), early data showed that about one out of every two pipeline “hits” resulted in either loss of containment or, even worse, dangerous incidents.

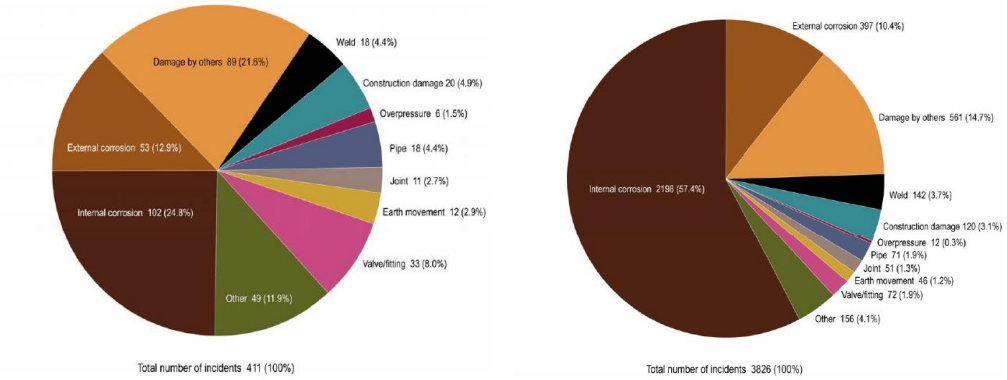

Figure 2-1: *Pipeline Incidents by cause (1990-2005); (a) Crude Oil and (b) Natural Gas pipelines [6].*

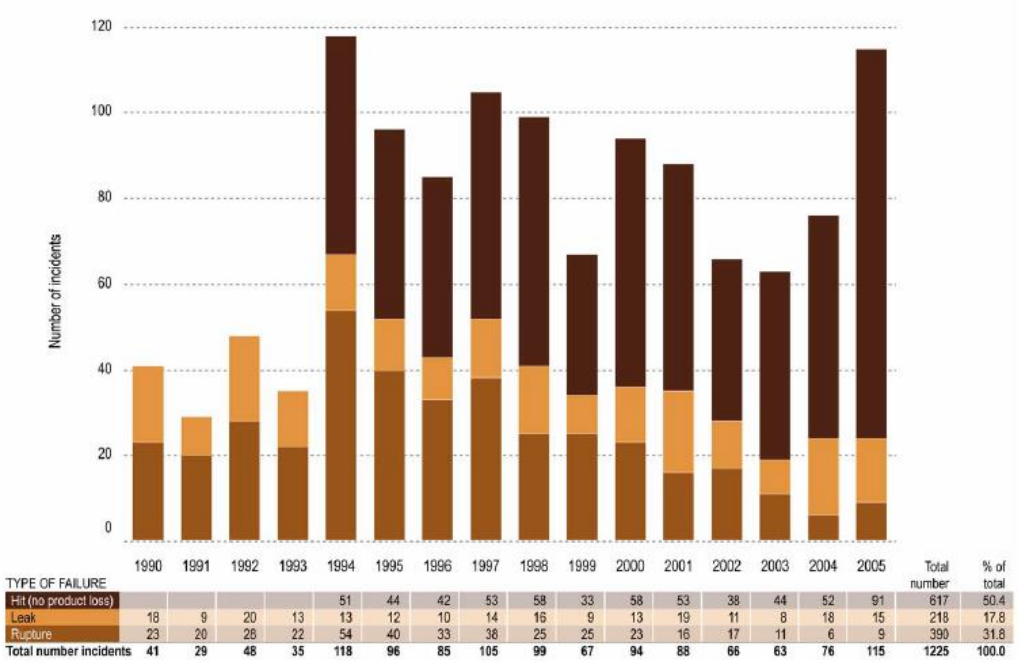

TYPE OF FAILURE	1990	1991	1992	1993	1994	1995	1996	1997	1998	1999	2000	2001	2002	2003	2004	2005	Total number	% of total
Hit (no product loss)					51	44	42	53	58	33	58	53	38	44	52	91	617	50.4
Leak	18	9	20	13	13	12	10	14	16	9	13	19	11	8	18	15	218	17.8
Rupture	23	20	28	22	54	40	33	38	25	25	23	16	17	11	6	9	390	31.8
Total number incidents	**41**	**29**	**48**	**35**	**118**	**96**	**85**	**105**	**99**	**67**	**94**	**88**	**66**	**63**	**76**	**115**	**1225**	**100.0**

Figure 2-2: Pipeline incidents due to third-party damage per year (1990-2005)[6].

A representative example of pipeline failure due to external "hit" occurred more recently, in North Texas: In 2010 a large natural gas line in North Texas, near Granbury, erupted after utility workers accidentally hit an Enterprise Products Partners natural gas pipeline. The pipeline exploded killing one worker. The ruptured pipeline and the damaged area after the explosion are shown in Figure 2-3. [Source: http://www.dailymail.co.uk/news/article-1284880/Texas-gas-pipeline-explosion-kills-worker-injures-seven.html#ixzz3dpBySx9h]

Moreover, many accidents have occurred due to insufficient pipeline inspection and monitoring system or damage assessment methods. In 2014, a catastrophic incident occurred to a buried gas transmission pipeline network in Taiwan, where gas leaks were not assessed directly. In this incident 32 people were killed and 321 others were injured by multiple explosions along the underground pipeline system in Kaohsiung, while the blasts ripped up roads, trapped and overturned cars and firetrucks (Figure 2-4).

[Source: https://en.wikipedia.org/wiki/2014_Kaohsiung_gas_explosions]

(a) (b)

Figure 2-3: Gas pipeline explosion in North Texas; (a) ruptured pipeline (b) the burned pipeline suroundings. [https://www.youtube.com/watch?v=RSCz-35M9hA]

(a) (b)

Figure 2-4: Multiple explosions of the underground Gas pipeline system in Taiwan. (https://www.youtube.com/watch?v=-1guX7YWuko)

It is well understood, from the above, that the evaluation of the remaining life of oil and gas transmission steel pipelines with local wall defects constitutes a crucial issue for maintaining a reliable level of pipeline condition and operation level, and has motivated significant amount of research for over 35 years [7], [8], [9], [10].

Towards this purpose, pipeline industry has developed defect acceptance criteria and several "defect-assessment" or "fitness-for-purpose" methods.

Furthermore, due to the global increase of energy demand, pipeline operators tend to the increase of basic design stress levels and operating pressures, in transmission pipelines, larger than the levels recommended by current standards [11], [12], [13], [14]. Towards this purpose, the information gained through the

investigation of the remaining life of damaged pipelines can contribute to enhanced, safer and more cost-effective operation of transmission pipelines.

The effect of various defects (dents, gouges, manufacturing or weld defects, corrosion) on the structural integrity of pipelines has been examined in a joint industry project based on existing experimental and numerical results. Considering a large number of publications regarding the ultimate capacity or the fatigue strength of defected or damaged pipelines this study is aimed at the enhancement of the current methodologies and the identification of "gaps" in existing knowledge towards a "fitness-for-purpose" pipeline assessment.

2.1 Literature Review

An extensive review on previous research work and currently used damage assessment methods referring to dented and dented/gouged pipelines is reported in the following paragraphs. The reader is also referred to the work of Iflefel [15].

2.1.1 Dented pipes

Local dents could be caused by impact of sharp objects. Short and long defects are defined on the basis of the axial length which should be less than, or greater than, twice the circumferential defect's width, respectively [16].

2.1.1.1 Denting of pipes

Full-scale tests on X42 and X52 steel pipes with diameter equal to 508 mm, and 660 mm, respectively, were presented by Belonos et al. [17]. Two different types of dents were studied, long continuous dents and local dents. Local residual stresses were recorded by the use of strain gauges at the dent region. The results demonstrated that these residual stresses are developed adjacent to the dent region.

Experimental and analytical work on dented pipes was presented by Alexander [18] and [19]. The tests were carried out on X52 steel grade pipe with diameter-to-thickness ratio D/t equal to 104.6. The pipe specimens were dented using two types of indenter, 'dome" type and a "long bar" type, under zero internal pressure. The maximum depth of the dent to the pipe diameter was d/D = 18%. Forty-four different dent configurations were considered in the course of testing. Analytical work was also performed to address dent mechanics using first-order quadrilateral shell,

S4R5, elements. Soil interaction was modelled using spring elements with a trial and error approach.

Denting of pressurized pipelines under local radial loading was modelled by Brooker [21]. A shell-to-solid approach technique was used for the numerical analysis and the finite element model consisted of 8-node full-integration solid elements in the dent region with five layers through wall thickness of the pipe, and 8-node shell elements away from the dent region. The shape of the impacting excavator tooth was modelled as a truncated wedge. Frictionless contact between the pipeline and the indenter has been assumed and the denting tooth was modelled using a 4-node rigid element.

A closed-form solution for the evaluation of stresses associated with long axial dents in a pressurized pipe can be found in [22]. It is concluded that for a long dent, the maximum bending stress always occurs at the root of the dent and its magnitude depends on both the dent's included angle and its profile. Sharp dent will induce a higher bending stress than a shallow dent. In addition, bending stresses induced by the development of local dent are smaller than those in a long dent.

The denting response of steel pipes subjected to transverse wedge loading, in the presence of internal pressure was examined in Gresnigt et al. [23]. The steel pipes, considered, with diameter-to-thickness (D/ t) ratio ranging between 34 and 50, exhibit significant inelastic deformations. First, nonlinear shell finite elements are employed to model the pipe response under lateral load imposed by a wedge-shaped denting tool. Following a comparison with available experimental data [24] on pressurized pipe specimens, a short parametric study is conducted and load-displacement curves are obtained for different levels of pressure, considering various denting tool sizes and orientations. In addition, a simplified two dimensional heuristic model is also presented. Considering the subsequent stage of denting deformation, the model describes the response through closed-form expressions, which illustrate the response of pressurized pipes in a clear and elegant manner. The model predictions are compared with the aforementioned test data.

2.1.1.2 Residual Capacity of dented pipes

Experimental and numerical study in order to investigate the strength of dented tubular members under axial compression is presented in [25]. Six (6) 2 meter-long seamless tubes of diameter-to-thickness ratio equal to 35 and yield stress equal to 280 MPa. The specimens were dented at the middle section via a knife-edge intender. The remaining dent depth after load removal was equal to 11.8 mm and 7.6 mm. After denting the specimens were tested under axial compression with pinned ends. Finite element models have been developed to simulate indentation and axial loading taking into account the existence of residual stresses. For the numerical modelling, eight-node thin shell elements with bilinear interpolation were implemented. It was shown that dents affect significantly the axial capacity of the tubular members, while the comparison of the experimental and finite element results validated the use of the finite element method for investigating these types of damage.

The influence of wall thickness on the resistance to external damage of gas transmission pipelines was examined in [26]. For this purpose, a calculation model was developed in order to examine the relation between vertical force applied during impact and the dent depth, the wall thickness, strength of the material and internal pressure. Another calculation model was developed for the estimation of burst pressure of notched dents. These models were substantiated by burst tests performed on 2'' and 4'' pipes and on 12'' tubes conducted earlier by Jones [27].

A parametric study was carried out by Rinehart et al. [28] to quantify dents which fall into transition region between the short and long dents. This analysis was based on the existing full-scale data and on finite element analysis. The study showed that, unrestrained, longer dents experience central cracking, re-rounding, and relatively short fatigue lives. Shorter dents experience cracking, little re-rounding, and also relatively short fatigue lives. Similar findings were also presented by Beller et al. [29] who used 3D finite element model.

Fifteen tests on pipeline ring specimens, made from X52, X65, and X60 steel grades, containing dented seam welds, are reported in [30]. The ring specimens were 75 mm wide slices of pipe, pressurized internally in a special test rig. Seven (7) specimens were dented and then pressurized to failure. Three specimens achieved stresses exceeding yield and they did not fail. The other rings exhibited failure at

stresses as low as 24% of the yield stress. Weld cracking was evident in some of the models after denting but prior to bursting.

Using four different two-dimensional shape functions to describe dent geometry, Ong [31] calculated local stresses at the pipe wall of a pressurized elastic pipe with a long smooth dent and found that the maximum local elastic stress varies between 14 and 21 times the value of the nominal hoop stress due to pressure.

In a later publication, Ong et al. [32] conducted 18 burst tests which revealed that the bursting strength of a pipe was generally insensitive to the existence of a local dent. The tests showed that the defect due to loss of thickness was the main factor governing the pipe failure. The finite element models were developed using shell elements to model plain, local dents without any surface-defect. The strain-gauging results, and the finite element results, on plain local dent showed that the strain distribution in the local dent is different from strain distribution obtained for a long dent. The peak stress in a local dent occurred at the axial flank of the dent, while in a long dent it occurred at the dent's root. Also, the magnitude of the peak stress in a local dent was much smaller than that in the long dent. It is worth noting that results given in [32] are within the elastic range, only.

Experimental work on pressurization of dented pipes is reported in [33]. These tests were performed on small-scale aluminum alloy pipes with diameter-to-wall thickness ratio (D/t) equal to 54.1. The pipes were dented at zero pressure via a spherical rigid denting tool producing a short dent. Two crescent-shaped zones of high strain values have been identified at the axial extremities of the dent. The location of these regions remained stationary as internal pressure was applied.

Collapse pressure tests on long cylinders with local dents were carried out by Park and Kyriakides. [34]. A series of stainless steel tubes (SS-304) with diameter-to-thickness ratios (D/t) equal to 33, 24, and 19, were dented up to various dent depths using spherical indenters with diameters 0.4, and 1.6 of the tube diameter. The denting process was carried out for all specimens at zero internal pressure. Subsequently, external pressure was applied to the dented specimens by enclosing each tube in a stiff 69 MPa- capacity pressure vessel until collapse. The results depicted that tubes with relatively small dents exhibited higher capacity on external pressure. The values of collapse loads were found to be insensitive to the detailed

geometry of a dent but they were dependent on the maximum of pipe ovalization (of its most deformed cross section).

A theoretical model describing the structural behaviour of dented pipe under pressure is given in [35]. It is reported that the model gave predictions for re-rounding that were in good agreement with results of tests. Tests also indicated that dent re-rounding is cycle-dependent.

An experimental and numerical investigation of the fatigue resistance of offshore pipelines with plain (smooth) dents under cyclic pressure has been reported in [36]. A longitudinal wedge shaped denting tool was employed to dent 12 in. steel pipe specimens at depths ranging between 5% and 20% of their diameter. It was found that plain (smooth) dents with a depth larger than 5% may result in a reduction of the pipeline fatigue strength. Buitrago and Hsu [37], using a finite element simulation, investigated the fatigue response of non- pressurized tubular members containing relatively smooth dents and provided stress concentration factors in the form of parametric equations in terms of geometric parameters for axial and bending loads.

Small-scale tests are carried out as reported in[38]. to evaluate the strain behavior of small-scale steel pipe specimens during denting simulation followed by cyclic internal pressure. Nine small-scale specimens with total length (L) of 510 mm, approximately 7D with external diameter (D) and wall thickness (t) equal to 73.03 mm and 3.05 mm, respectively, which refer to a D/t ratio of 23.96. The strain history results are used to validate a nonlinear three-dimensional finite element (FE) model, which is developed to estimate stress concentration factors induced by plain dents on steel pipes under internal pressure. Using the validated FE model, several analyses are carried out in a parametric study to generate SCF values for different pipe and dent dimensions. Each analysis comprises an elastic–plastic simulation of the denting process followed by an elastic determination of the stress concentration factor. Finally, fatigue tests are conducted to evaluate the finite life behavior of small-scale damaged pipes under cyclic internal pressure and to validate the proposed methodology of fatigue analysis.

More recently, the effect of local dents on the collapse curvature of pressurized pipes under bending has been investigated experimentally and numerically by Limam et al. [39]. Seamless stainless steel pipe specimens with D/t of 52 were initially dented

up to various levels. Subsequently the pipes were filled with oil and pressurized up to using a stand-alone, closed-loop control pressurizing system and subjected to four-point-bending applied through displacement control conditions. The tube denting, the pressurization and bending to collapse have been simulated using solid finite element models. In the present study it was found that local dents do not affect the elastic and the early part of the inelastic response of the tube. They do however reduce its collapse curvature (or bending strain) quite significantly by up to 50%. All predicted collapse curvatures were slightly lower than measured values. The cause of this discrepancy was traced to small misalignments of the experimental dents, each of which tends to delay collapse somewhat.

2.1.1.3 Dent Assessment-Current Standards and Methodologies

The presence of dents has been recognized as a threat to pipeline integrity, mainly in terms of burst pressure capacity. Current standards have addressed dent acceptability limits [14] and dent assessment methodologies [13]. International pipeline codes usually consider plain dents non-acceptable if they exceed a depth of 6% of the nominal pipe diameter. In a methodology proposed in Appendix R of the ASME B31.8 code [13], it is possible to estimate the maximum strain in a dent assuming the total strain is the combination of bending strain in the circumferential direction, the bending strain in the longitudinal direction and the membrane (stretching) strain in the longitudinal direction. Each of those strain components is evaluated separately; then, assuming that each component occurs coincidently at the dent apex, the components are combined appropriately to determine the total strain.

The following equations are proposed in [14], [40], [41], for the evaluation of the bending strain in the circumferential direction (ε_1), and the bending and membrane strains in the longitudinal direction (ε_2 and ε_3):

$$\varepsilon_1 = \frac{t}{2}\left(\frac{1}{R_0} - \frac{1}{R_1}\right) \tag{1.1}$$

$$\varepsilon_2 = -\frac{1}{2R_2}t \tag{1.2}$$

$$\varepsilon_3 = \frac{1}{2}\left(\frac{d}{L}\right)^2 \tag{1.3}$$

where R_0 is the radius of curvature of the undeformed pipe surface (equal to half of the nominal pipe outside diameter), and t, D, L correspond to the wall thickness, dent

depth and dent length respectively in the longitudinal direction. The external surface radii of curvature R_1 and R_2 (see Figure 2-5) are measured, respectively, in the transverse and longitudinal planes through the dent. The value of R_1 is positive when the dent partially flattens the pipe, i.e. when the curvature of the pipe surface in the transverse plane is in the same direction as the original surface radius of curvature R_0. Otherwise, if the dent is re-entrant (corresponding to wall inversion), the value of R_1 is negative. The curvature R_2 as used in the code always has a negative value. Subsequently, the total strain on the inner and outer pipe surfaces (respectively ε_i and ε_0) are then given by the following expressions:

$$\varepsilon_i = \sqrt{\varepsilon_1^{\,2} - \varepsilon_1\left(\varepsilon_2 + \varepsilon_3\right) + \left(\varepsilon_2 + \varepsilon_3\right)^2} \tag{1.4}$$

$$\varepsilon_o = \sqrt{\varepsilon_1^{\,2} + \varepsilon_1\left(-\varepsilon_2 + \varepsilon_3\right) + \left(-\varepsilon_2 + \varepsilon_3\right)^2} \tag{1.5}$$

The dent is considered as acceptable when the larger of the values of ε_i and ε_0 is lower than the allowable strain limit. For smooth dents, which do not include gauges or welds, the allowable strain limit is 6%.

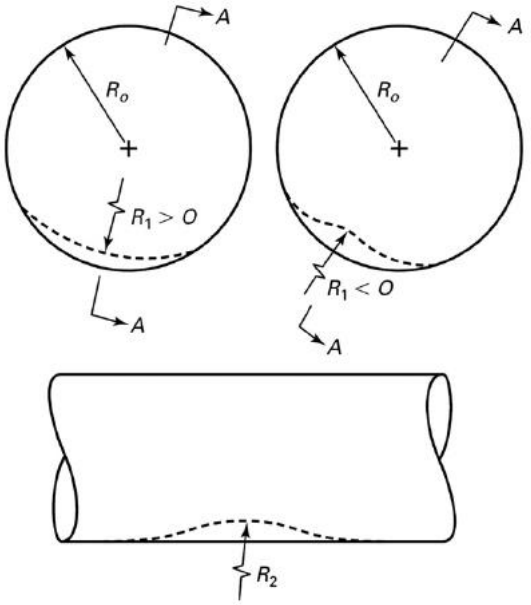

Figure 2-5: Local curvatures of pipe wall for estimating strain in smooth dents [14].

Norohna et al [42] have proposed an enhancement of the strain criterion developed by ASME B31.8 [14] including the influence of the combination of plane strain state and the existence of radial strain components. The aforementioned

criterion is based on ultimate damage resistance to monotonic loading conditions. Enhanced evaluation process is, also, suggested by Baker et al. [43], which contain an additional check for susceptibility to pressure cycle fatigue for all dents but restrained bottom-side dents.

Several codes are available for assessment of defects in the transmission pipelines. British Standard, BS 7910, [44] is widely used for assessing crack-like flaws on damaged pipelines comprising of three levels: the lowest level accounts for linear elastic fracture mechanics. The second level is based on the R-curve, which is used when failure is likely to occur. This level takes, also, into the account the effects of plasticity. The third level is based on J-integral, which accounts for crack arrest. Furthermore, Part 12 of API 579-1/ASME FFS-1 [13] code addresses the assessment of gouged or non-gouged (smooth) dents in cyclic pressurized components. For the case of non-gouged dents, the assessment methodology consists of three levels. The first (lowest) level is based on simple geometric criteria concerning the dent depth. In the second assessment level, the maximum acceptable pressure cycles can be calculated using the maximum cyclic circumferential stress values. These values are calculated using the stress concentration factors computed employing the dent geometrical characteristics and damage growth rate parameters defined at the critical area of the dent. The last level consists of a more detailed assessment employing numerical stress and temperature analysis and local material properties.

In addition to the above standards, guidelines for the assessment of girth weld defects, mechanical damage, and ductile fracture propagation have been produced by the European Pipeline Research Group (EPRG)[45]. Other methodologies presented in [7] and [9], mentioned earlier, have been developed for the assessment of dents, gouges and dent/gouge combinations under cyclic internal pressure.

2.1.2 Buckled Pipes

2.1.2.1 Buckling Development

Buckling of steel pipes in the form of pipe wall wrinkles may occur due to extreme axial or bending loading. In onshore pipelines, ground-induced actions are the primary sources of such extreme loading. Examples of ground-induced actions are seismic fault displacements, landslides due to slope instability, liquefaction-induced

lateral spreading, or permafrost action. In the above extreme loading cases, bending constitutes the dominant loading pattern, however, axial compression may also occur in some cases.

Longitudinal bending of a pipeline induces ovalization of the pipe cross-section, known as "Brazier effect" [46] which reduces pipe bending stiffness because of flattening, increases the local radius of the tube cross-section at the maximum compression location, and introduces a biaxial stress state, because of ring bending, leading to early yielding of the pipe. Upon increasing bending deformation, structural instability of the compressed tube wall occurs, in the form of a localized wavy pattern, referred to as "local buckle", "wrinkle" or "kink". For typical onshore pipes, the wrinkles have a half-wavelength equal to about 10 times the pipe thickness, which is a short-wave wrinkling pattern. Such wrinkles may also occur in the case of excessive axial compression of the pipe.

The bending response of metal pipes has been investigated experimentally numerous times in the last decades. Early experimental work was conducted by Moore and Clark [47] on specimens machined from aluminum-alloy rolled rod with D/t ratios ranging from 2 to 150. Their scaled experiments include bending, compression and torsion testing of which the former two are of interest for the current research. Specimens with D/t ratios larger than 15, were found to be prone to instabilities either due to progressive ovalization, or due to local buckling development. The influence of axial tension on local buckling was found to be positive by Wilhoit and Merwin [48] in similar scaled bending experiments. A large number of small scale bending tests has been performed by Johns et al. [49]. The use of small scale experiments allowed the application of combined load of external pressure and bending. By validating the large number of scaled tests with a limited number of full scale four-point bending tests, understanding of the local buckling mechanism was further increased. More bending tests on small scale specimens were performed by Tugcu and Schroeder [50], whose research includes mainly tests on tube branches besides a few tests on plain tube, and Reddy [51], who tested tubing with D/t ratios up till 80 made of steel and aluminum. The latter investigation also includes the measurement of longitudinal profiles of the tubing at the onset of local buckling. Testing on slender tubes (D/t=81-102) of intermediate scale was performed by Van Douwen *et al.* [52], focusing on the application of pipelines in settlement

areas. More recently, small-scale specimens have been tested by Kyriakides and Shaw [53] and Kyriakides and Ju [54]. In these two publications combined, more than twenty tests on steel and aluminum specimens under monotonic or cyclic bending are reported. The experiments in [54] were carefully analyzed in [55], using analytical methods.

2.1.2.2 Residual Capacity of Buckled Pipes

Limited information is currently available for the structural capacity of buckled pipelines, especially under cyclic bending conditions caused by temperature variations or permafrost actions.

Das et al. [56] conducted full-scale tests to investigate the post-wrinkling ultimate behavior of 305 mm diameter steel pipelines. The pipe specimens exhibited extreme ductile behavior and did not fail in fracture under monotonically increasing axisymmetric compressive axial loads and displacements. Fracture has developed at the wrinkled region, however, when a wrinkled pipe specimen was subjected to cyclic strain reversals due to unloading and loading of primary loads.

Developing a fracture life assessment model requires wide range of full-scale tests; a procedure which is considered expensive and time consuming. Therefore, Das et al. [57] has proposed a series of small-scale tests on strip specimens extracted from pipes. The strips were initially, bent up to 45° and subsequently subjected to cyclic load reversals. The better understanding of local strain reversal behavior of wrinkled pipes subjected to low-cycle fatigue loadings was provided and a simple fracture life assessment model was proposed. The fracture-life model is based on a parameter that defines the unit of cycle energy absorbed by the crest of the strip specimen. The specific model was able to predict, rather conservatively, the fatigue life of full-scale tests performed earlier by Das et al. [56].

In a more recent study, Das at al. [58] investigated, experimentally and numerically, the behavior of a wrinkled energy pipeline subjected to sustained monotonic axial compressive deformation. Two full-scale laboratory tests were performed on X52 grade steel pipes with a diameter-to-thickness ratio equal to 45 with moderate and high internal pressure values. These pipe specimens were considered extremely ductile while rupture did not occur under axisymmetric

compressive axial deformation. However, the specimens failed due to the excessive deformation upon the formation of multiple wrinkles. Subsequently, a detailed parametric study using a numerical technique was undertaken to determine the failure condition and failure mode of this pipeline for various realistic internal pressures and diameter-to thickness ratios. A nonlinear finite element method was used for the numerical study. The numerical model was validated with the data obtained from the two full-scale tests.

Dama et al. [59] presented experimental and numerical research conducted to assess the structural condition of buckled pipes, subjected to both bending and internal pressure. Fatigue failure under repeated loading and pipe burst has been investigated, through three full-scale buckled pipe specimens and nonlinear finite element tools. Using the maximum strain range from the finite element computations, and a simple *"Δε-N"* approach gave reasonable predictions for the number of cycles to failure observed in the tests. The results of that study demonstrate that under repeated loading, fatigue failure occurs in the buckled area at the location of maximum strain range. It is also concluded has been concluded that the presence of local buckles does not affect the burst pressure of pipes, even after a substantial part of the pipe fatigue life has passed.

2.1.2.3 Buckle Assessment-Current Standards and Methodologies

There is lack of assessment methods for buckled piped. Although several provisions exist in current codes and standards are implemented in order to prevent buckling on the stages of pipeline design, such type of a local damage can occur at construction stages or during operation. Pipeline standards do not provide acceptance criteria for buckles in terms of ultimate capacity or fatigue strength. However, in the case of extreme loading conditions, local buckling of the pipe can occur and the corresponding strains can be well beyond the strain limits specified in [60], [61], [62].

ASME B31.8 [13] Code committee is considering the acceptance of wrinkles with peak-to-valley heights over 1% of the pipe diameter based on recent work of Rosenfeld et. al [63]. However, as buckles are characterized of a more complex geometry than dents; their "depth" may not be the most reliable parameter for determining the pipeline integrity.

According to a recent report by Baker [64], the strain–based method described in ASME B31.8 [13] could be used for specifying acceptance criteria for buckles. The accumulated strain in a buckle (due to the associated curvature) is calculated and then, if the buckle is not located near welds, it is compared with the strain 6% acceptance level (for plain dents). Essentially, the 6% limit was chosen within the 3% strain limit for field bends (ASME B31.4 (2006) [65] and ASME B31.8 [13]) and the material strain level (12%) at which the likelihood of cracks appears to increase [63].

Furthermore, Baker [64], also, proposes an assessment procedure for corroded buckles in order to evaluate the pressure integrity and potential fatigue life of corroded wrinkles. A specific procedure is followed where, after the pressure strength is estimated for the corroded region, the fatigue integrity is estimated disregarding the effect of corrosion. Annual "histograms" and global pipeline models are developed so that global loads and stress fields are estimated. Subsequently, "local" FEA model of the wrinkle geometry is used to calculate the stress concentration factor in the wrinkle region, so that the localized fatigue stress demands for internal pressure and bending moment loads are identified. "S-N" curves are used to compute the fatigue life of the wrinkle. If the design fatigue life is longer than the design life of the pipeline, the buckle satisfies the fatigue criteria that would be useful for the design pipelines, including a significant safety factor. Otherwise, the wrinkle would be considered as acceptable depending on the safety factor adopted through the design "S-N" curve used. Once the fatigue life is identified, the fatigue analysis may be extended in order to include corrosion effects with the same evaluation procedure described previously, while the FEA model developed includes corrosion characterization.

2.2 Importance and Innovative Features of Present Research

Hydrocarbon pipeline systems constitute a major component of our economy, allowing for the transmission of large quantities of energy resources. However, pipelines are frequently susceptible to various kinds of damage, particularly caused by external interference or by ground-induced actions. As a result, their structural integrity may be seriously threatened, leading to major accidents and loss of containment, with severe consequences for human lives, the environment and the economy. Therefore, it is very important to monitor and assess damages

systematically, in a systematic and cost-effective manner in order to estimate the remaining operational life of pipelines and maintain a reliable level of structural performance.

Towards the above purpose, several methods and practices have been proposed in the past and used for the assessment of limited cases of local defects on pipeline wall. Nevertheless, there exist several modes of damage that require more attention and further investigation. The literature review and evaluation stated in the previous sections show that there exist dent acceptability limits, based on a large number of tests on dented pipelines under pressure cyclic loading and burst. However, limited information is currently available for the mechanical response of damaged pipelines, under cyclic structural loadings (e.g. bending), caused by temperature variations or permafrost actions. On the other hand, it was also found that very limited data exist for the influence of local buckles on the integrity of steel pipeline, both on fatigue resistance under cyclic pressure and on their burst pressure capacity. In particular, few works are currently available on the fatigue capacity due to bending loading, and this constitutes an issue open for research.

The present dissertation consists of novel work following an integrated approach that combines full-scale and small-scale tests supported by numerical finite element simulations leading to a simplified assessment methodology. The scope of the present research is to address the above issues regarding the assessment of dents and buckles, where limited and no sufficient information exists. The ultimate purpose of this research effort consists of developing simple and efficient assessment tools enhancing current methodologies regarding the damage types under consideration, towards more reliable evaluation of damaged hydrocarbon pipelines and pipeline integrity management.

2.3 Research Outline

The work plan followed in the present research can be outlined as follows. In Chapter 3, the performance of the experimental campaign is described in detail. The experiments mainly refer to full-scale 6-inch-diameter X52 pipe specimens, under various loading conditions at the laboratory of Technology and Concrete Structures of the University of Thessaly. Denting or buckling of the pipes is conducted first, and subsequently, the specimens are subjected to cyclic loading of bending or pressure, or

monotonic increase of pressure until burst. In addition to full-scale testing, small-scale tests on bent strip specimens are also performed, for the purpose of correlating those results with the available material fatigue data of the X52 steel material, obtained elsewhere.

Apart from experimental testing, an extensive finite element study is conducted and presented in Chapter 4, aiming at simulating the loading pattern of each experiment, and providing the local strain variation at critical locations of the dented/buckled area. In Chapter 5, the experimental and numerical results are considered and correlated, towards (a) performing a fatigue analysis of the cyclic-loaded specimens and (b) proposing a simple and efficient methodology for the structural assessment of dented/buckled pipelines, validated through the above experimental and numerical results. Finally, in Chapter 6, some important conclusions are stated, together with some suggestions for further research.

Chapter 3 EXPERIMENTAL PROCEDURE

3.1 Introduction

Local distortions on pipeline wall in the form of dents or buckles may constitute a threat for the structural integrity of the steel pipeline. In the present paper, experimental research supported by numerical simulation is reported to investigate the structural integrity of smoothly dented and buckled steel pipes. A series of sixteen (16) full-scale experiments on 6-inch X52 pipes has been carried out, and numerical simulations have also been conducted at the Laboratory of Technology and Concrete Structures of the University of Thessaly (Department of Civil Engineering) in Volos Greece. The dented/buckled steel pipes are subjected to cyclic loading (bending or pressure) in order to estimate their residual strength and remaining fatigue life. Additionally, a series of small tests on strip specimens extracted from the X52 pipe specimens has been performed at the Laboratory of Mechanics and Strength of Materials of the Department of Mechanical Engineering at the University of Thessaly (Volos, Greece) to further investigate the cyclic response of pipe material in the critical area of damage under cyclic loading. Following the full-scale testing, the strips are initially bent monotonically under three (3) point- bending conditions up to a certain angle (90° and 120°), simulating the creation of a dent or a smooth buckle on the pipe wall, and then they are subjected to cyclic vertical loading in correspondence with the full-scale pipes under cyclic bending as described in Section 3.7.

3.2 Specimen Description

The full-scale experimental program consists of two testing groups. The first one (group 1) consists of ten (10) tests and refers to denting of six (6) pipe specimens with a nominal thickness equal to 4.78 mm (∅168.3/4.78) [67], corresponding to D/t=35 and four (4) with nominal thickness equal to 3 mm (∅165/3), corresponding

to D/t= 55. The latter group of specimens has been machined from the original geometry (∅168.3/4.78) in order to investigate the cyclic response of thinner specimens with higher diameter-to-thickness ratios. The second group (group 2) consists of six (6) tests and refers to buckling of pipe specimens with nominal thickness equal to 3 mm (∅165/3), corresponding to D/t= 55.

The machining of specimens was performed in order to examine the buckling behavior of thinner pipes with D/t larger than the value of 35. Through this process the specimens' thickness was reduced about to a constant mean value of a 2.8mm for 50cm-long central pipe region. There exists a 10cm-long transition zone on both sides of the specimen, out of the 50cm-long region, where the thickness is gradually decreased from the pipe ends, producing a smooth slope of less than 2^o degrees. This was considered to avoid geometrical discontinuities which might have affected the experimental results. In the following paragraphs, the procedure of buckling, cyclic bending and pressure loading are described.

Furthermore, 1.5″-diameter holes have been drilled in the wall of both types of specimens(D/t=35 and D/t=55) at a distance of 15 cm far from each end-plate on the same side to implement pressure valves and facilitate the application of internal air pressure during the tests. The pipe specimens ∅168.3/4.78 and ∅165/3 are shown in Figure 3-1.

After the formation of denting or buckling, the specimens of both groups were further subjected to cyclic loading of bending or pressure in order to estimate their residual strength and the remaining life. Buckling was induced through the application of monotonic four-point bending up to a certain post-buckling level. The schematic configuration of the bending set-up is shown in Figure 3-2. Cyclic bending loading was applied with the same four-point bending set-up until fatigue cracking occured in the low-cycle fatigue range (Figure 3-2).

Cyclic bending loading was applied until fatigue cracking occured in the low-cycle fatigue range, while cyclic pressure was applied for a significant number of cycles (5000 cycles) and then the pressure was raised monotonically until burst. Moreover, the specimen ends are capped with thick plates, to enable the application of internal pressure and the connection with adjacent pipe parts for the experimental set-up.
The specimens of group 1 are dented with a wedge indenter at zero pressure, and subsequently, they are subjected to cyclic loading. Similarly, group 2 specimens were

buckled up to different levels and, subsequently, they were subjected to further cyclic loading (bending or pressure). The experimental program can be summarized as follows:

- Group 1: ten (10) dented specimens:
  - six (6) subjected to cyclic bending loading
  - four (4) subjected to cyclic pressure loading.
- Group 2: six (6) buckled specimens:
  - four (4) subjected to cyclic bending loading
  - two (2) subjected to cyclic pressure loading.

In the following paragraphs, the procedure of denting, buckling, cyclic bending and pressure loading are described in detail. It is noted that denting and cyclic bending has been conducted at the "Reinforced Concrete Technology and Structures" Laboratory of the Department of Civil Engineering at the University of Thessaly, whereas the the pressure tests have been performed at the facilities of EBETAM S.A., located in Volos, Greece.

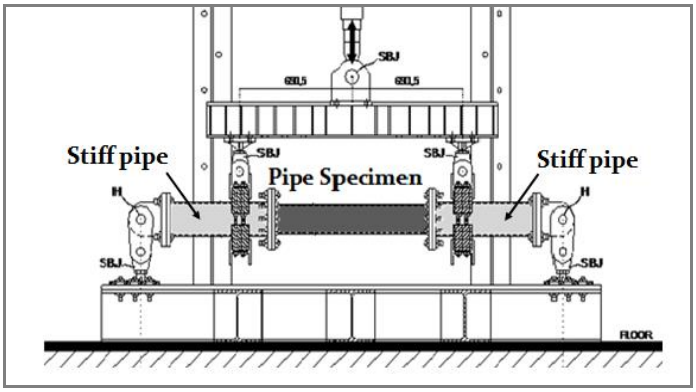

Figure 3-1: Schematic configuration of four-point bending set-up.

(a)

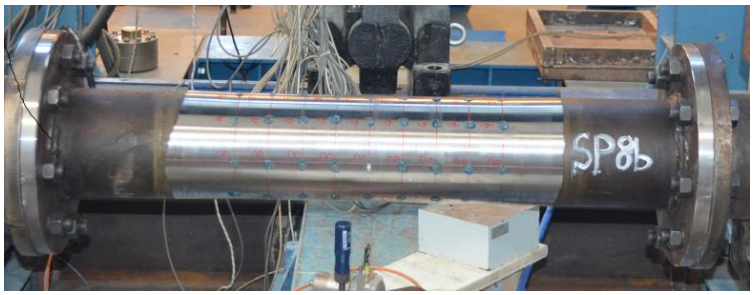

(b)

Figure 3-2: X52 pipe specimens (a) 6-inch and (b) machined at 2.8mm thickness

3.3 Material properties

Material testing to characterize material properties has been performed, in the facilities of University of Porto (FEUP) [68]. Monotonic and cyclic behavior of X52 steel material of the pipes under consideration has been obtained. Monotonic and low-cycle fatigue tests were performed on the X52 steel (API 5L) material from a seamless 6″×4.78mm pipe supplied by University of Thessaly, to determine material properties. The coupon specimens were extracted in the longitudinal direction of the pipe. The dimensions of the specimens are in accordance with the ASTM E606 standard, as shown in Figure 3-3. The side faces of the specimens were flattened and finished in order to remove the hoop curvature and the surface imperfections.

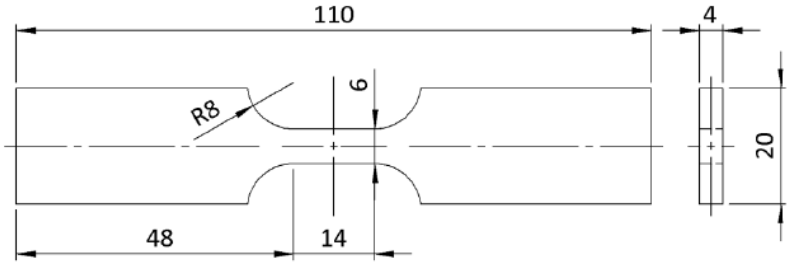

Figure 3-3: Coupon tensile tests [68].

The monotonic and cyclic tests have been performed at room-temperature in air. The fatigue tests were conducted under constant strain amplitudes and with a frequency adjusted to result an average strain rate of 0.008s-1. The longitudinal strain was measured using a clip gauge with limit displacements of ±2.5 mm with a gauge length of 12.5 mm (INSTRON 2620-602). This extensometer was also used in two monotonic tensile tests allowing for measuring longitudinal strains up to approximately 17 %. Four specimens named as “M_LD_1” -“M_LD_4” have been

tested under monotonic loading to derive the monotonic load-displacement and stress-strain experimental curves. The material stress-strain curve was obtained from tensile coupon tests as shown in Figure 3-4, indicating a yield stress value (σ_y) equal to 364MPa, quite close to the nominal value, and ultimate stress (σ_{UTS}) equal to 525.8 MPa at about 18% uniform elongation.

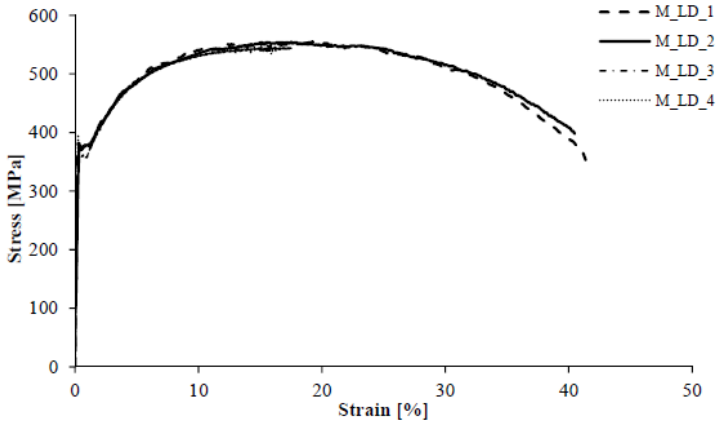

Figure 3-4: Material curve of X52 steel grade[68]

In addition to tensile testing, a total of thirty (30) cyclic tests have been performed by FEUP on strip specimens with loading ratios -1 and 0 [68]. The stabilized hysteresis loops and the evolution of the cyclic stress amplitude with the number of cycles were derived for the tested strain ranges, covering fatigue lives in the range $\sim 10^2$ - 10^4 cycles (Figure 3-5).

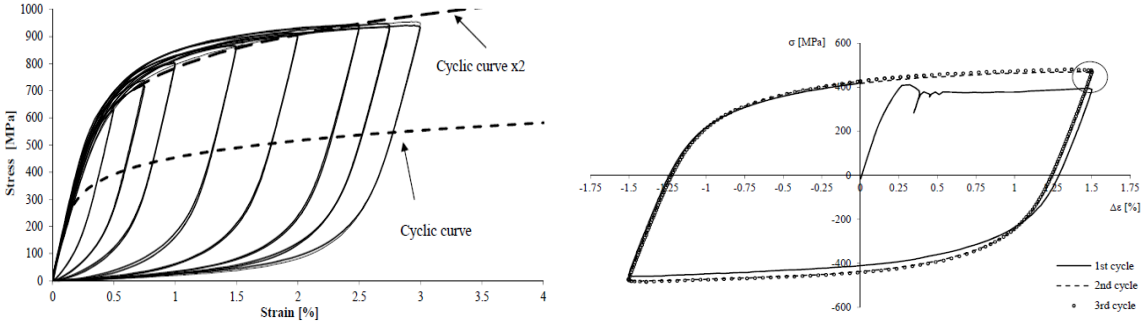

(a) (b)

Figure 3-5: (a) Hysteresis loops and cyclic curve under R =0; and (b) first three hysteresis loops for Δε= 3%, under R=-1([68])

The strain-life data has been correlated to compute Morrow's constants used in the fatigue curve of the X52 material expressed through a Coffin-Manson-Basquin

equation Eq(2.1) [[68]. The schematic configuration of the X52 fatigue curve is shown in Figure 3-6.

$$\Delta\varepsilon = 0.0104(2N)^{-0.1133} + 0.333(2N)^{-0.4807} \tag{2.1}$$

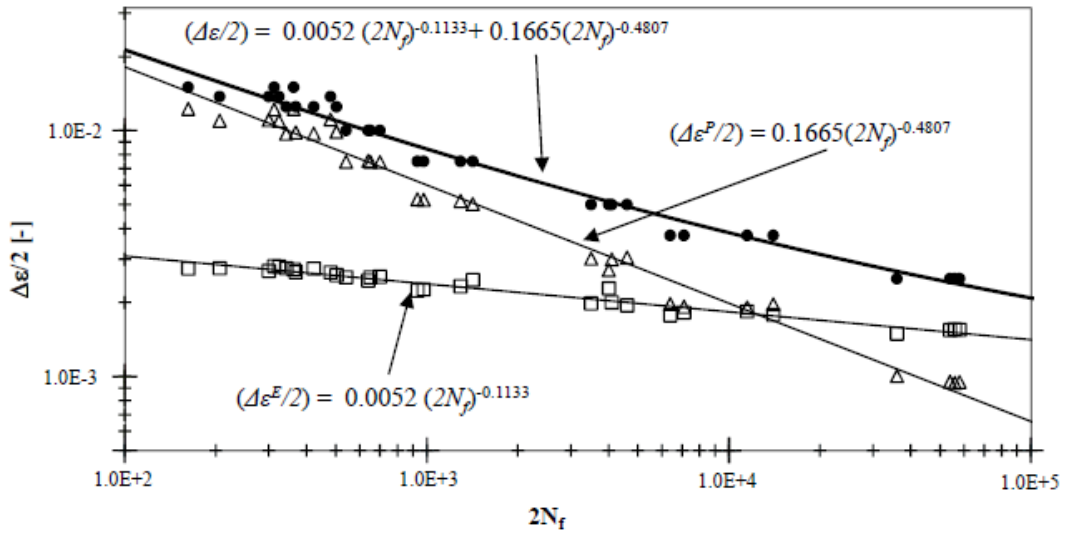

Figure 3-6: Global strain-life curves for the X52 steel, according to the Morrow's model [68].

3.4 Thickness Measurements

Prior to testing the specimens, thickness measurements were obtained using an ultrasonic device at specific points around several cross sections along the specimen's length Figure 3-7. A mean thickness value was obtained equal to 5.026mm for the ∅168.3/4.78 specimens, which is greater than the nominal value (4.78mm) while for specimens ∅165/3 a mean value equal to 2.794 was recorded.

(a) (b)

Figure 3-7: (a) Thickness measurements on ∅168.3/4.78 pipe specimens via ultrasonic device and (b) marked ∅165/3 specimens.

The geometrical properties of the specimens under consideration are summarized in Table 1 and Table 2. It is observed that in local regions the measurements did show a considerable variation of thickness with respect to the mean thickness values.

Table 1.Geometrical characteristics of pipe specimens∅168.3/4.78 and ∅165/3

	Dented Specimens		
Specimen	**D (mm)**	**t_{mean} (mm)**	**D/t_{mean}**
SP1d	168.3	5.016	33.55
SP2d	168.3	4.974	33.83
SP3d	168.3	5.056	33.28
SP4d	168.3	4.988	33.74
SP5d	168.3	5.078	33.14
SP6d	168.3	4.987	33.74
SP7d	166.03	2.508	66.19
SP8d	166.25	2.735	60.78
SP9d	166.38	2.865	58.07
SP10d	166.57	3.054	54.54

Table 2.Geometrical properties of pipe specimens ∅165/3

	Buckled Specimens		
Specimen	**D_{nom} (mm)**	**t_{mean} (mm)**	**D/t_{mean}**
SP3b	166.79	3.268	51.03
SP4b	166.2	2.680	62.02
SP5b	166.27	2.747	60.53
SP6b	166.33	2.808	59.23
SP7b	166.31	2.750	59.52
SP8b	166.46	2.943	56.56

3.5 Experimental Set-up

3.5.1 Denting Procedure

Denting is applied on the ten (10) pipe specimens through the application of a rounded wedge indenter, shown in Figure 3-8, oriented perpendicular to the pipe axis, so that a smooth dent is formed on the pipe wall.The total wedge height is equal to 80 mm, the horizontal length is equal to 85 mm, and the radius of the rounded wedge is equal to 5 mm (Figure 3-9). As shown in Figure 3-9, the steel plate is bolted at the bottom of the hydraulic actuator.

During denting, the specimen is supported on a wooden base (300×280×200) shown in Figure 3-10. The wooden base was developed longitudinally, by connecting 50mm-long wooden parts. The top surface of each wooden part was properly curved so, after connecting these parts, the top surface of the entire base could prevent movement of the tubular specimen. Moreover, to avoid the development of strain and stress concentration in the pipe at the edge of the wooden base, the radius of base curve was chosen greater than the value of the nominal radius of the pipe. Furthermore, as shown in Figure 3-11, the wooden base was stiffened along both directions (length and height) with the use of steel rods in order to avoid excessive deformations of the wood material during the application of denting load. The test set-up is shown in Figure 3-12.

(a) (b)

Figure 3-8: The Wedge Denting tool; (a) Side view and (b) Bottom view

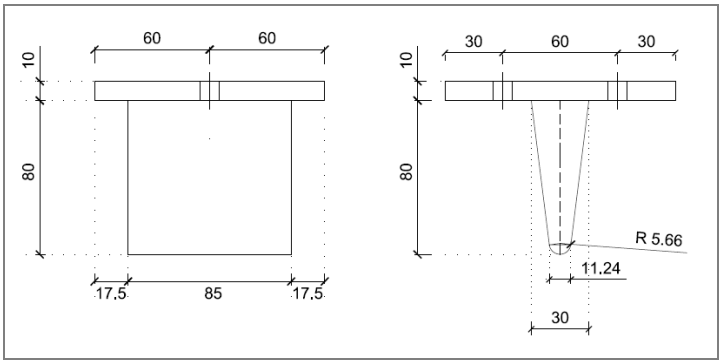

(a)

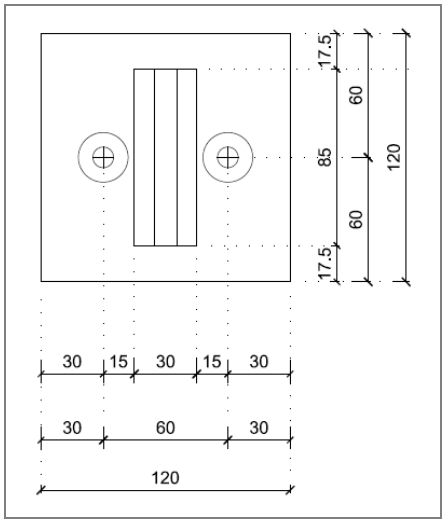

(b)

Figure 3-9: Drawings of the denting tool; (a) Side views and (b) bottom view

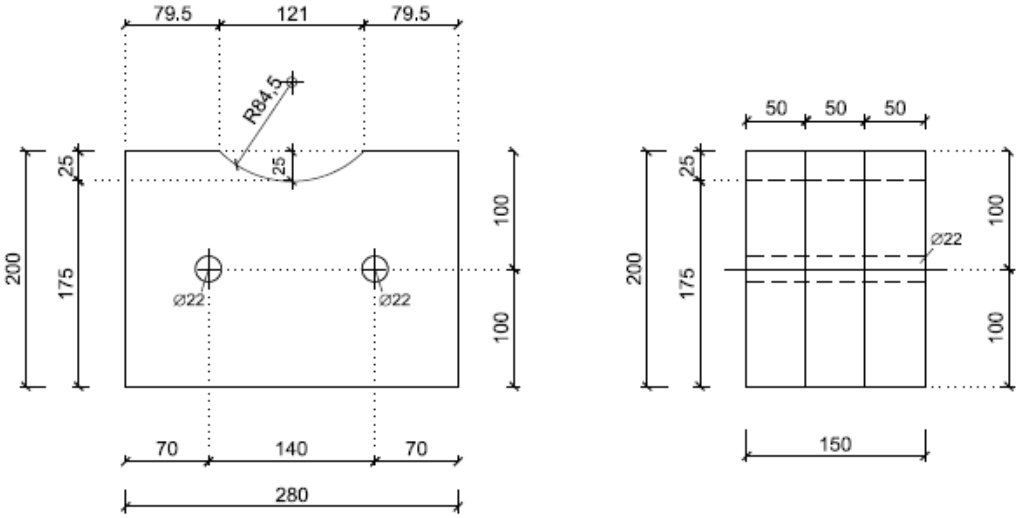

Figure 3-10: Drawings of wooden base; (a) view along the width and (b) view of half length

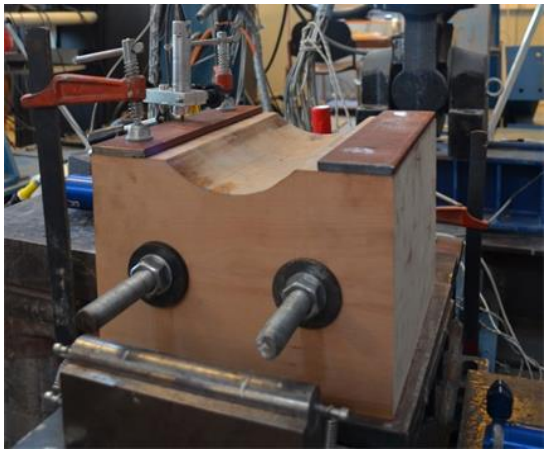

Figure 3-11: The stiffened wooden base

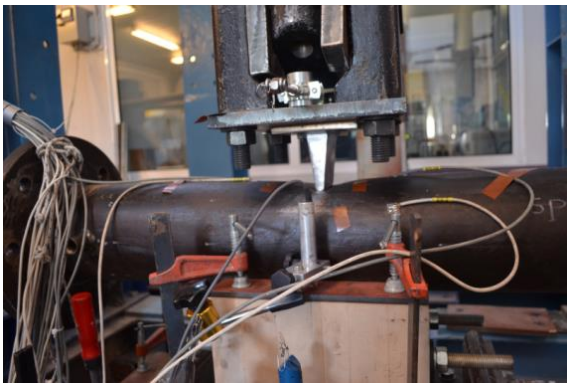

Figure 3-12: Denting set-up.

Prior to denting, uniaxial strain gauges were installed on several critical points along the outside surface of the specimens and close to the region where the dent would be developed, in order to define the evolution of local strains during the denting procedure (Figure 3-13 and Figure 3-14). Additionally, two LVDT's were implemented, to record the indenter downward movement during the denting force application. The one end of each LVDT was fixed on a stable part of the steel frame set-up, while the moving end was hinged on the horizontal steel plate of the denting tool.

Furthermore, DCDT transducers were instrumented via special purpose supports in order to measure the relative displacement of the top surface of the wooden base during denting (Figure 3-12)

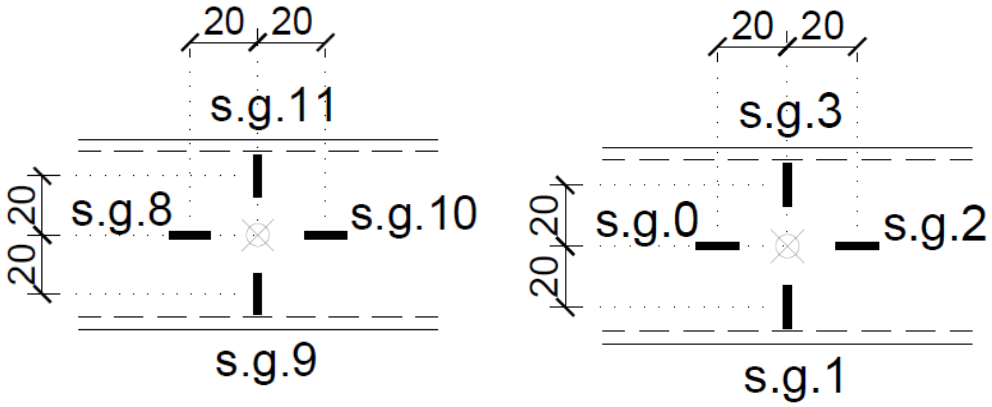

Figure 3-13: Schematic view of the strain gauges implemented at the denting region for (a) SP5d and (b) SP6d specimens

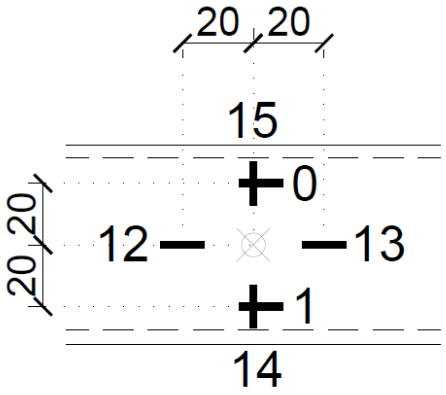

Figure 3-14: Schematic view of the strain gauges implemented at the denting region for SP9d and SP10d specimens

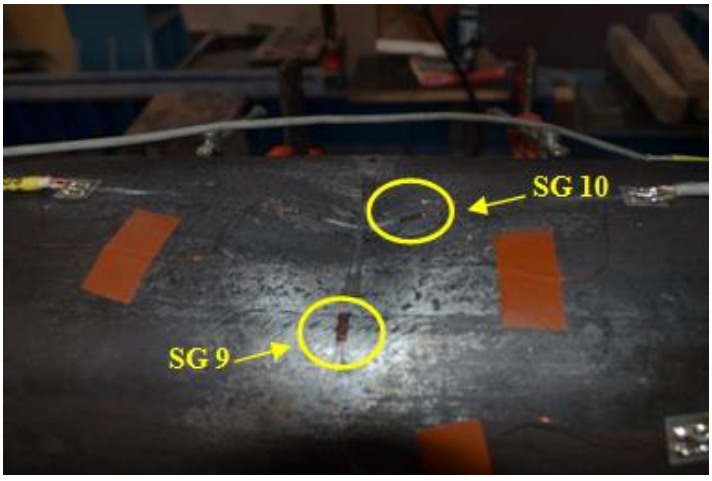

Figure 3-15: The strain gauges of SP5d pipe specimen after denting.

3.5.2 Monotonic and Cyclic bending set-up

The set-up employed for buckling development and cyclic bending on the dented/buckled specimens is shown in Figure 3-16. To carry out these experiments several special frames and ball-joint hinges had to be manufactured.

The 1-meter long specimens are connected on either side to two heavy-walled 7-inch-diameter 650-mm-long tube segments (∅193.7/10) made of high-strength steel using a bolted connection referred to as "stiff- pipe". The entire system, 2.615-meters long, is supported using a double-hinge 'roller' system with ball joint hinges. The bending load is applied from the 600-kN-force-capacity hydraulic actuator through a stiffened horizontal steel beam with a system of two special ball-joint hinges and appropriate wooden grips. The two wooden clamps (Figure 3-17) have been manufactured for the purposes of these tests. The wooden grips consist of properly curved wooden slices strongly glued together and stiffened. The cutting curve of the wooden slices was chosen larger than the nominal diameter of the "stiff" pipes. The "stiff" pipes' were griped by the wooden clamps around their circumferences as shown in Figure 3-16. The wooden grips are connected with the horizontal steel beam through appropriate hinges allowing the rotation in the bending plane.

The set-up shown in Figure 3-18 corresponds to a four-point bending structural system, where monotonic and cyclic bending is applied through the vertical motion of the hydraulic actuator. The actual experimental set-up is shown in Figure 3-19. The details of the supports and the wooden grips are shown in Figure 3-20. The entire experimental design was based on the basic restriction of the application of tensile loading conditions to avoid out-of-plane instabilities.

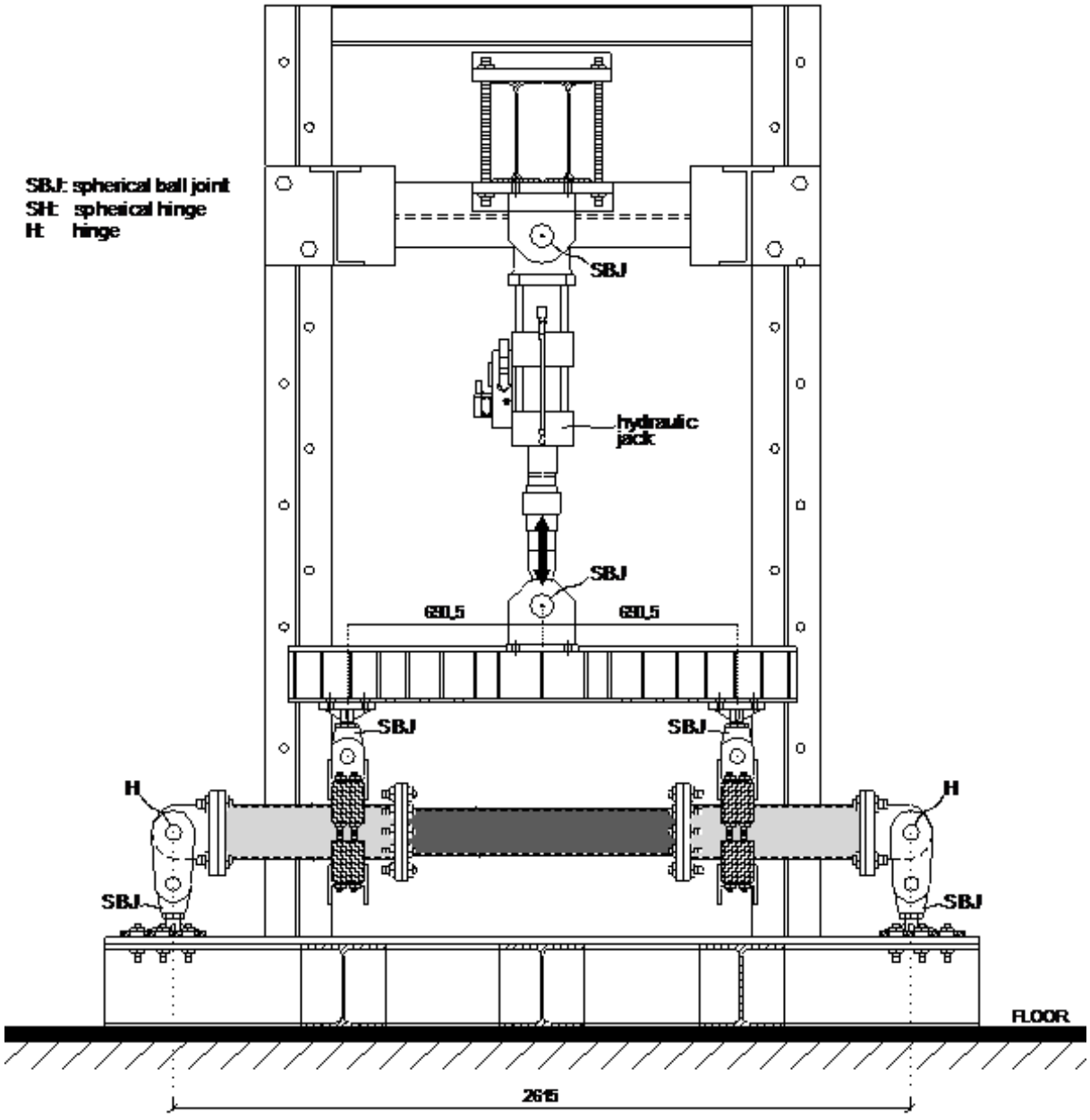

Figure 3-16: Schematic illustration of the experimental set-up during monotonic and cyclic bending

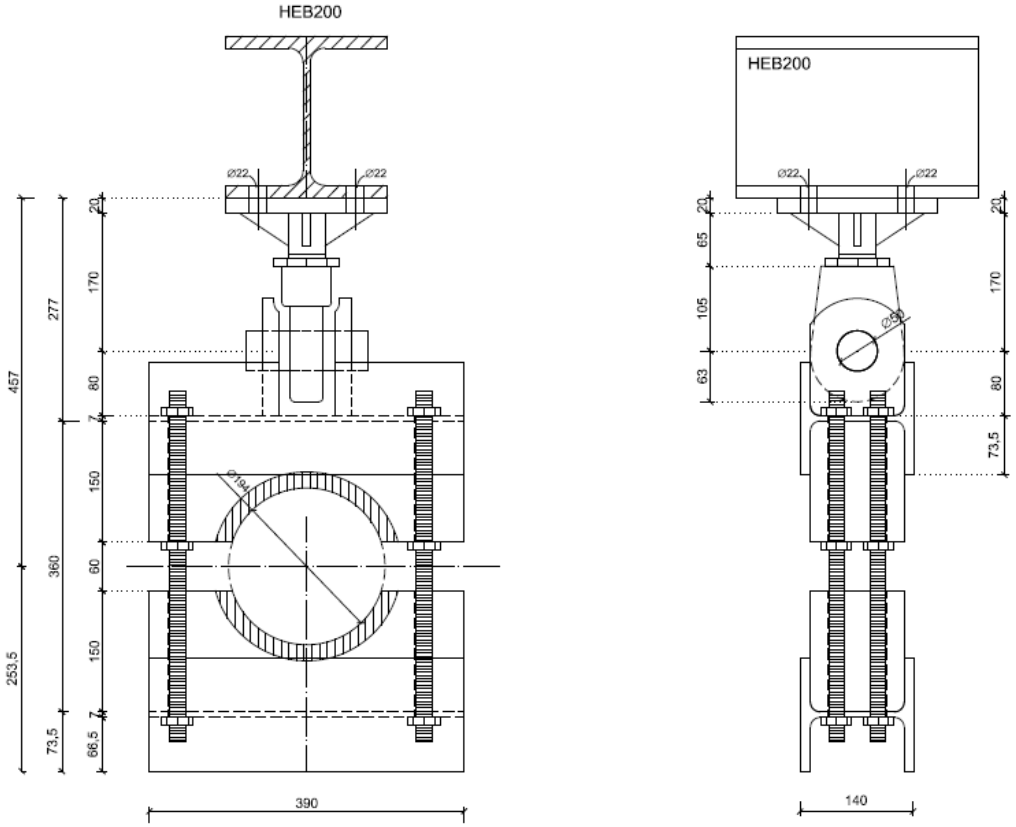

Figure 3-17: Wooden clamps' drawing

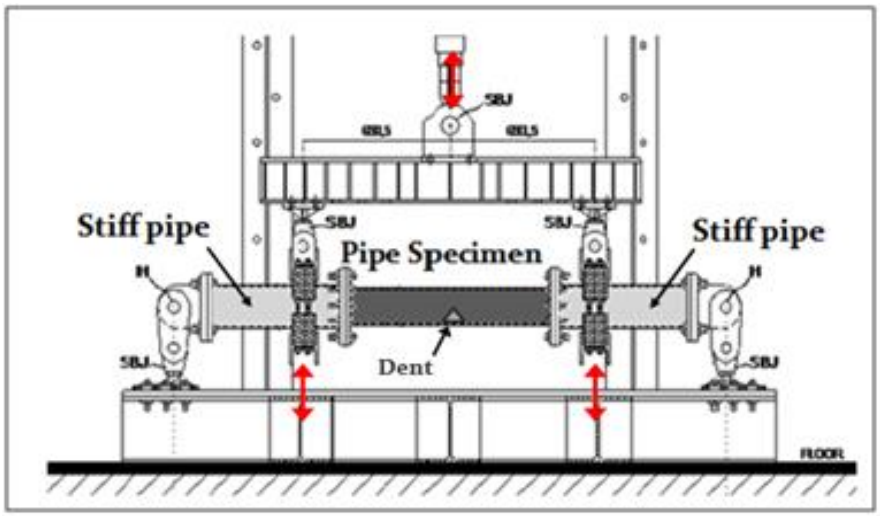

Figure 3-18: Configuration of the four-point bending experimental set-up.

Figure 3-19: Four-point bending experimental set-up.

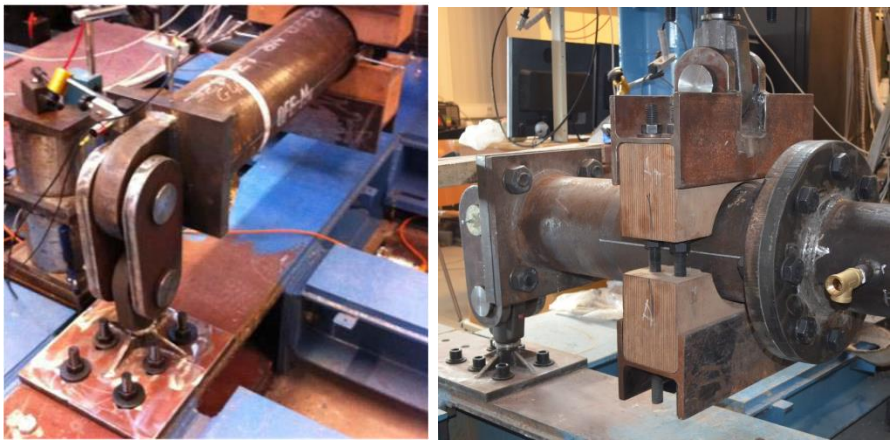

(a) *(b)*

Figure 3-20: (a) bending specimen hinges and (b) wooden clamp.

Furthermore, local strains are measured throughout the experimental procedure through strain gauges located at several positions along the pipe specimens as shown in Figure 3-21, Figure 3-22 and Figure 3-23. Prior to cyclic loading, additional strain gauges have been implemented in the critical region of the dent or buckle (after its occurrence) in order to measure local strain variations before crack initiation.

Furthermore, the main concern during the 4-point set-up design was the elimination of the axial load that could be developed during the application of pure bending. Eventually, the four (4) hinged support design of this set-up minimized the axial load introduced during the monotonic loading, because of the type of

constraints applied by the wooden grips and the supports. In fact, using the appropriately located strain gauges, the maximum value of axial load at maximum bending load axial force was calculated equal to less than 8% of the cross-sectional axial yield strength and it is considered negligible.

Moreover, internal pressure up to 0.1 bar was applied in the specimens. As shown in Figure 3-24, a manometer was placed in the one hole, while the other was used as the gate valve. The internal pressure was kept constant and measured during the cyclic tests. The failure of the specimen was determined by a through-thickness crack resulting in pressure leakage.

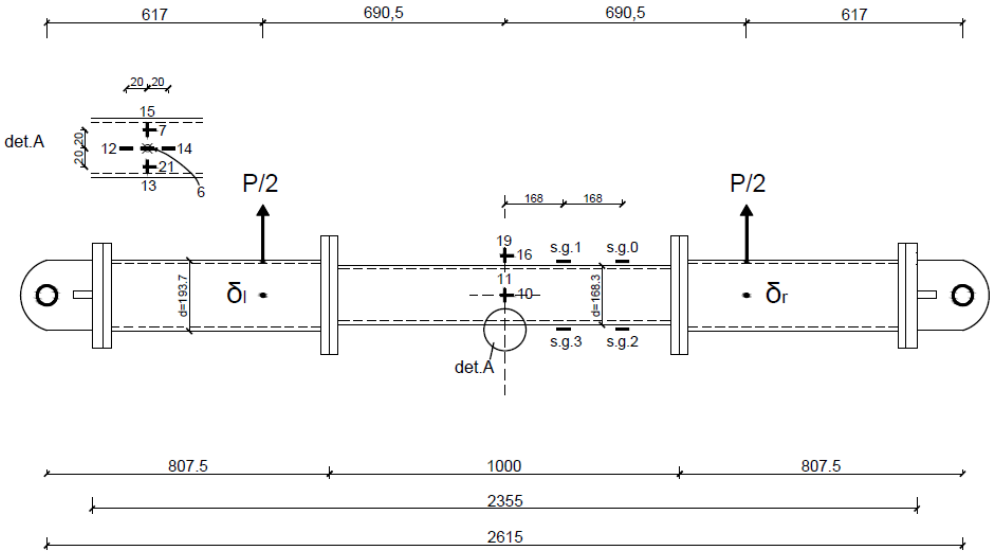

Figure 3-21: Strain gauges instrumentation of SP1d and SP3d specimens prior cyclic bending tests

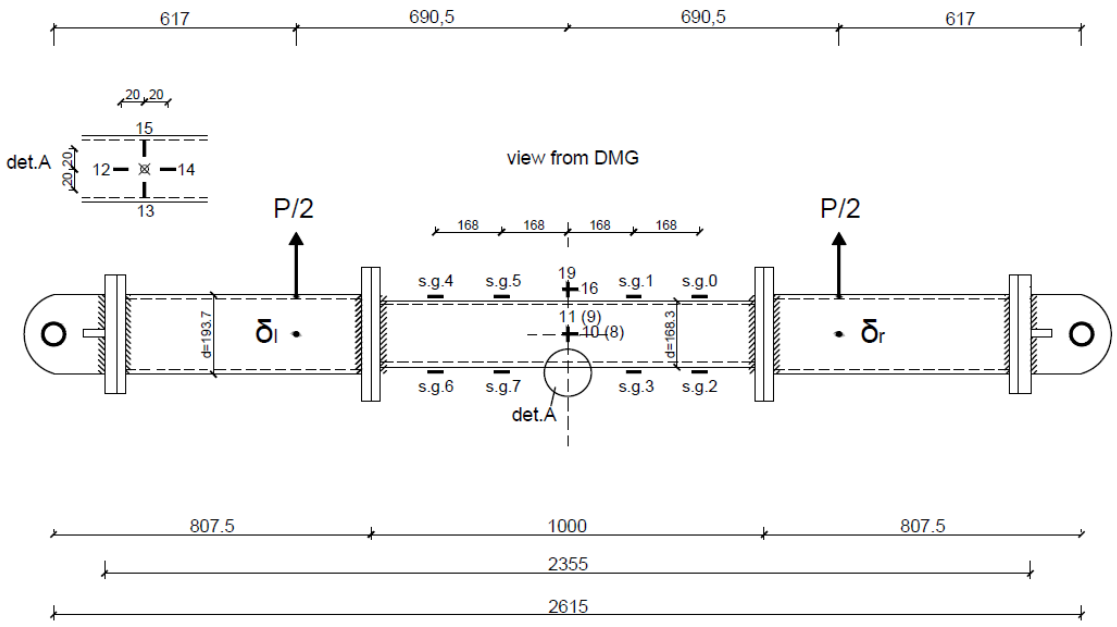

Figure 3-22: Strain gauges instrumentation of SP5d specimen prior cyclic bending tests

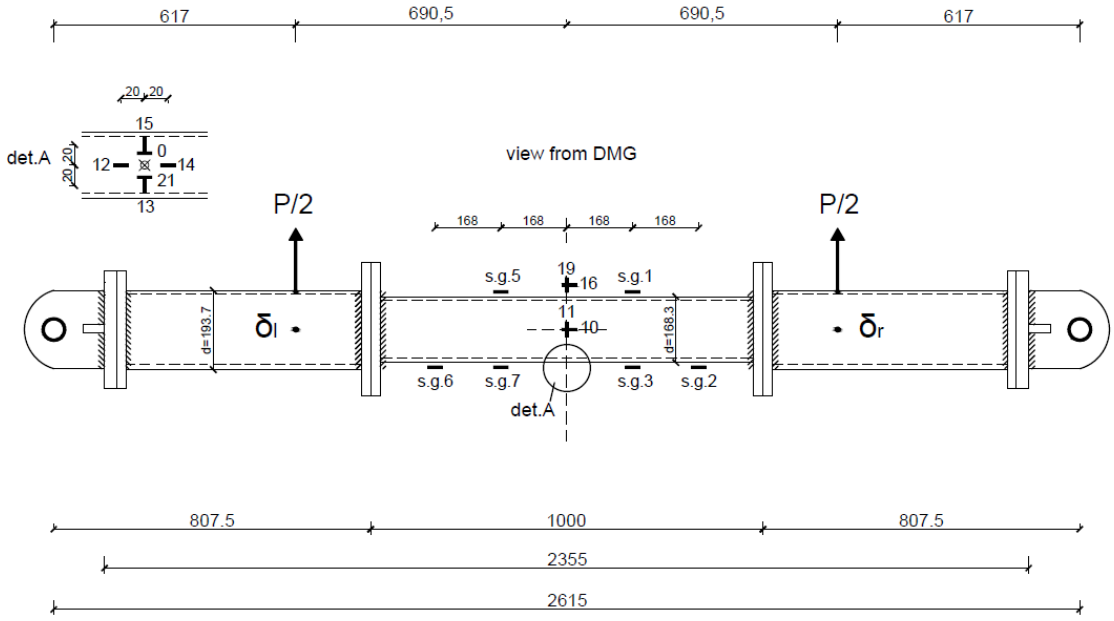

Figure 3-23: Strain gauges instrumentation of SP6d specimen prior cyclic bending tests

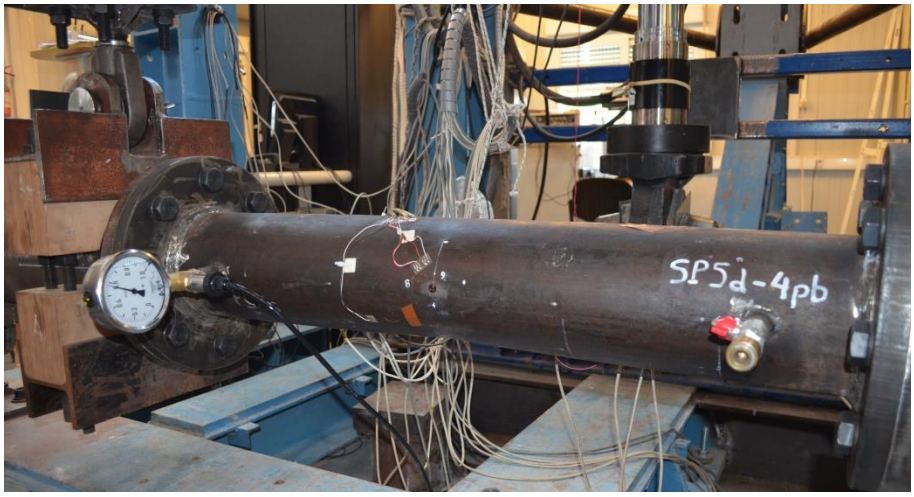

Figure 3-24: Detail of the pressure valve and manometer implemented for the internal pressure during cyclic bending

3.5.3 Pressure test procedure

The total six (6) specimens have been connected with a 450-bar-capacity water pump instrumented with several manometers of various recording ranges Figure 3-25 and Figure 3-26. Cyclic pressure has been applied to ∅168.3/4.78 specimens with a pressure range (Δp) equal to 135 bar, while specimens ∅165/3 were subjected to Δp equal to 83 bar with loading ratio (R) equal to 0.1 and at a frequency of about 0.1 Hz. Following cyclic testing, the specimens were pressurized monotonically until burst.

Figure 3-25: Pressure application on specimens ∅168.3/4.78.

Figure 3-26: Pressure application on specimens ∅165/3.

3.6 Experimental Results

For the first group of dented specimens, two values for the dent depth d/D have been considered equal to 6% and 12%. The first value is equal to the dent acceptability limit used in practical applications and pipeline assessment manuals, [14] whereas the second value was chosen equal to twice this limit. During denting, the specimen was simply supported by the wooden base while its ends were totally unrestrained.

For the buckle development the specimens were subjected to monotonic 4-point bending and were connected to the experimental set-up shown in Figure 3-19. The monotonic bending is subjected until the desired size of buckle is developed in the post buckling regime. The level of buckling is defined from the ratio of P_b/ P_m, where P_b value refers to the predefined vertical load level reached on the post buckling brunch and P_m is the maximum sustained vertical load before buckling development. Two levels of buckle have been mainly investigated corresponding to P_b/ P_m ratios equal to 0.5 and 0.75.

Subsequently, cyclic bending was applied to six (6) out of ten (10) dented specimens and four (4) out of six (6) buckled specimens. During the monotonic and cyclic tests, the reaction forces of the frame against the vertical movement of the actuator are considered as the load values used for the display of the experimental results (load- displacement and load –strain values curves).

On the other hand, pressure loading was applied for the rest four (4) dented specimens and for the rest two (2) buckled specimens connected with the pressure pump.

3.6.1 Denting results

The denting load is applied vertically through a hydraulic actuator at a very low speed until a dent depth of about 16 mm (for SP1d, SP4d and SP6d) and 27 mm (for SP2d, SP3d and SP5d), and subsequently, the load was removed. The permanent dent depth after the elastic "spring back" is measured about 11mm and 21mm corresponding to d/D=6% and d/D=12% respectively. The dent results are summarized in Table 3. Several observations could be made from this table. At first, for the case of specimens (D/t=33.5) the denting force required for a dent with

d/D=12% is about 17% larger than the force applied for a dent with d/D= 6%. Moreover, for the thinner specimens (∅ 165/3 and D/t=55) the maximum denting load required for a dent with d/D=12% becomes about 60% larger than the maximum force applied for a dent with d/D= 6%. Furthermore, the peak denting force in order to obtain a final dent of 12% of the nominal diameter of ∅ 165/3 specimen is about 65% lower than the load achieved for the same dent depth on the ∅ 168.3/4.78 specimen's wall. Similarly, in order to obtain a final dent of 6% D on a ∅165/3 specimen, the maximum load obtain is about 75% lower than the development of a similar dent depth on the ∅ 168.3/4.78 specimen's wall.

The denting load-stroke curves for specimens SP1d, SP3d, SP5d and SP6d are presented and compared in Figure 3-27. As shown in Figure 3-29, load-stroke curves are compared, also, with the load vs LVDT's displacement curves for each specimen (Figure 3-28). The latter displacement values have been calculated as the average value of the two LVDT transducers placed during denting procedure. Furthermore, the maximum stroke is 0.5mm larger than the average value recorded from the transducers implemented on the denting tool. Nevertheless, the residual displacement value on the pipe specimens' wall is identical either obtained from stroke or LVDT's recordings.

Moreover, as shown in Figure 3-33, during denting, a relatively small elastic movement of the surface of the wooden base is recorded from the DCDT's with a maximum value of 0.85mm and 0.05mm in the case of ∅ 168.3/4.78 and ∅ 165/3 specimens, respectively.

Furthermore, the dented region and axial and hoop strain gauges instrumented are shown in *Figure 3-30*. The evolution of axial and hoop local strains at the dented region of specimens SP5d, SP9d and SP10d is indicatively illustrated in Figure 3-31 and Figure 3-32.

Table 3: Pipe denting results.

Specimen	Residual depth d(mm)	Normalized depth d/D(%)	Maximum Force F_{max} (kN)
SP1d	10.245	6.08	69.26
SP2d	20.310	12.06	81.35
SP3d	20.198	12.00	83.29
SP4d	10.593	6.29	69.11
SP5d	20.263	12.04	81.75
SP6d	10.658	6.33	67.39
SP7d	5.97	9.78	18.40
SP8d	12.19	20.03	29.18
SP9d	5.97	9.83	24.60
SP10d	11.92	19.66	33.10

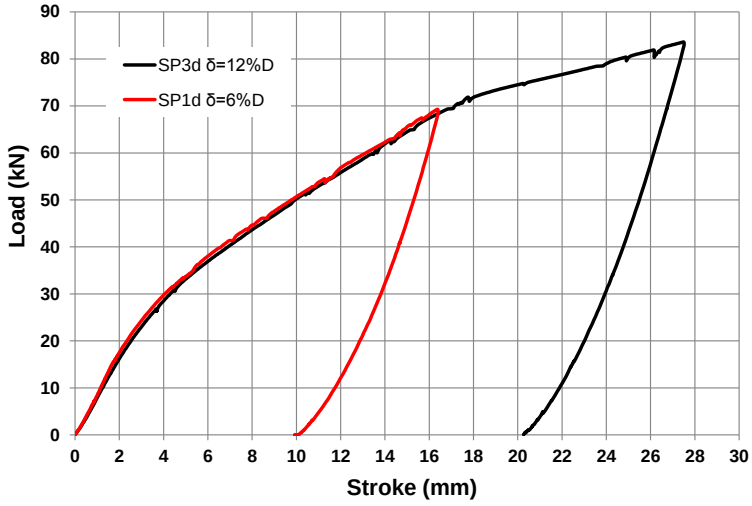

(a)

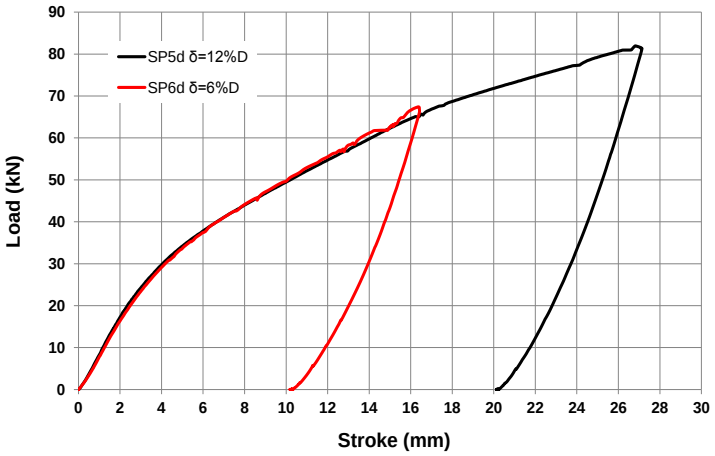

(b)

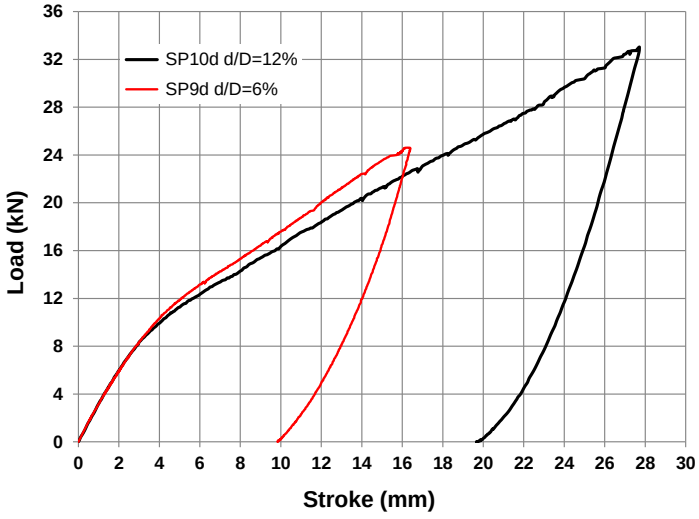

(c)

Figure 3-27: Load-Stroke curves during denting procedure, for specimens (a) SP1d and SP3d(b) SP5d and SP6d and (c) SP9d and SP10d.

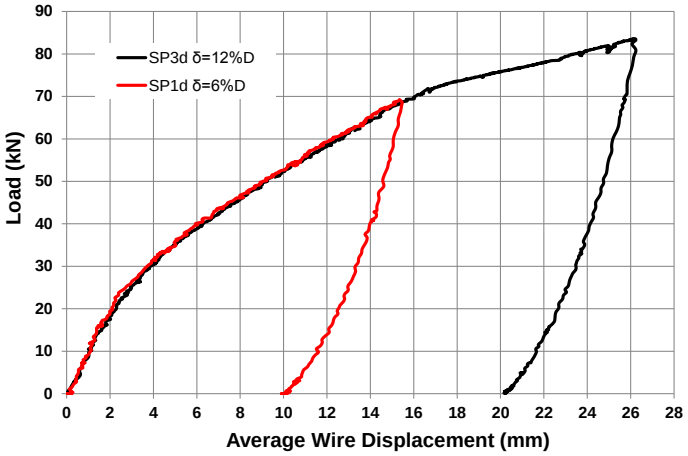

(a)

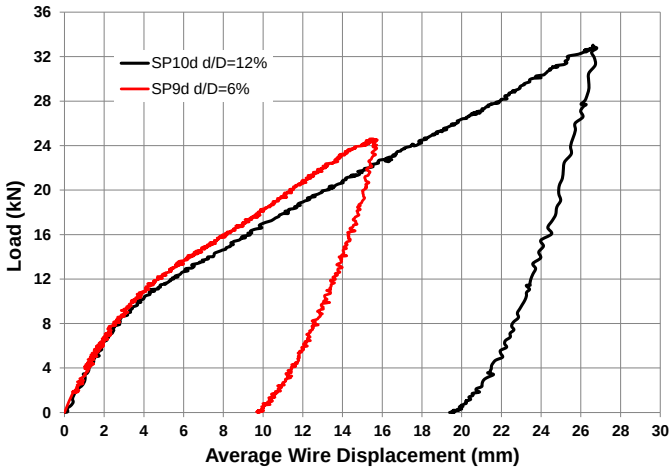

(b)

Figure 3-28: Load- Displacement curves obtained from LVDT's recording during denting (a) SP1d in comparison with SP3d and (b) SP9d in comparison with SP10d

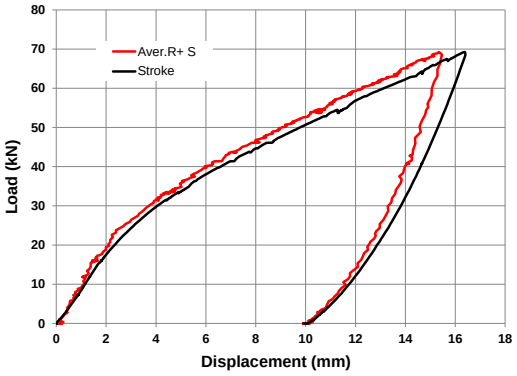

(a)

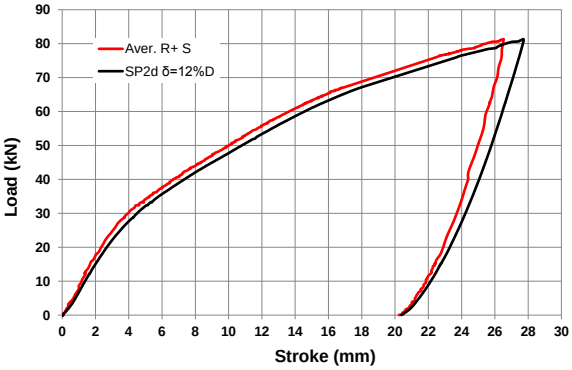

(b)

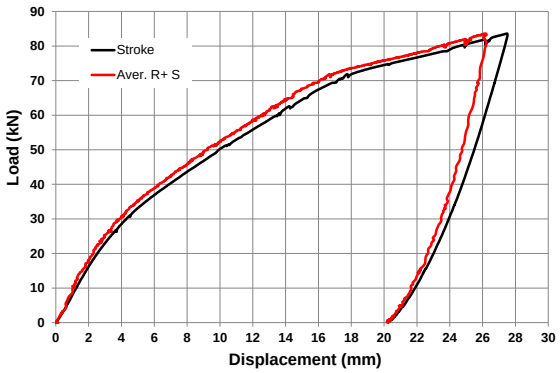

(c)

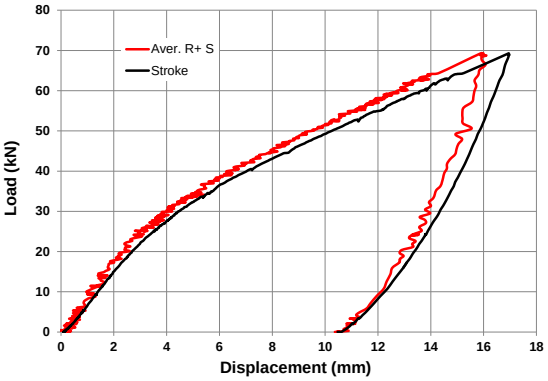

(d)

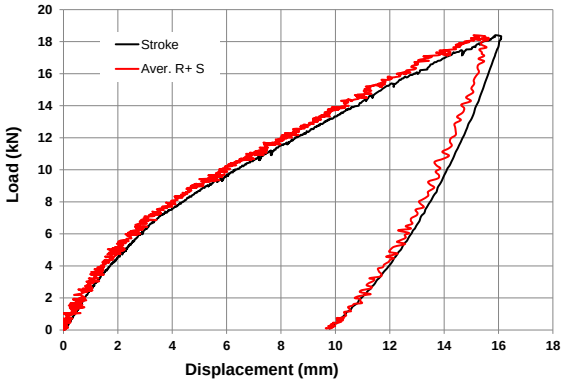

(e)

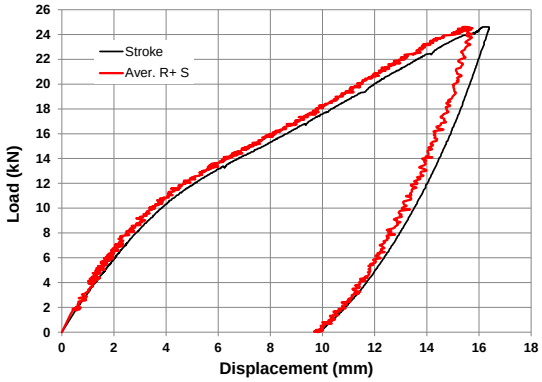

(f)

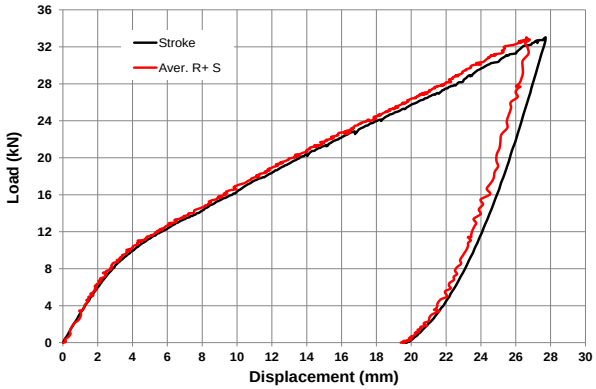

(g)

Figure 3-29: Load-stroke curves during denting procedure in comprison with load-displacement curves of LVDT's, for specimens (a) SP1d, (b) SP2d, (c) SP3d (d) SP4d, (e) SP7d, (f) SP9d and (g) SP10d specimens

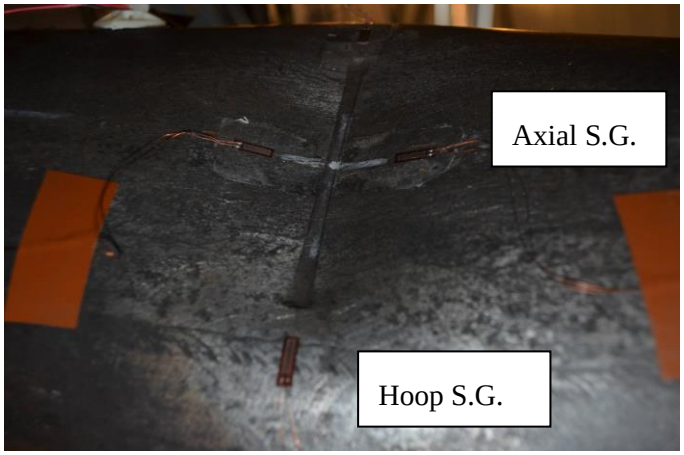

Figure 3-30: Denting region of SP5d specimen after load removal

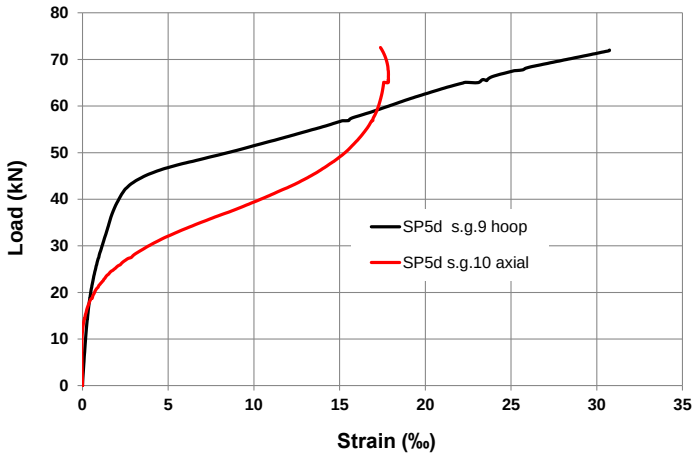

(a)

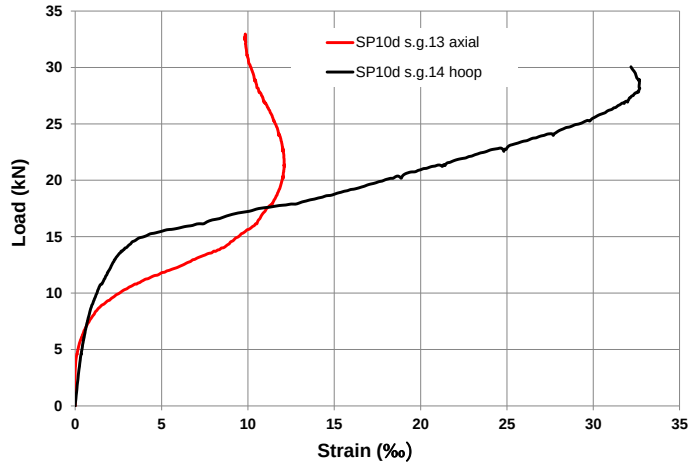

(b)

Figure 3-31: Longitudinal and hoop strain distribution during denting for specimens (a) SP5d and (b) SP10d (d/D= 12%).

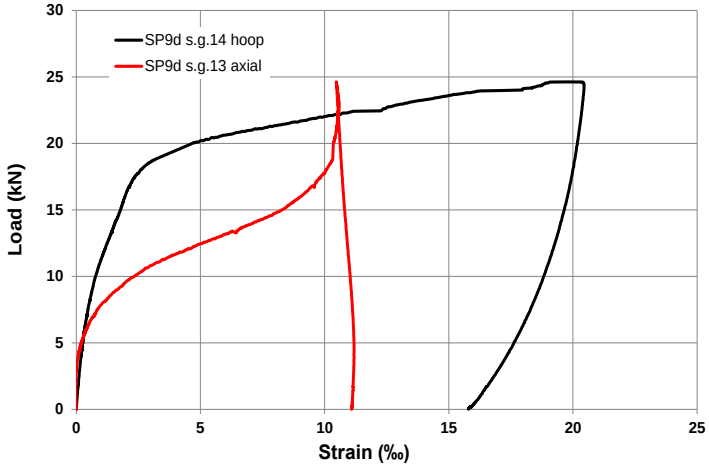

Figure 3-32: Longitudinal and hoop strain distribution during denting for specimen SP9d (d/D= 6%).

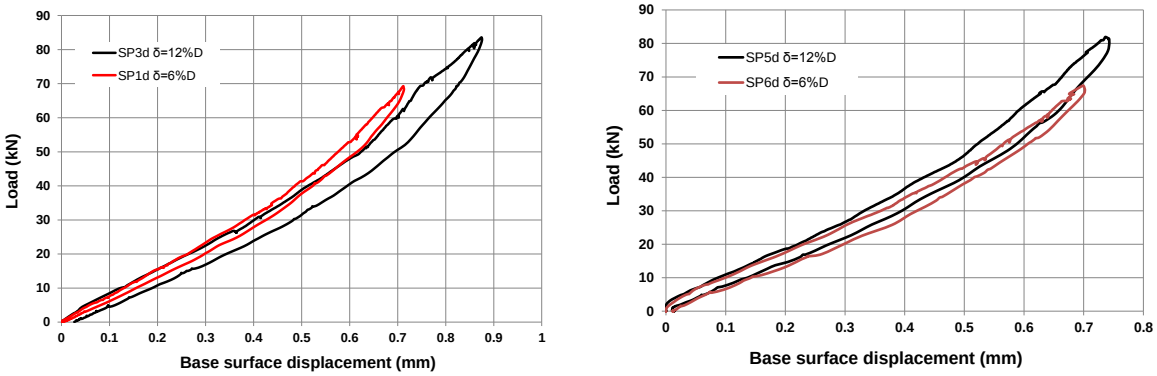

(a) (b)

Figure 3-33: Load vs Displacement curves of the wooden base top surface during denting of (a) SP3d and SP1d and (b) SP3d and SP1d.

3.6.2 Cyclic bending results on dented specimens

After denting six (6) dented pipe specimens (SP1d, SP3d, SP5d, SP6d, SP9d and SP10d), these pipes were subjected to cyclic four-point bending using the set-up described earlier (Figure 3-18) , and a displacement-controlled pattern. The results are summarized in Table 4.

The loading sequence followed in dented specimens SP5d and SP6d is shown in Figure 3-34. Figure 3-35, represents the comparison between the corresponding load-stroke curve and load- LVDTs' displacement curve for SP5d during cyclic testing. Specimens SP5d and SP6d were first bent up to a stroke of 40mm, beyond the maximum bending load, and subsequently, were subjected to cyclic loading at two stages. During this procedure the dent was at the compression side of the specimen and the load ratio was equal to 0.1.

Furthermore, an alternative representation of the cyclic bending results is shown in Figure (Figure 3-36). In this figure moment-curvature curves for SP5d and SP6d specimens are shown. For the computation of the bending moment and curvature values, the displacement recorded from LVDT's was taken into account. In addition, in order to compute the global curvature of each specimen from the test data, the auxiliary pipe members of the test set-up. The moment and curvature values are normalized with the values $M_0 = \sigma_y D_m^2 t$ and $k_0 = \frac{t}{D_m^2}$, respectively, where σ_y refers to the yield stress of the material equal to 364 MPa, D_m the mean diameter of the pipes and t the nominal thickness value.

Following a number of loading cycles of the bent specimens shown in Figure 3-37, each specimen failed because of fatigue crack at the dent "ridge". The number of cycles to failure is equal to 1,100 and 950 for specimens SP5d and SP6d respectively. The crack configuration for specimen SP5d is shown in Figure 3-38.

On the other hand, specimens SP1d and SP3d were subjected to a different cyclic bending pattern, shown in Figure 3-39 and Figure 3-40, respectively. Both specimens were bent beyond the limit bending load [dent in compression]. Subsequently reverse bending was applied, so that the dented region is under tension, whereas the opposite region of the pipe is in compression. This loading situation results in local buckling diametrically opposite side to the dent due to excessive compression (Figure 3-42 and

Figure 3-43). As shown in Figure 3-44, under cyclic loading, fatigue cracks develop at the buckle "ridge". The crack is quite similar to the one shown in Figure 3-38.

In addition, specimens SP9d and SP10d (∅ 165/3) were both subjected to bending loading up to the maximum bending load and the dent was at the compression side of the specimen. Subsequently, cyclic bending was applied with a loading ratio of about 0.1. This loading pattern was considered different from the other dented specimens. In this case, we wanted to investigate the response of the dents after the application of monotonic bending not far beyond the maximum bending load. The corresponding loading curves are shown in Figure 3-41 and a typical failure of the SP9d specimen is shown in Figure 3-45. As depicted in Table 3, specimens SP9d and SP10d failed under the application of 2300 and 125 bending cycles, respectively.

Table 4: Cyclic bending results on dented specimens

	1st Stage: Denting	**2nd Stage: Cyclic Bending**	
Dented Specimen	**d/D (%)**	**Δu(mm)**	**Nf_{tot}**
SP1d	6.08	16	1400
SP3d	12	16	1100
SP5d	12.04	13	950
SP6d	6.33	13	1100
SP9d	5.97	9	2300
SP10d	11.92	8	125

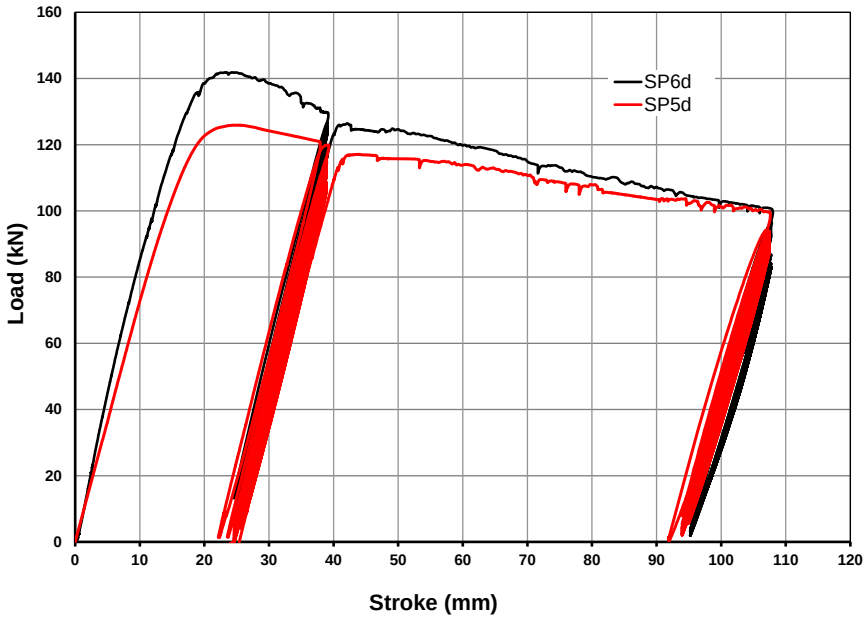

Figure 3-34: Load vs displacement curves for specimens SP5d and SP6d; monotonic and cyclic bending load.

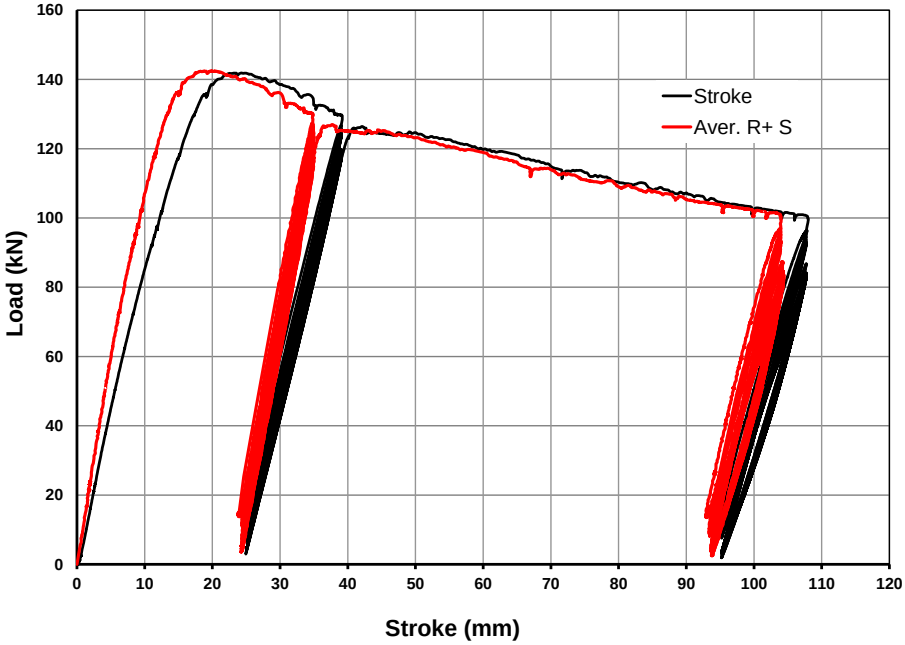

Figure 3-35: Load vs stroke curve in comparison with the load vs average LVDT's displacement curve for SP6d specimen; monotonic and cyclic bending.

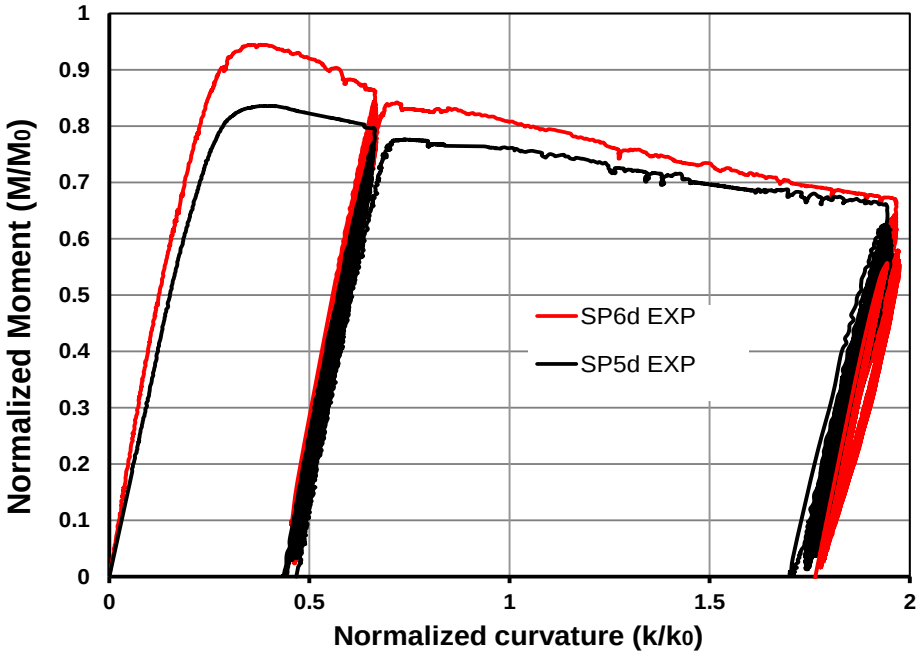

Figure 3-36: Normalized moment-curvature curves for specimens SP5d and SP6d monotonic and cyclic bending.

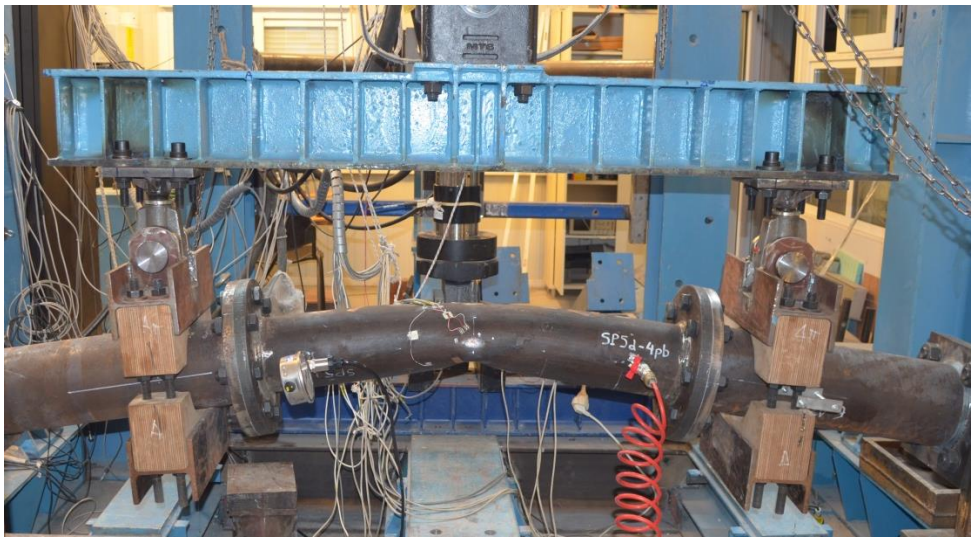

(a)

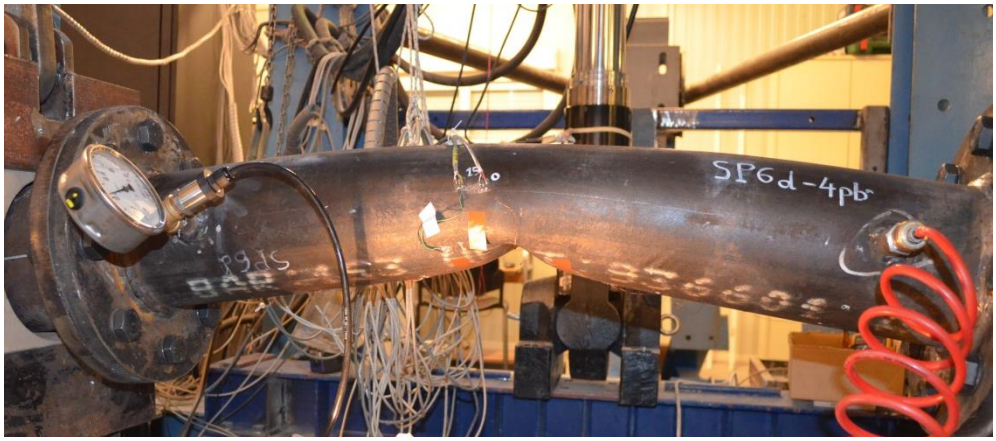

(b)

Figure 3-37: Side view of dented specimens (a) SP5dand (b) SP6d during cyclic 4-point bending.

Figure 3-38: Pipe wall rupture of specimen SP5d due to cyclic bending loading at the dent "ridge".

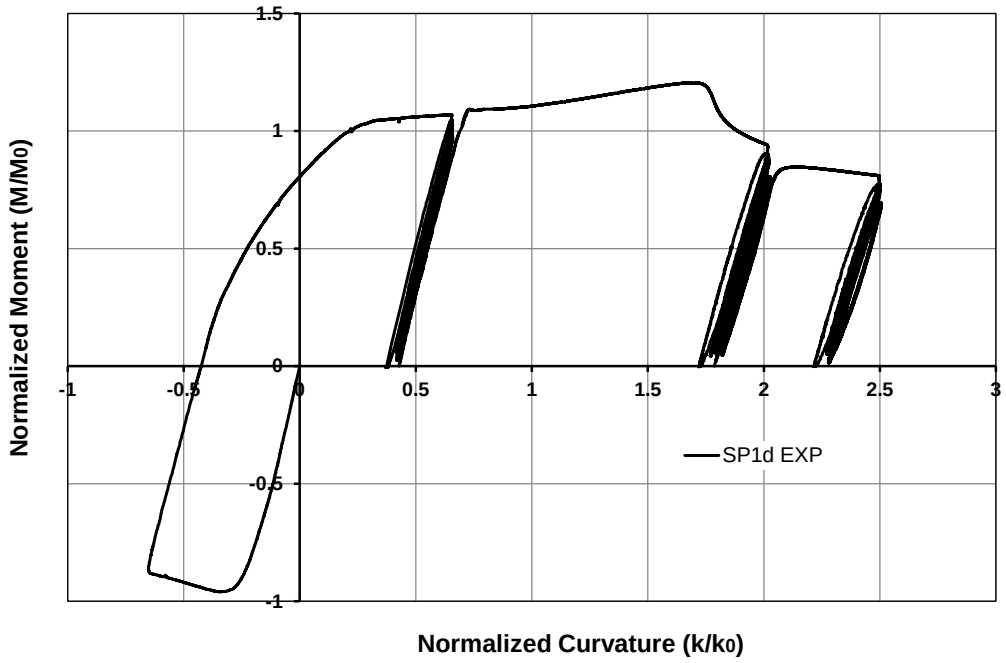

Figure 3-39: Normalized moment-curvature curve for SP1d specimen during monotonic and cyclic bending

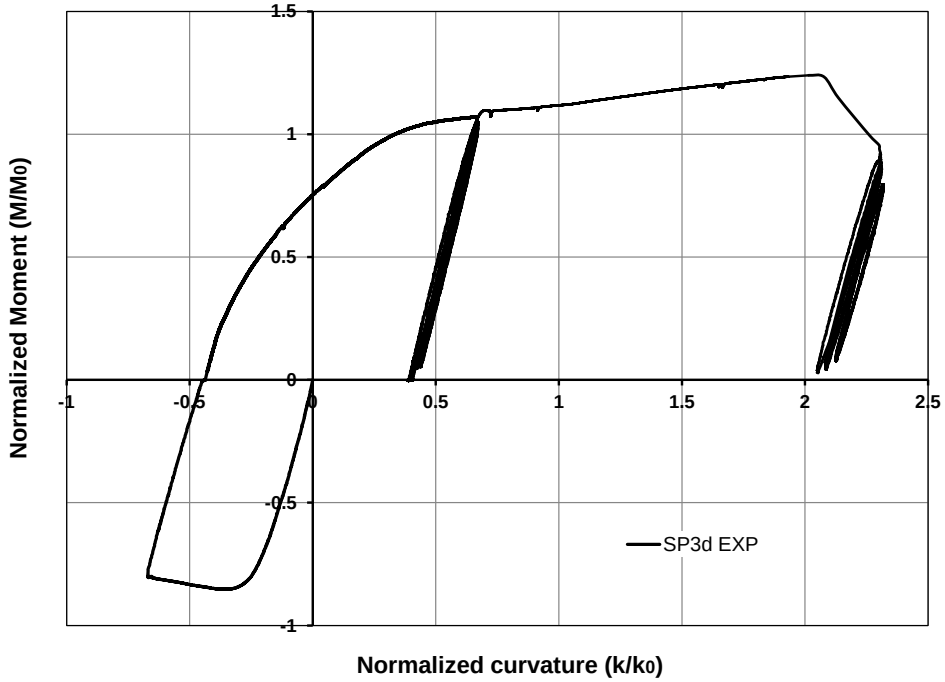

Figure 3-40 Normalized moment-curvature curve for SP3d specimen during monotonic and cyclic bending

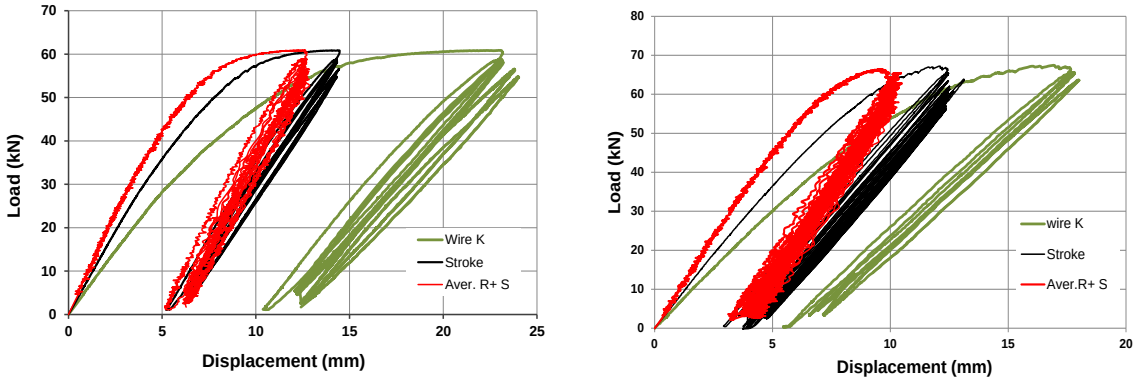

(a) (b)

Figure 3-41: Load vs displacement curves for specimens (a) SP9d-4pb and (b) SP10d-4pb; monotonic and cyclic bending load.

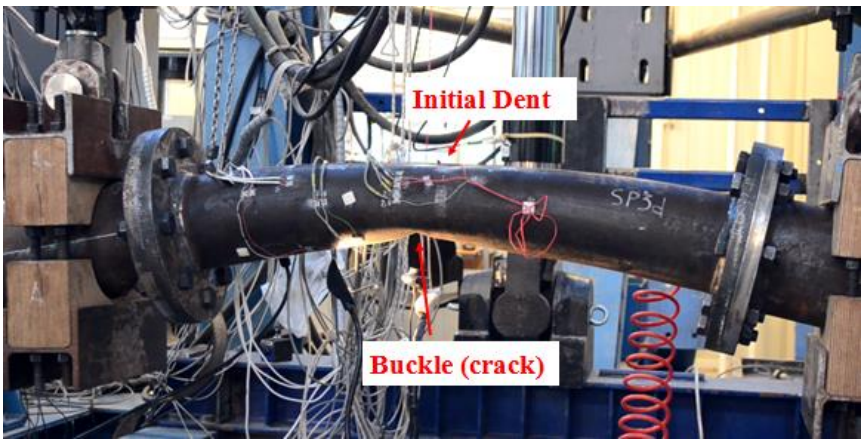

Figure 3-42: Dented specimen SP3d during monotonic and cyclic 4-point bending

(a) (b)

Figure 3-43: (a) Side view of dented specimen SP1d and (b) detail of the buckle development at the opposite of the dent during monotonic and cyclic 4-point bending

(a) (b)

Figure 3-44: Final cracks detected at the buckle "ridges" on (a) SP1d at 1400 Cycle and (b) SP3d at 1090 Cycle (3cm-long crack)

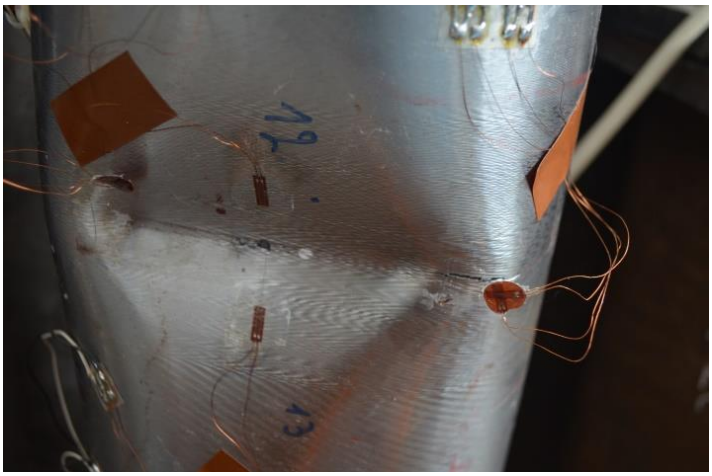

Figure 3-45: Pipe wall rupture of specimen SP9d-4pb due to cyclic bending loading at the dent "ridge".

3.6.3 Buckling of specimens

To form a buckle on the pipe wall, the specimens (SP3b-SP8b) are subjected to monotonic 4-point bending using the experimental set-up shown in Figure 3-19. Monotonic bending is applied into the post buckling regime until the desired size of buckle is developed on the compressive side of the specimen. The level of buckling is defined from the ratio of P_b/ P_m, where P_b value refers to the predefined load level reached on the post buckling brunch and P_m is the maximum load sustained by the specimen. Three levels of buckle have been investigated corresponding to P_b/ P_m ratios equal to 0.55, 0.65 and 0.75.

The loading sequence for SP3b-SP8b specimens during buckling development and cyclic loading are shown in Figure 3-46 in terms of load-stroke curves. From Figure 3-46, it is shown that each specimen exhibits different buckling and post-buckling behavior. This is mostly attributed to the fact that buckling capacity of thin pipes is rather sensitive in thickness variations and the presence of initial imperfections produced during the machining of specimens.

Furthermore, the displacements measured via wire transducers are recorded and compared with the stroke applied through the actuator for specimens SP4b-SP8b, as shown in Figure 3-47. Wire K was located in order to measure the movement of the central pipe section during monotonic and cyclic bending, while wires R and S were placed in order to measure the movement of the pipe configuration at the location of the wooden grips. During monotonic bending, strain values are recorded from the strain gauges which were instrumented at several points and critical regions along the pipe wall (Figure 3-48). Moreover, tensile and compressive axial strain values in the central cross-section are obtained. Figure 3-49 shows the maximum tensile and compressive axial strain values obtained from specific points located diametrically opposite around the central cross section of the SP4b specimen during monotonic bending.

The graphs in Figure 3-49 show that the axial tensile strain values follow the trend of load-displacement curves, while the curve corresponding to the strain values in the compressive region, changes abruptly due to local buckle development of the local buckle in the compressive side and the formation of the wrinkling pattern.

For all specimens, a local buckle is developed after the formation of uniform wrinkles in the compression side of the pipe specimen (Figure 3-50a). With increasing applied load, compressive strains also increase, resulting in the localization of damage, producing a non-symmetric buckle (Figure 3-50b).

Table 5: Experimental Results for buckled specimen - Monotonic bending

	1st Stage: Buckling Development				**2nd Stage:**
Buckled Specimen	**P_m (kN)**	**P_b/P_m**	**δ_m (mm)**	**δ_b-δ_m (mm)**	**Type of loading**
SP3b	80.59	0.50	17.8	54.5	4-Point Bending
SP4b	66.67	0.50	15.2	43.8	
SP5b	79.4	0.75	30	6.4	
SP6b	78.4	0.65	18.2	19.8	
SP7b	89.25	0.55	34.53	36.9	Pressure
SP8b	91.40	0.75	43.53	7.58	

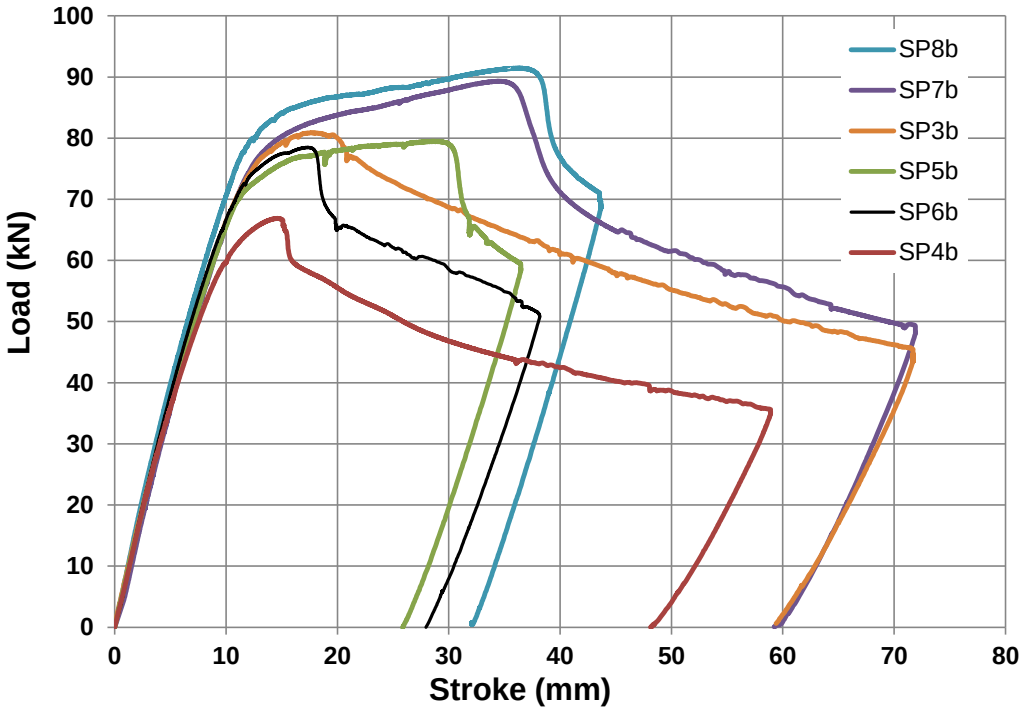

Figure 3-46: Monotonic bending of specimens SP3b-SP8b; Load vs Stroke curves

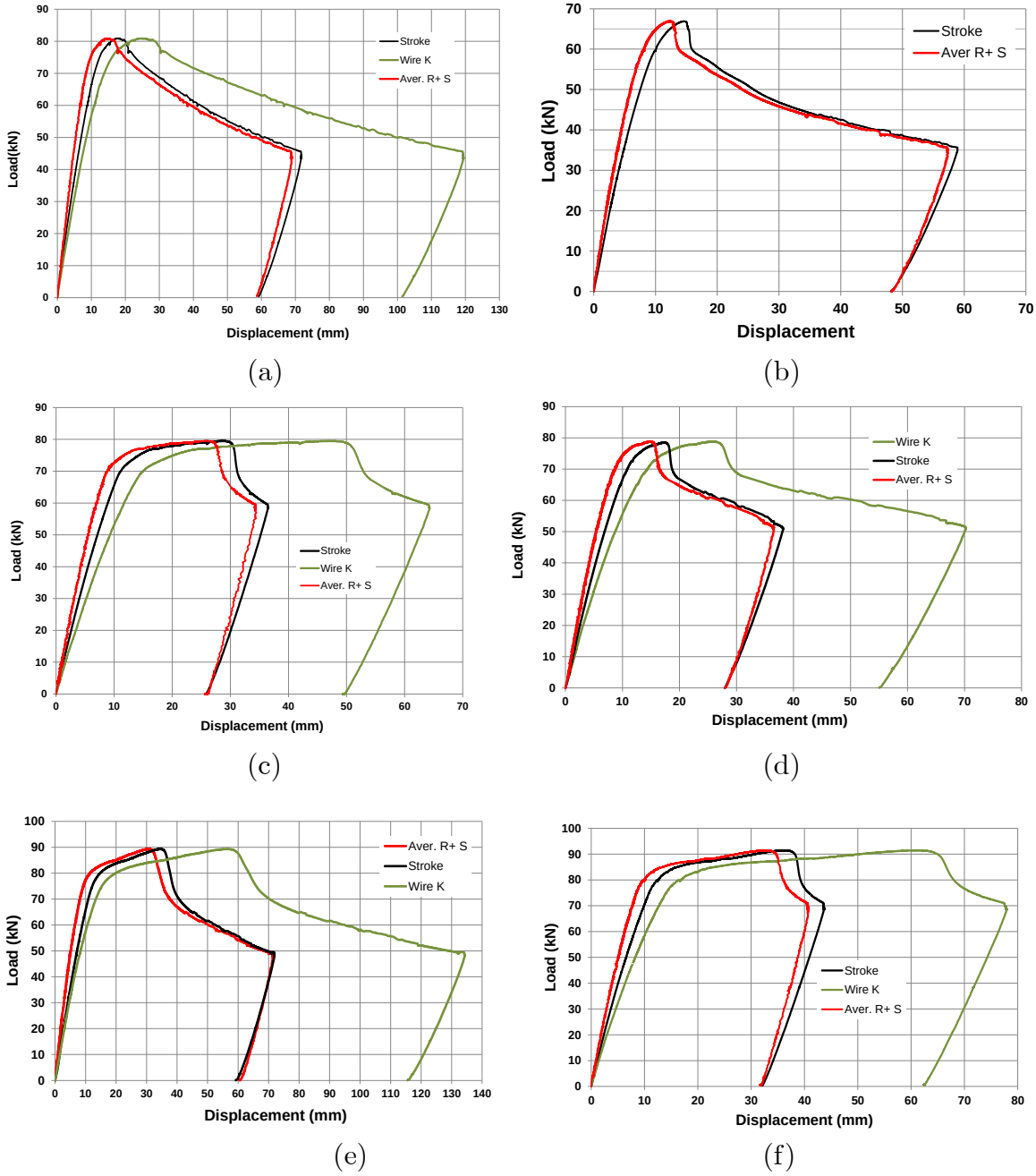

Figure 3-47: Monotonic bending of specimens (a) SP3b, (b) SP4b, (c) SP5b, (d) SP6b, (e)SP7b and (f) SP8b; Load vs Stroke curves in comparison with load vs LVDT's displacement curves

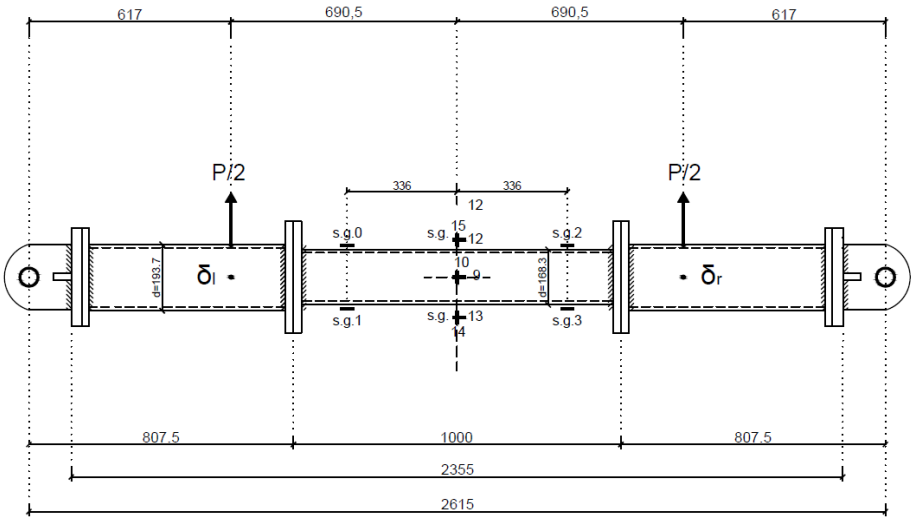

Figure 3-48: Strain gauges instrumentation of specimen SP6b for the monotonic bending tests.

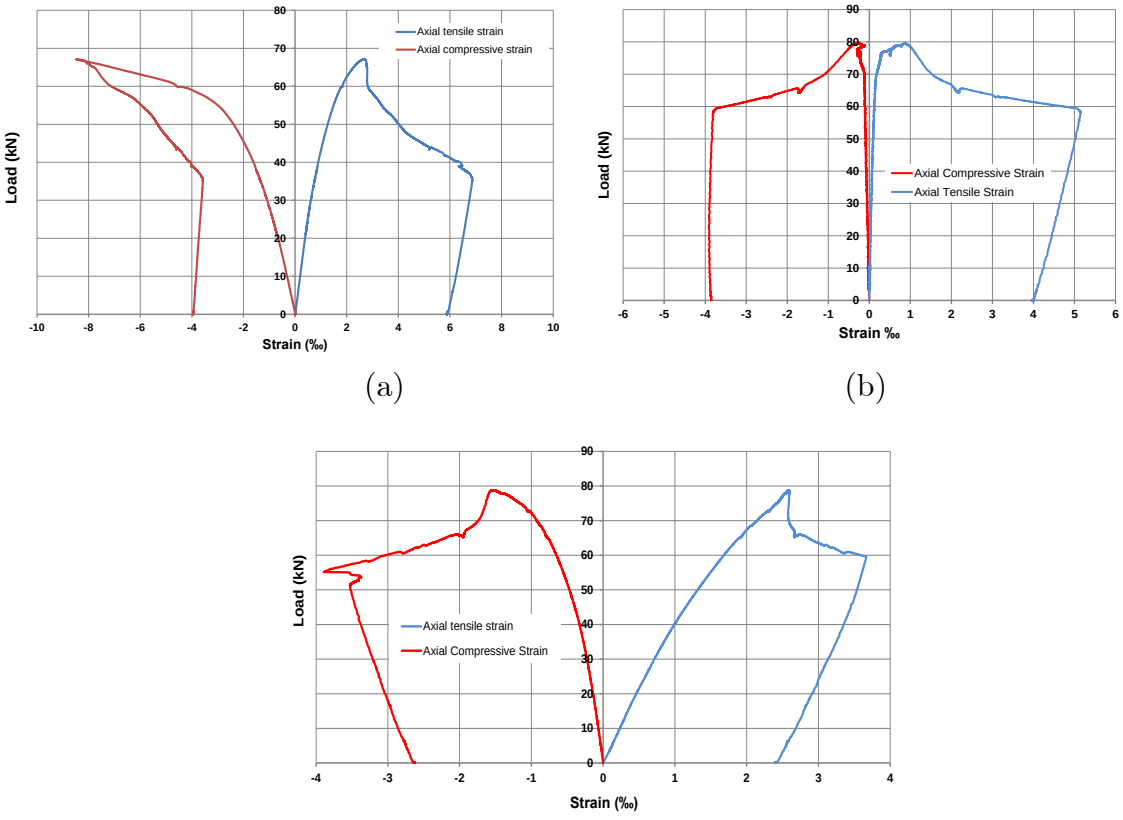

Figure 3-49: Strain evolution in terms of load during monotonic bending; (a) specimen SP4b, (b) SP5b and (c) SP6b

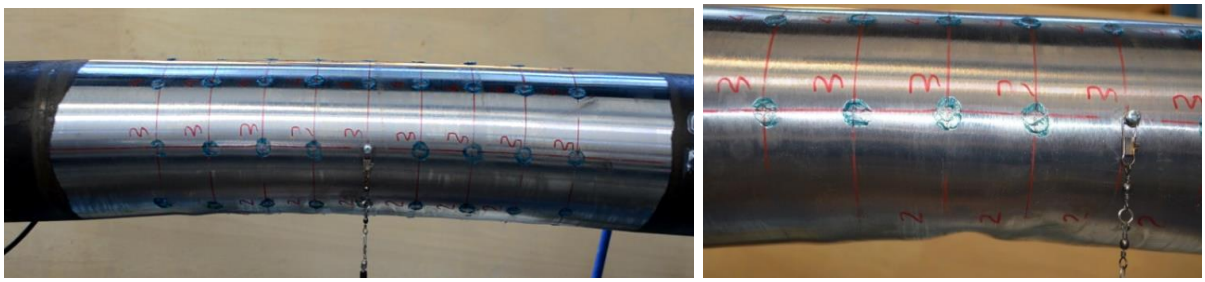

(a) (b)

Figure 3-50: (a) Initial uniform wrinkling and (b) wrinkling localization upon buckle development during monotonic bending; SP8b specimen

The final buckled shapes of the specimens before the application of cyclic bending are shown in Figure 3-51. In particular, Figure 3-51c, shows that specimen SP6b buckled almost exactly at the mdspan. For the most cases of pipe specimens the buckling pattern consisted of a diamond-type shape with one major and two minor buckles on each side of the bending plane, as shown clearly in Figure 3-52b. On the other hand, the buckled mode of specimens SP5b and SP8b, consisted of two main buckles perpendicular to the pipe main axis on each side of the bending plane (Figure 3-52c).

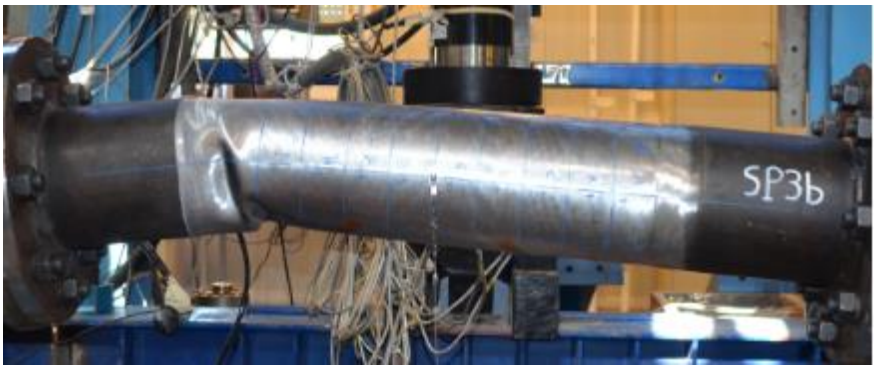

(a)

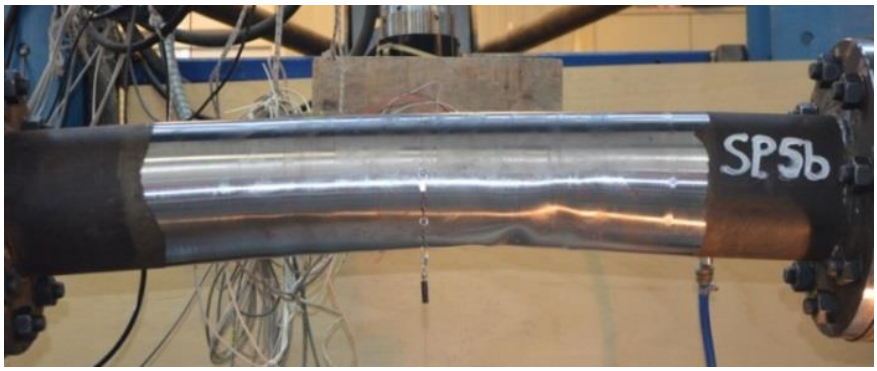

(b)

(c)

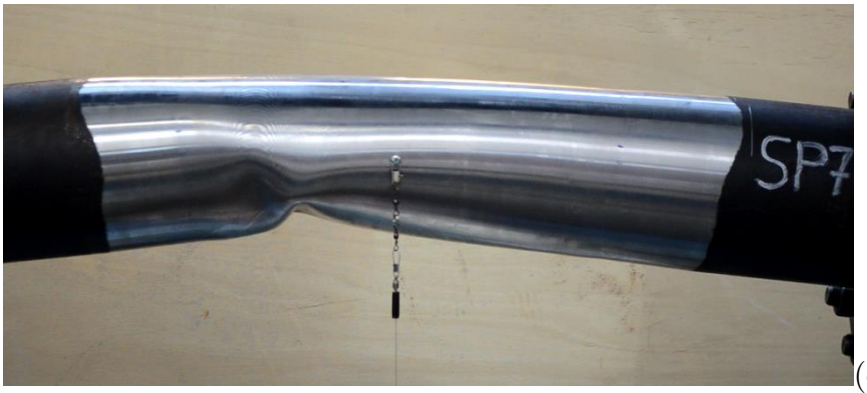

(d)

Figure 3-51: Side views of buckled specimens (a) SP3b, (b) SP5b, (c) SP6b and (d) SP7b buckled specimens.

Figure 3-52: Detail of the non-symmetric buckle for (a) SP3b, (b) SP4b and (c) SP5b (d) SP6b (e) SP7b and (f) SP8b specimens.

3.6.4 Cyclic bending results on buckled specimens

After the formation of a smooth buckle (of different levels) on specimens SP3b-SP6b, cyclic loading via displacement control conditions was applied (Δu equal to about 10mm) until failure. Table 6, summarizes the results on buckled specimens under consideration for both buckle development and cyclic loading. The loading sequence applied in specimens SP3b- SP6b (monotonic and cyclic) is presented in *Figure 3-53* in terms of load-stroke curves.

Table 6. Experimental Results on buckled specimen - Cyclic bending

	1st Stage: Buckling Development				**2nd Stage: Cyclic Loading**	
Buckled Specimen	**P_m (kN)**	**P_b/P_m**	**δ_m (mm)**	**δ_b-δ_m (mm)**	**Δu (mm)**	**Nf_{tot}**
SP3b	80.59	0.50	17.8	54.5	10	830
SP4b	66.67	0.50	15.2	43.8	10	590
SP5b	79.4	0.75	30	6.4	10	920
SP6b	78.4	0.65	18.2	19.8	9	200

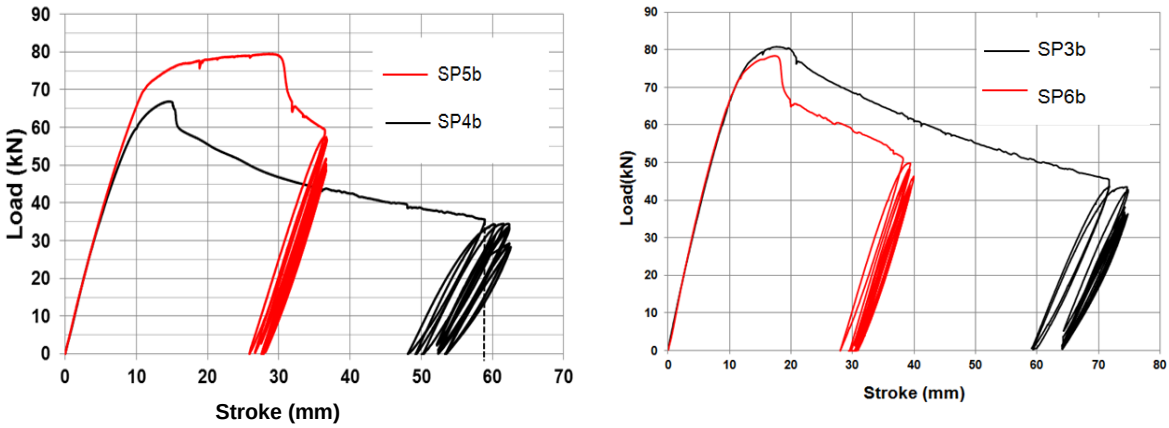

(a) (b)

Figure 3-53: The loading sequence for the specimens (a) SP4b & SP5b and (b) SP3b & SP6b under monotonic cyclic bending

Moreover, prior to cyclic testing, one tri-axial strain gauge was implemented on the critical region where a crack was most probable to occur (Figure 3-54) at the critical buckle region in order to obtain local strain values along the axial, hoop and the diagonal direction (along the direction of 45° from the axial)of the pipe during cyclic loading. Local strain variations during cyclic loading were calculated and the hysteresis loops are shown in Figure 3-55. It is observed that the hysteresis loops grow wider with the increase of the local strain accumulation resulting in fatigue cracking. Furthermore, axial strain values appear to be larger than the hoop values. More specifically, with the application of a constant amplitude of Δu equal to 10mm, an increase of the local axial strain variations ($\Delta\varepsilon_x$) is observed initiating from values of 0.05% increasing up to about 2% at failure. This, also, explains the fact that, upon cyclic loading, the cracks propagated along the hoop direction perpendicular to the pipe axis.

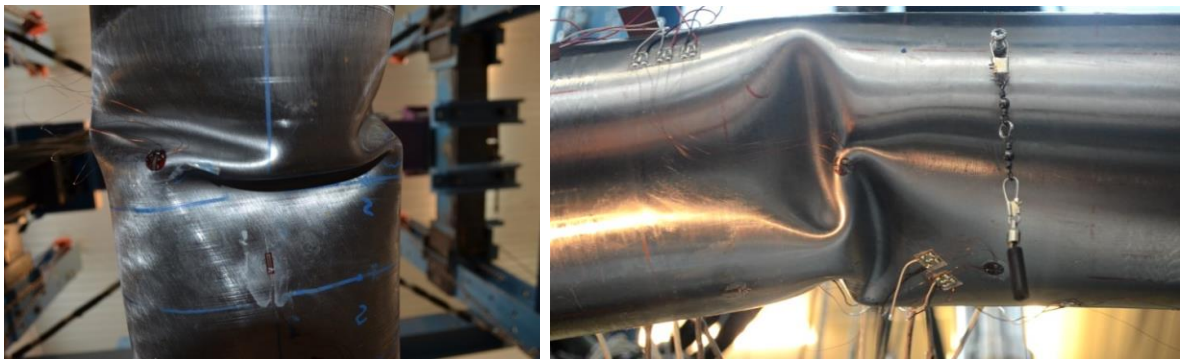

(a) (b)

Figure 3-54: Tri-axial strain gauge attached at the critical region after buckle development for (a) SP3b and (b) SP4b Specimens

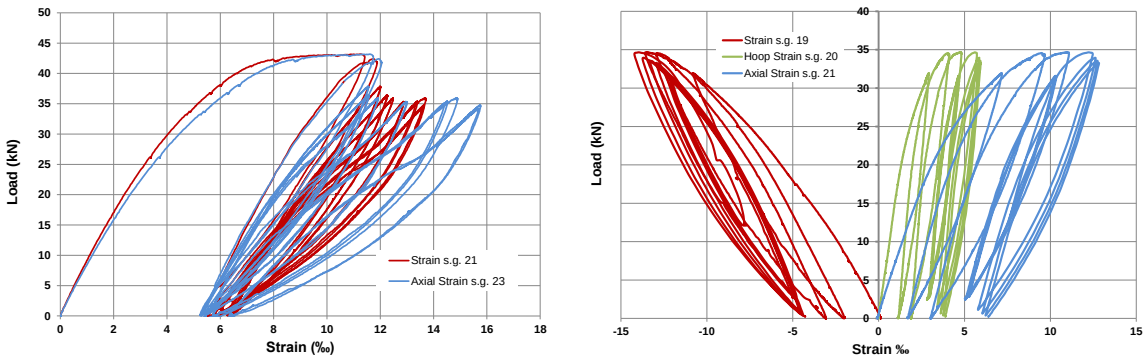

(a) (b)

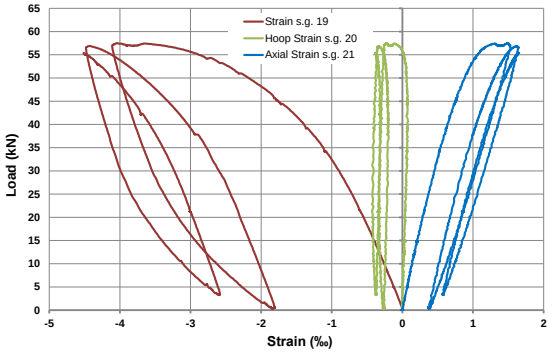

(c)

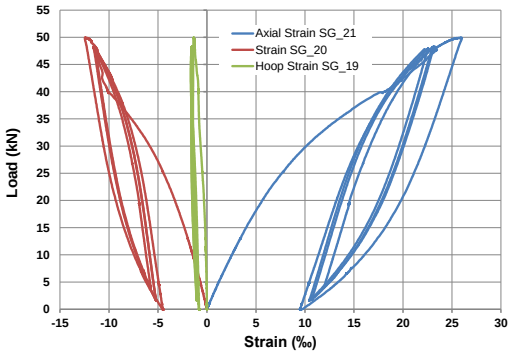

(d)

Figure 3-55: Strain variations measured on the buckle region, during cyclic loading for (a) SP3b, (b) SP4b (c) SP5b and (c) SP6b specimens.

The locations of the final cracks on the buckled specimens SP4b-SP6b are presented in Figure 3-56. It is observed that for SP5b and SP6b, the crack was initiated at the location where the tri-axial strain gauge was initially placed before the cyclic loading stage, and propagated along the hoop direction.

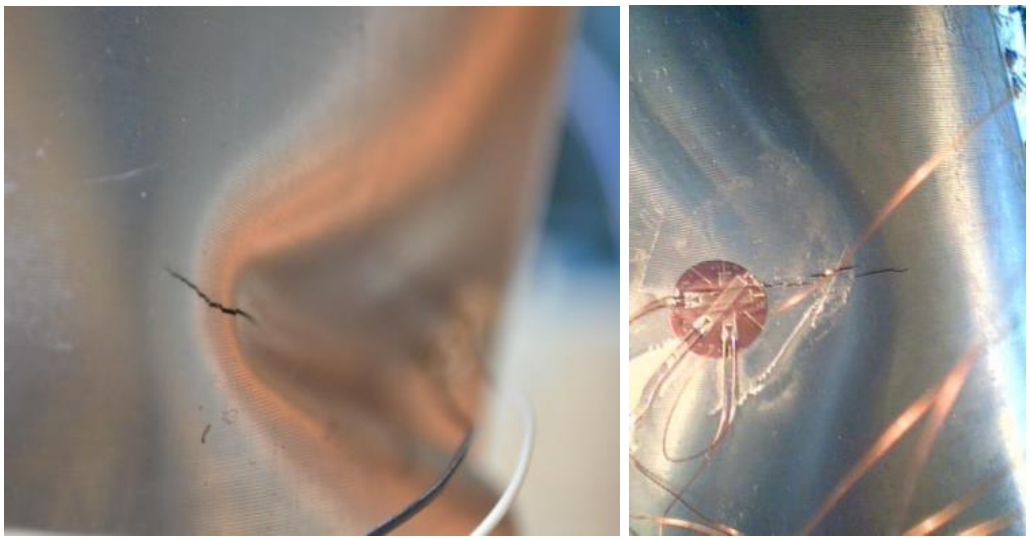

(a) (b)

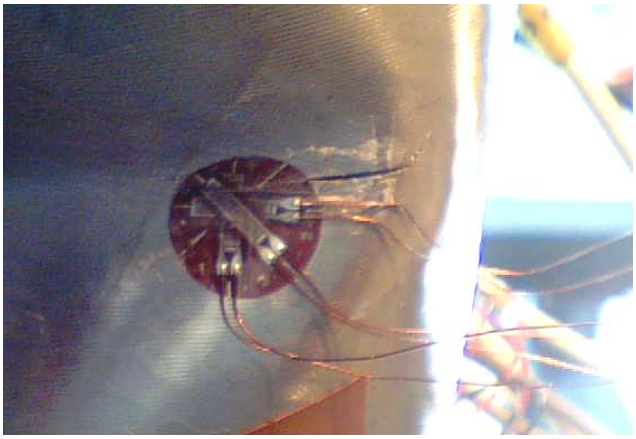

(c)

Figure 3-56: Location of final cracking; (a) SP4b and (b) SP5b and (c) SP6b specimens

3.6.5 Pressure tests results

Four (4) dented specimens, (SP2d, SP4d, SP7d and SP8d) and two (2) buckled (SP7b and SP8b) are tested under pressure loading. Internal pressure loading was applied via a 450bar water pump described in Chapter 2 .

The results refering to the dented specimens are summarized in Table 7. The specimens are subjected to 5,000 cycles of pressure loading with p_{min}=1.5MPa and p_{max} =15MPa, refering to ∅168.3/4.78 specimens and 0.92 MPa to 9.20 MPa for ∅165/3 specimens. The maximum pressure p_{max} corresponds to 72% of the nominal yield pressure σ_y equal to 20.55 MPa and 13.2 MPa for ∅168.3/4.78 and ∅165/3 specimens, respectively. Sunsequently, the specimens, are subjected to monotonically increasing pressure up to burst. No failure or damage has been detected due to cyclic loading ecxept from the SP8d specimen which was cracked at the "ridge" of the dent location at about 2500 cycles (Figure 3-57). The pressure level at which rupture occurs for the rest of the dented specimens SP2d and SP4d is 32MPa and 31.6MPa respectively. For the case of SP7d specimen, the pressure level is found from tests equal to 16.7 MPa. It is interesting to notice that these values are quite close to the theoretical values of burst pressure estimated from the following simplified formula, $p_{burst}=2\sigma_{UTS}(t_{actual}/D_{nom})$, equal to 30 MPa and 19.12 MPa for ∅168.3/4.78 and ∅165/3 specimens, respectively, where σ_{UTS} is the ultimate tensile stress. This result shows that the presence of a smooth dent on the pipe wall has no effect on the burst capacity of the pipe. In addition, rupture of the pipe wall occurred away from the dent area, as shown in Figure 3-58, which was also observed in a similar test on a buckled pipe reported by Dama et al (10).Furthermore, as shown in Figure 3-58c, the application of internal pressure resulted in a reduction of the dent size and a “smoothening” of the dented area.

Figure 3-57: Rupture ∅165/3 pipe specimen SP8d due to cyclic internal pressure; wall rupture location at the "ridge" of the dent location.

(a) (b)

(c)

Figure 3-58 (a) Detailed view, (b) side view of ruptured specimen SP2d (∅168.3/4.78) and (c) failed SP7d specimen (∅165/3) due to increased internal pressure; wall rupture location (different than the dent location)

Table 7.Pressure loading of dented specimens

Specimen	**d/D(%)**	**Δp(MPa)**	**Applied Cycles Ni**	**P_{burst} (MPa)**
SP2d	12.07	13.5	5,000	32.0
SP4d	6.10	13.5	5,000	31.6
SP7d	5.97	8.3	5,000	16.7
SP8d	12.19	8.3	2,500	--

Additionaly, the results for the two (2) buckled specimens, named as SP8b and SP7b, are tested under pressure loading similar with the case of dented specimens. The corresponding results are summarized in Table 8. Similar to specimens SP7d and SP8d, the buckled specimens, SP7b and SP8b, have been, initially, subjected to pressure cycles with minimum and maximum pressure values equal to P_{min}=0.92 MPa and P_{max}=9.20 MPa, respectively. The value P_{max} corresponds to 72% of the nominal yield pressure p_y equal 13.2 MPa.

Specimen SP7b failed after 570 pressure cycles (Figure 3-59) when fatigue cracking occurred at the buckled region. On the contrary, no failure or damage has been detected for the SP8b specimen after 5000 pressure cycles.After 5000 pressure

cycles, SP8b was subjected to monotonic internal pressure until burst. The specimen ruptured at 15.7 MPa away from the buckle area, as shown in Figure 3-60. The application of internal pressure resulted in a "smoothening" of the buckled area, as shown in Figure 3-61. It is interesting to notice that this value is somewhat lower than the theoretical value of burst pressure estimated from the simplified formula, $p_{burst}=2\sigma_{UTS}(t_{actual}/D_{nom})$, where σ_{UTS} is the ultimate tensile stress (σ_b=19.12MPa). This could be attributed to the fact that at the location of the rupture the measured thickness value of the specimen was lower than the mean measured thickness values of the specimen. This result, also, shows that the presence of a smooth buckle on the pipe wall has a rather small effect on the burst capacity of the pipe.

Table 8. Pressure loading of buckled specimens

	1st Stage: Buckling		**2nd Stage: Cyclic Pressure**		
Buckled Specimens	**P_m (kN)**	**P_b/P_m**	**ΔP (Mpa)**	**Nf_{tot}**	**P_{burst} (MPa)**
SP7b	89.25	0.55	8.3	570	--
SP8b	91.40	0.75	8.3	5000	15.7

Figure 3-59: Ruptured ∅165/3 pipe specimen (SP7b) due to cyclic internal pressure; wall rupture location at the buckle location

Figure 3-60: Rupture of SP8b specimen, away from the buckled area

Figure 3-61: Buckled specimen SP7b: (a) buckle region prior to pressure application and (b) after cyclic internal pressure

Furthermore, two perfect tube specimens have been tested under burst pressure. The geometry of the first specimen is similar with the ∅165/3 pipe specimens, while the second is similar with the ∅ 168.3/4.78 pipes. The main difference in comparison with the rest tested specimens is that both ends of each

specimen were capped with steel caps. The perfect ∅165/3 tube failed at a level of 50 bar (5MPa) which is about the 1/4 of the theoretical value of burst pressure. As shown in Figure 3-62, the rupture occured at the one side of the pipe machined central part, close to the transition thickness zone. This "early" failure can be atributed to the fact that, with the application of internal pressure, the thickness value at the rupture region was decreased to 1mm. On the other hand the ∅ 168.3/4.78 specimen failed at a burst pressure 35MPa, which is somewhat larger than the theoretical burst value. The rupture was located at the center of the specimen.

Figure 3-62: Rupture of prerfect ∅165/3 pipe specimens;(a) thickness wall reduction at the critical region and (b) the location of the rupture.

Figure 3-63: Rupture of perfect ∅ 168.3/4.78 specimen

3.7 Small-Scale tests

In order to obtain reliable fatigue curves, a wide range of the full- scale tests on pipes should be performed. However, this kind of testing is expensive, time consuming and difficult to carry out, so a new small scale testing procedure has been designed and developed towards the better understanding of the cyclic response of a wrinkle.

At first, ten (10) 300mm-long and about 40mm wide longitudinal strips (Figure 3-64) were cut from pipe material X52 the same used for the full-scale pipe specimens. The bent strips were used to simulate an equal fiber along the longitudinal direction of a pipe during the formation of a severe wrinkle where the maximum strains are developed. At the 1st loading stage, the strips were bent monotonically at mid length to an angle of 90° or 120° through a 3-point bending loading configuration (Figure 3-65) at the laboratories of EBETAM S.A. and then, at the 2nd loading stage, were subjected to cyclic reverse axial loading of various amplitudes (Δu=10, 15 & 20mm) at the Laboratory of "Mechanics and Strength of Materials" of the Department of Mechanical Engineering at the University of Thessaly. Before the initiation of the 2nd loading stage, two custom-made mounts were bolted to the straight portions of the bent strips and also gripped by the machine with the help of its hydraulic grips (Figure 3-66). These loading mounts consist of pin hinges in order to allow the rotation of the straight portions of the bent strips following the upward and downward movement of the lower testing machine loading head, while the upper head remains still. As the lower machine head moved up and down, the specimen was forced opened and closed, respectively. Longitudinal strain reversals, produced during the cyclic bending, were measured at both (inner and outer) faces of the strip at the crest location, where 5mm long strain gauges where instrumented (Figure 3-67). In order to record the strain data, an independent data acquisition system was used while the axial load and stroke measurements were recorded through the machine control system. The strain values were recorded during the first 5 loading cycles due to a limitation of the recording system regarding the strain ranges specified by the system. The purpose of using two different initial values of angles was to simulate two different depths/ severity of pipe wall wrinkles. The strips were subjected to severe reverse axial loading via displacement control conditions. The stroke amplitudes applied were determined in order to investigate the

cyclic behavior and fatigue life of severe wrinkles under ultra-low cycle fatigue loading conditions.

Figure 3-64: Geometry of Strip specimens

Figure 3-65: Monotonic 3-point bending loading

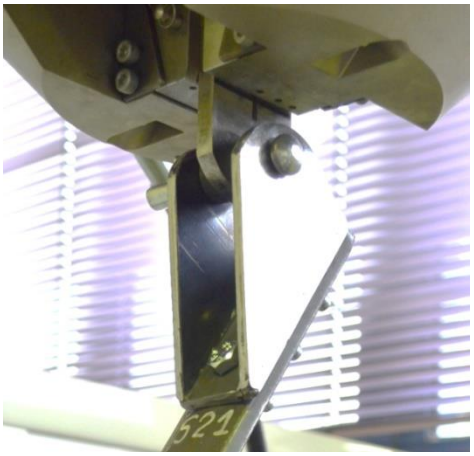

Figure 3-66: Detail of the upper hinge configuration gripped by the machine loading head

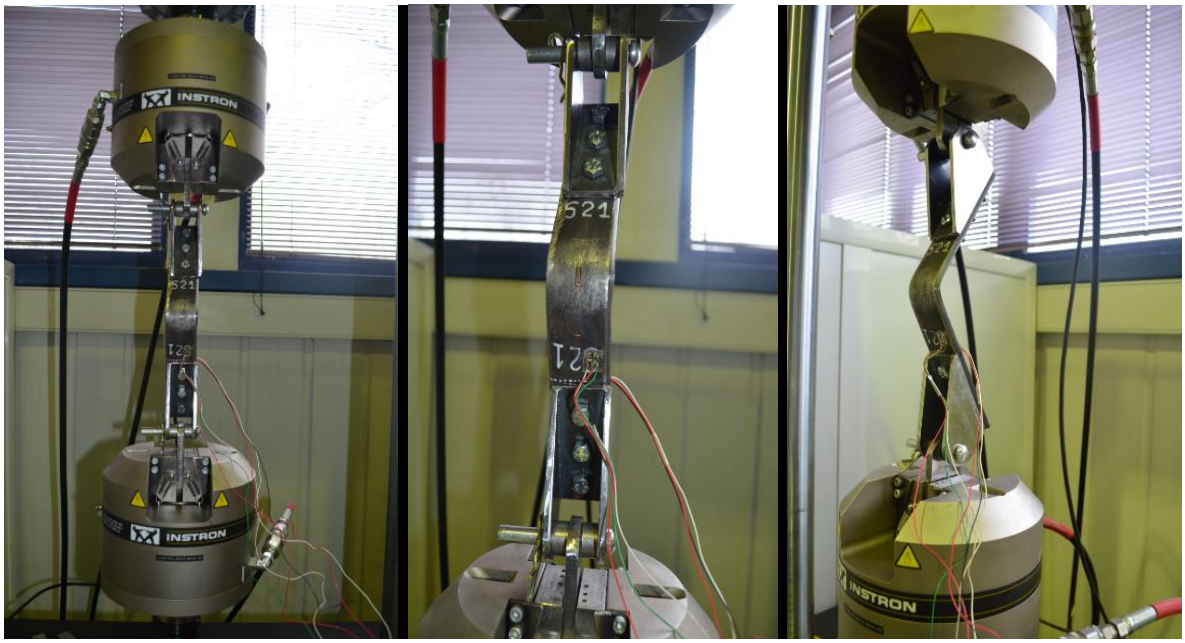

Figure 3-67: Different views of the strip - specimen instrumentation and general set-up

The results are summarized in Table 9 and represented graphically in Figure 3-68. Load vs stroke curves have been derived for each specimen (Figure 3-69and Figure 3-70) and longitudinal strain hysteresis plots have been obtained. Furthermore, comparison of load displacement curves and hysteresis loops are also shown in the following figures for different amplitudes of applied stroke and initial bent angles.

Table 9: Results of the small scale tests

Specimen	**φ (degrees)**	**Δu (mm)**	**N_f**
S11	95°	10	6743
S12	93.6°	20	515
S13	89.5°	15	1889
S15	92.8°	10	9222
S16	93.8°	15	1668
S21	114.9°	10	599
S22	112°	10	585
S23	115°	15	267
S25	114.9°	15	270
S26	117.5°	20	147

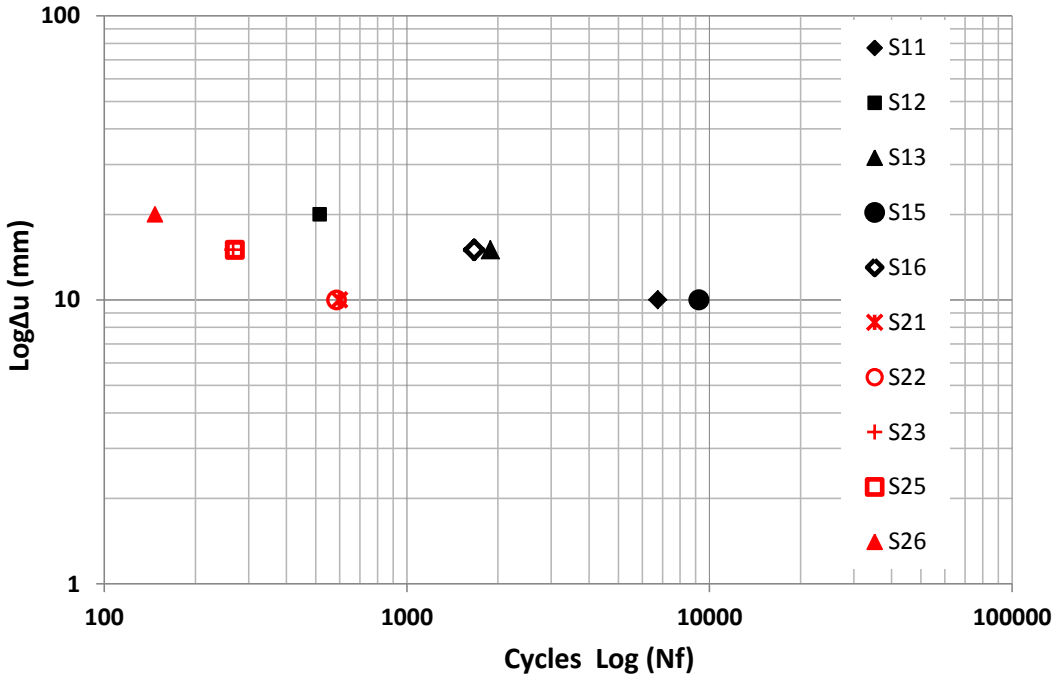

Figure 3-68: Logarithmic fatigue curves of stroke amplitude vs fatigue life

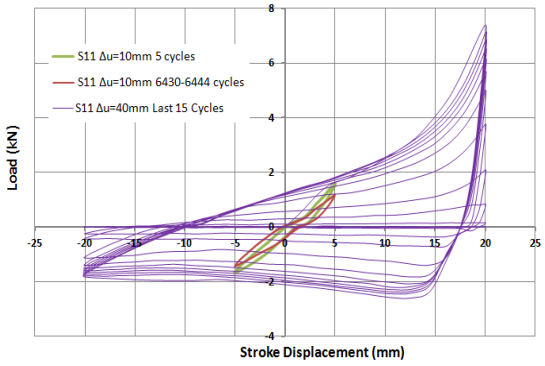

(a)

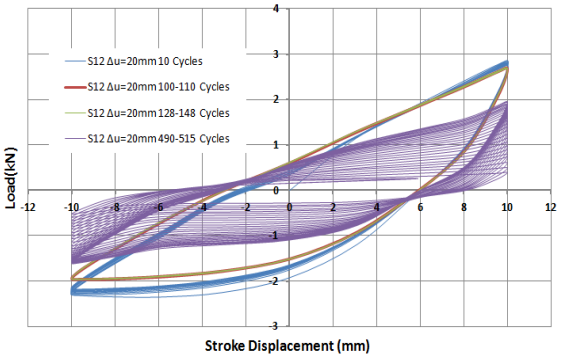

(b)

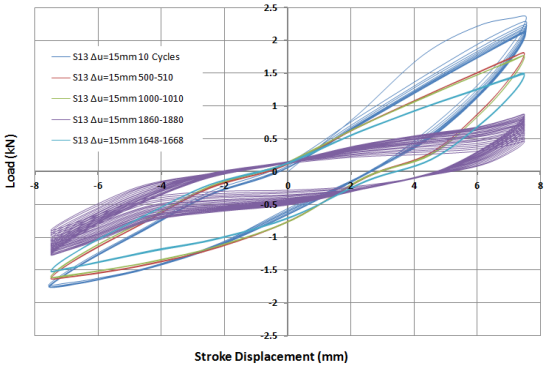

(c)

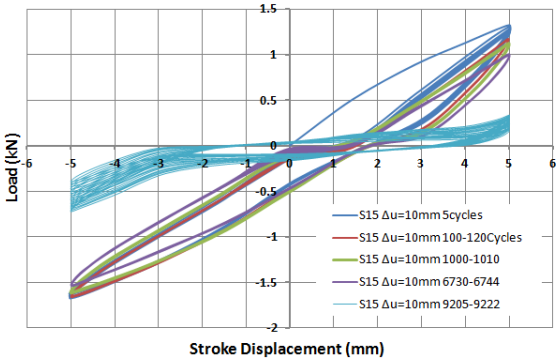

(d)

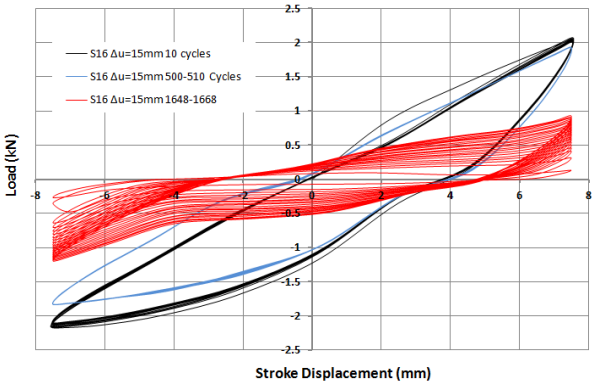

(e)

Figure 3-69: Load vs Stroke curves of the S11-S16 specimens (a)-(e) under cyclic loading

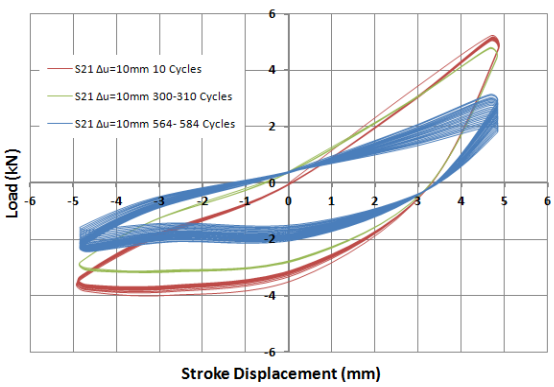

(a)

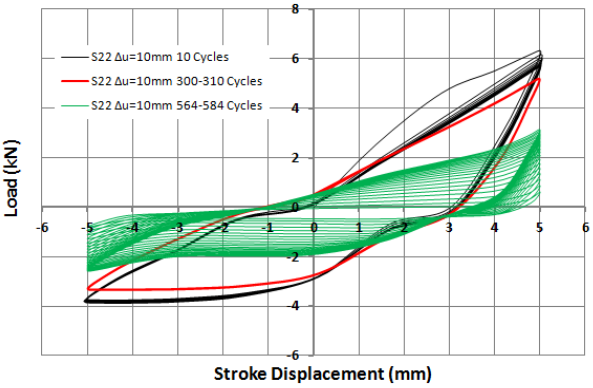

(b)

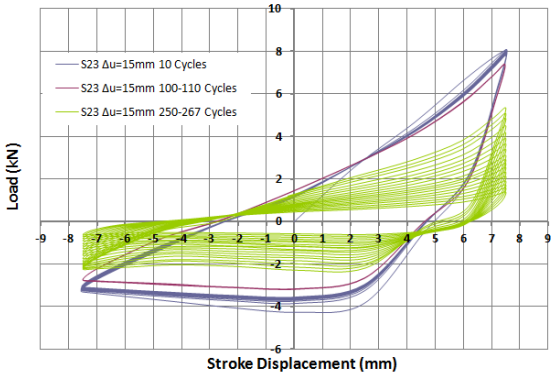

(c)

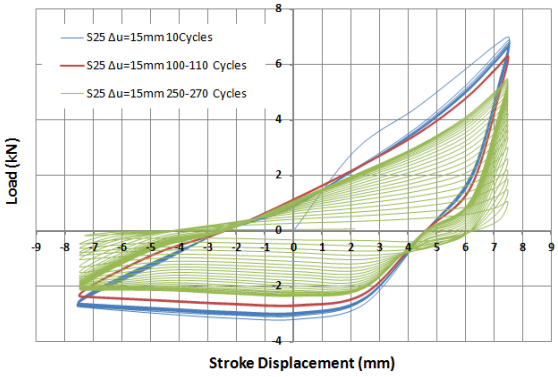

(d)

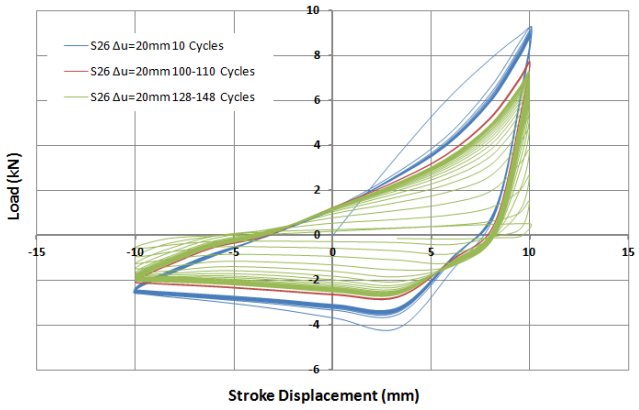

(e)

Figure 3-70: Load vs Stroke curves of the S21-S26 specimens (a)-(e) under cyclic loading

Comparison of load-displacement curves are shown for specimens with different loading amplitudes and similar bent angles (Figure 3-71-Figure 3-74). Moreover, Figure 3-75-Figure 3-77 present load displacement curves of specimens with different bent angles and similar amplitude of applied stroke.

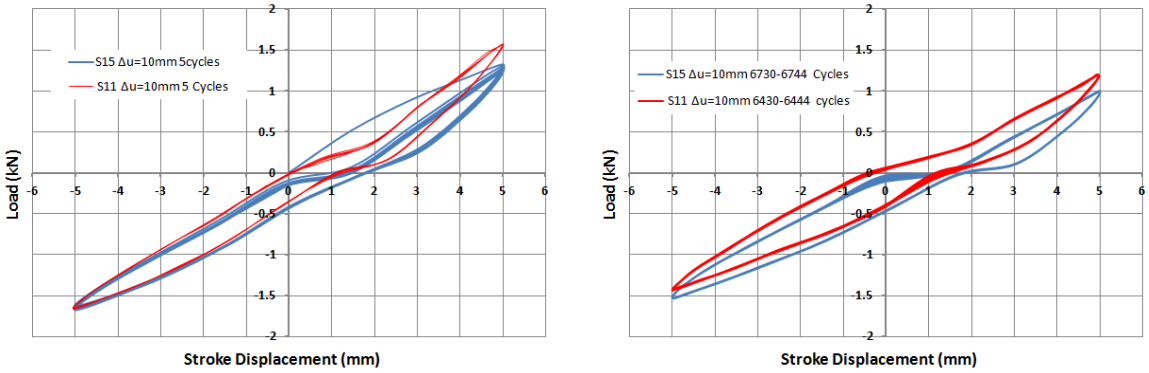

(a) (b)

Figure 3-71: Comparison of load vs stroke curves for the S11-S15 specimens during (a) the first 5 cycles and (b) during a later loading stage close to failure

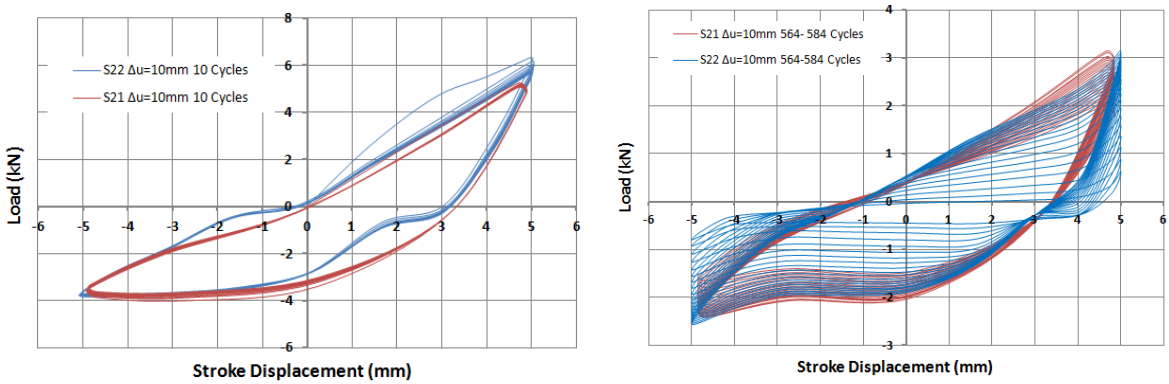

(a) (b)

Figure 3-72: Comparison of load vs stroke curves for the S21-S22 specimens during (a) the first 10 cycles and (b) during a later loading stage close to failure

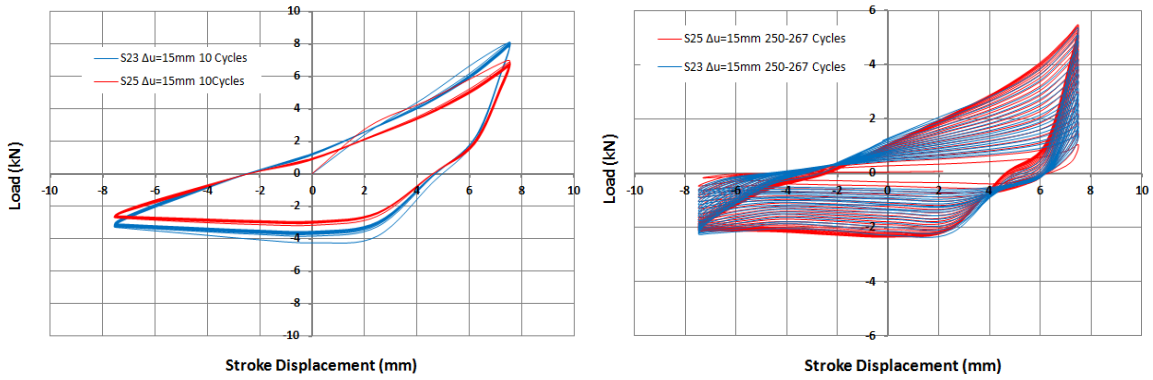

(a) (b)

Figure 3-73: Comparison of load vs stroke curves for the S23-S25 specimens (a) during the first 10 cycles and (b) during a later loading stage close to failure.

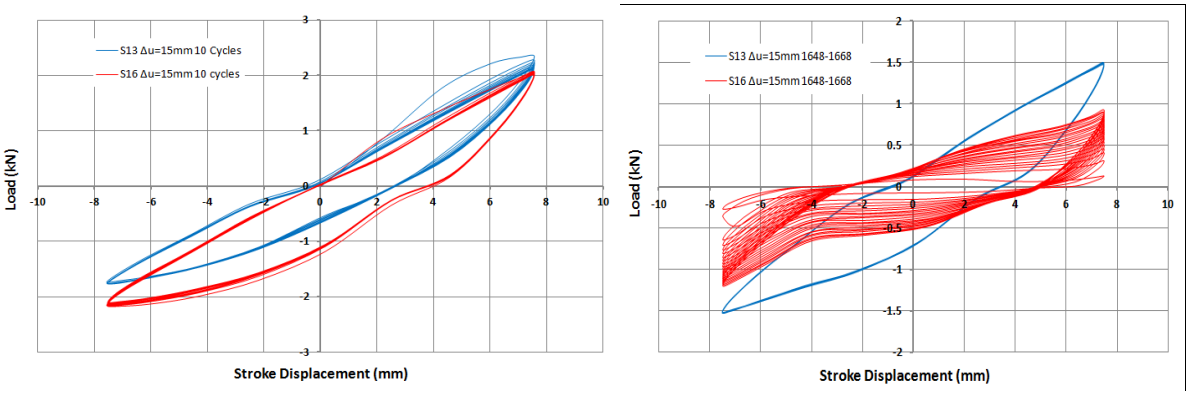

(a) (b)

Figure 3-74: Comparison of load vs stroke curves for the S13-S16 specimens (a) during the first 10 cycles and (b) during a later loading stage

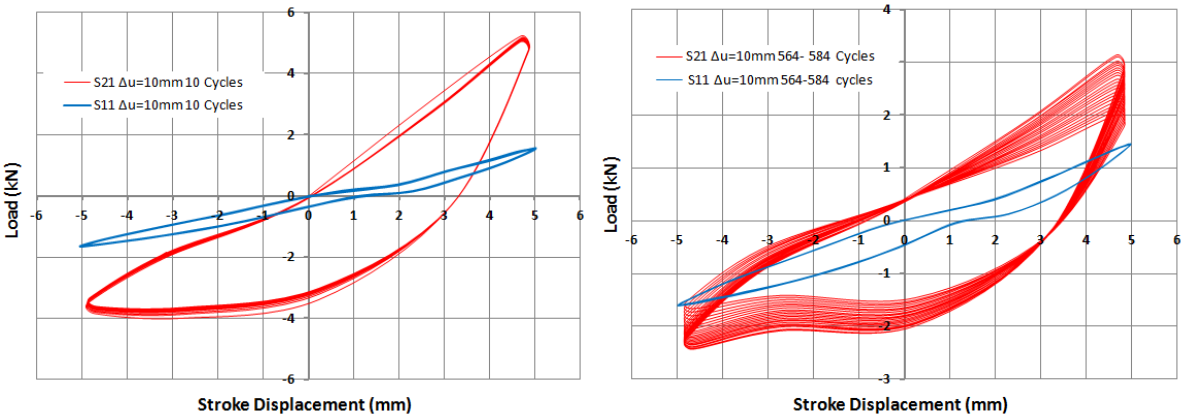

(a) (b)

Figure 3-75: Comparison of load vs stroke curves for the S11-S21 specimens (a) during the first 10 cycles and (b) during a later loading stage

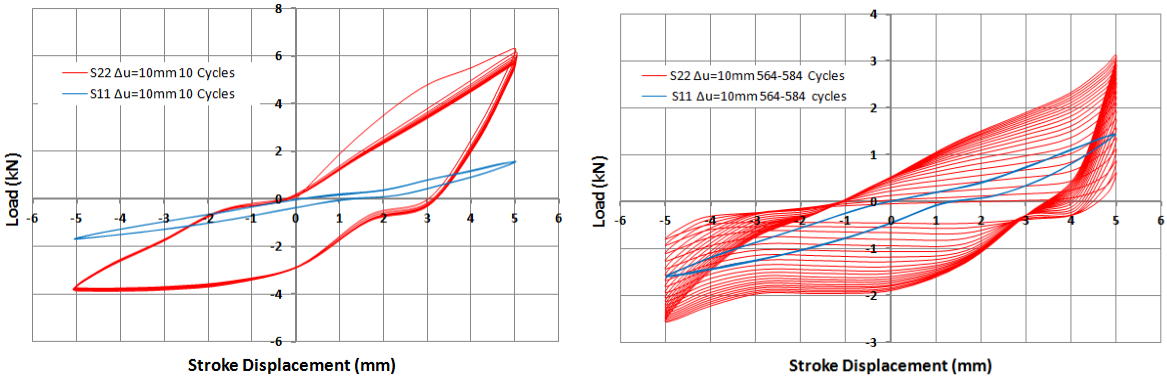

(a) (b)

Figure 3-76: Comparison of load vs stroke curves for the S11-S22 specimens (a) during the first 10 cycles and (b) during a later loading stage

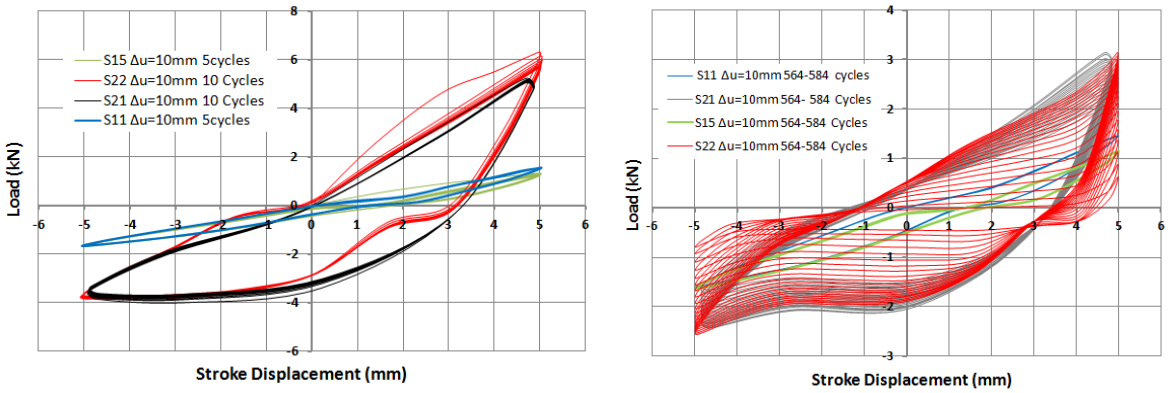

(a) (b)

Figure 3-77: Comparison of load vs stroke curves for the S11-S15 & S21-S22 specimens (a) during the first cycles and (b) during a later loading stage

Furthermore, the evolution of the peak load of each loading cycle has been identified for each specimen. In Figure 3-78 the peak-load for every loading cycle is represented for specimen S11.

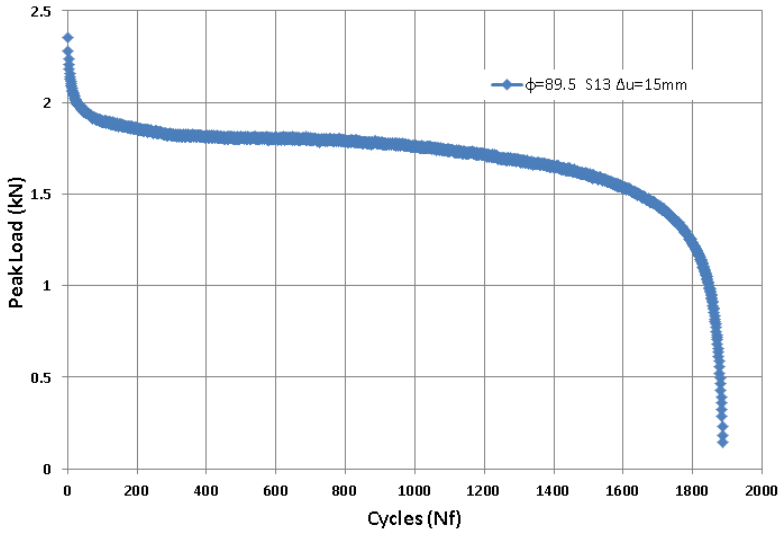

Figure 3-78: The descending path of the peak load values during the application of cyclic loading for S13 specimen.

In conclusion, after the completion of the small-scale tests two main observations should be made about the fatigue life and the crack development process:

1) Greater strain ranges are developed at the crest of the strips that were bent up to a 120° angle and as a result they exhibit lower fatigue life than the ones bent up to a 90° angle. This is also verified by the fatigue analysis reported in Chapter 5.

2) In Figure 3-78, it can be seen that the peak load per cycle is abruptly decreased due to material softening within the first 50-100 cycles, while after 1600 cycles the peak load per cycle decreases abruptly indicating that a crack has been initiated. More specifically, two cracks have been initiated the first at the inner and the second at the outer face of the strip, along the transverse direction with respect to the axial axis of the bent- strip. Upon cyclic loading the cracks start to propagate from both surfaces of the strip towards the center of the strip thickness until each strip specimen is cut symmetrically at the mid-length.

Upon the application of cyclic loading (tensile and compressive), the values of longitudinal strains have been recorded at the crest location. Strain hysteresis plots are presented for specimens S11 and S15 under imposed stroke range, Δu, equal to 10mm as shown in Figure 3-79 -Figure 3-80. The final crack is shown indicatively for the specimen S21 in Figure 3-81.

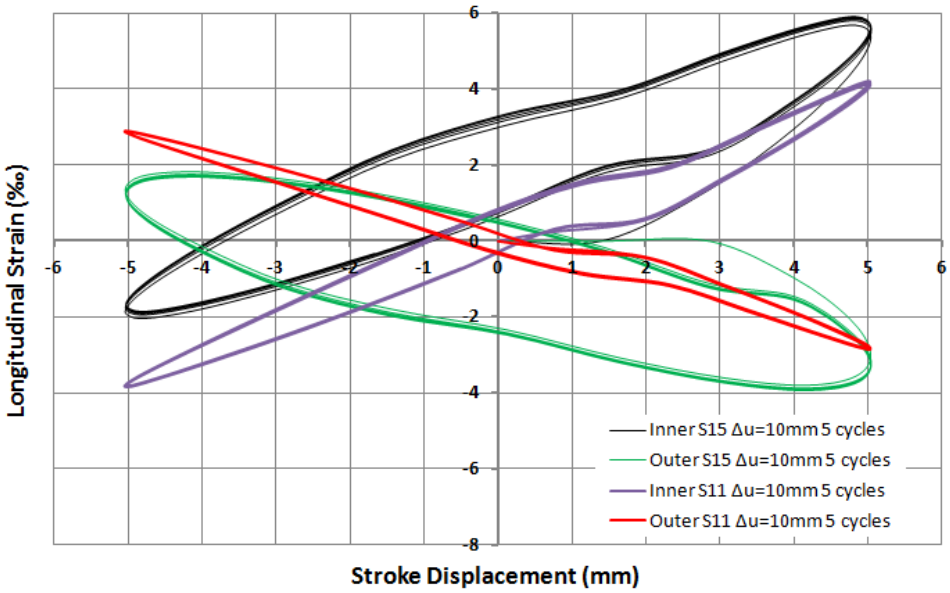

Figure 3-79: "Local strain vs stroke displacement" curves for S11 and S15 during the first 5 loading cycles (Δu=10mm)

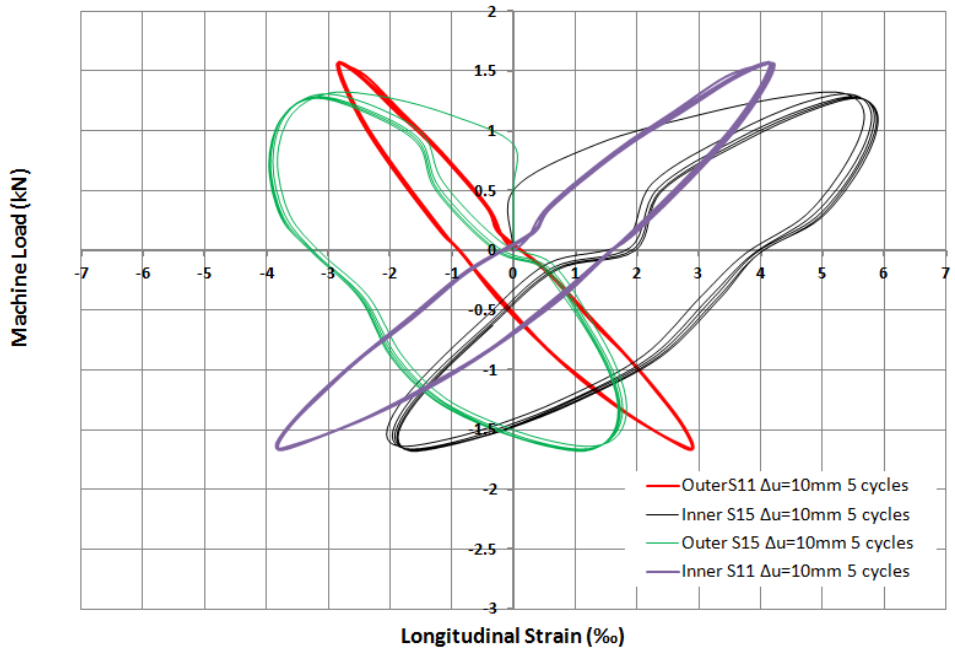

Figure 3-80: Load vs strain curves for the S11 and S15 specimens during the first 5 loading cycles (Δu=10mm)

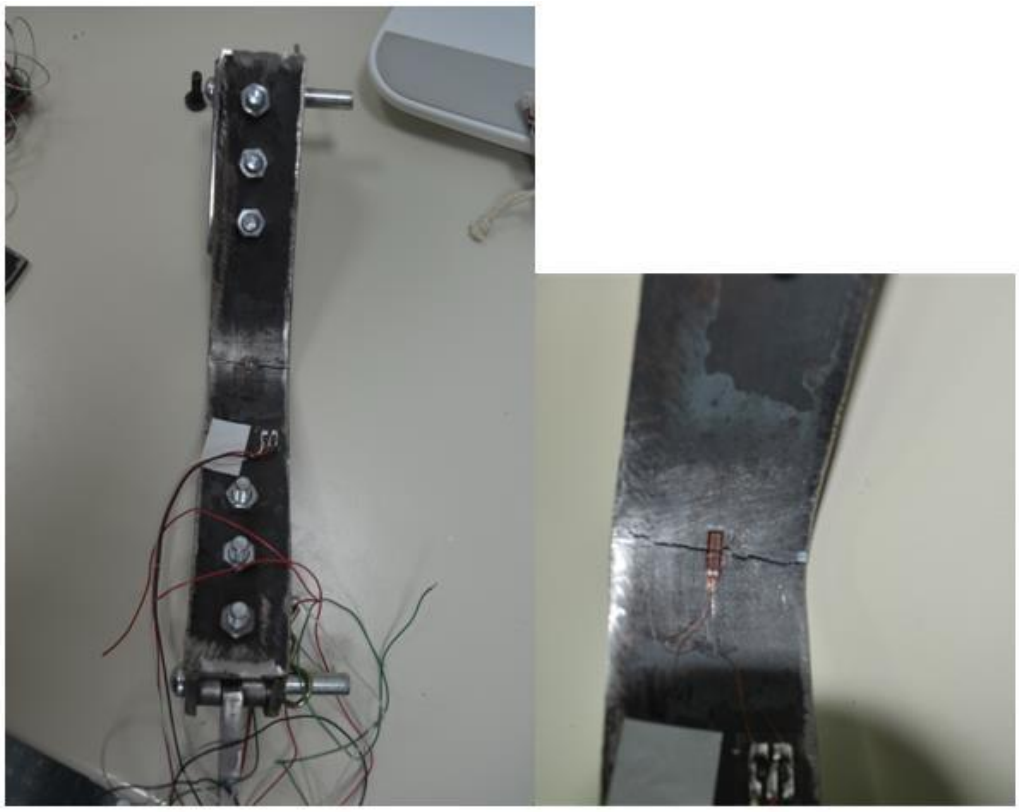

Figure 3-81: Crack development of specimen S21-View from the inner face of the strip. The crack propagated along the transverse direction.

Chapter 4 NUMERICAL SIMULATIONS

Nonlinear finite element tools have been employed to simulate the experimental procedure described in Chapter 2. General-purpose finite element program ABAQUS [69] is employed to simulate the development of denting/buckling and the behavior of the dented/buckled pipes under cyclic bending and pressure loading. The analysis considers nonlinear geometry through a J_2 flow (von Mises) large-strain plasticity model with isotropic hardening.

The plasticity model is calibrated through appropriate uniaxial tensile tests on steel coupon specimens, extracted from the X52 6-inch pipe specimens. The yield stress has been measured equal to 364 MPa and ultimate stress equal to 554.7 MPa as reported in Chapter 2, paragraph 2.1.

4.1 Dented specimens

The finite element model for the denting stage consists of five parts; the denting tool, the pipe specimen, the wooden base that supports the pipe movement during indentation, and the two stiff pipe segments (see Figure 4-1) on either side of the specimen. The entire pipe specimens have been simulated with four-node reduced-integration shell elements (S4R), which have shown to perform very well in nonlinear analysis problems involving large inelastic deformations of relatively thick-walled steel cylinders. In order to simulate accurately the formation of a dent profile, and the development of the corresponding local stress and strain distribution, the element mesh is rather dense in a two-diameter-long region, at the middle section of the pipe, where maximum deformation due to dent is located. On the other hand, a less dense finite element mesh is considered outside this region.

The stiff pipe segments are simulated with beam elements of appropriate cross-sectional and material properties, and simply-supported conditions at the two ends.

The thick plates, welded at the end of the specimens, were modeled through a "kinematic coupling" constraint at the end nodes.

4.1.1 Simulation of Denting

According to the experimental set-up (Figure 3-12), the wedge-type denting tool is oriented in a direction perpendicular to the pipe axis. For the purpose of reducing computational time, only the curved part of the wedge tool, which is in contact with the pipe, is modeled. The radius of the rounded wedge is equal to 5 mm, identical to the one used in the experiments. The denting tool is designed as a non-deformable "discrete rigid" part. Contact interaction without friction is imposed between the wedge surface and the outer surface of pipe wall.

The geometry of the wooden base, shown in Figure 4-2a, is similar to the one used in actual testing conditions (Figure 4-2b) with dimensions 300mm×300mm and the upper surface properly curved in order to support the pipe model. The wooden base is designed as discrete rigid part, implementing four-node reduced-integration shell elements (S4R). Frictionless contact conditions are imposed between the surface of the support and the pipe outer surface, which prevent penetration, but allow for pipe uplifting and sliding.

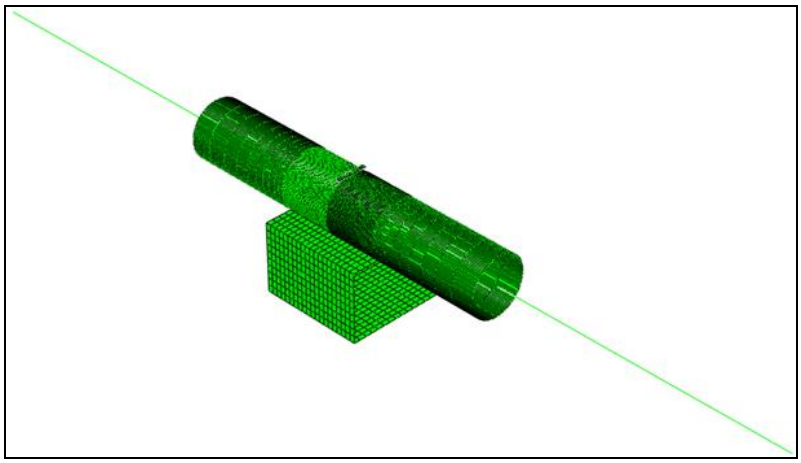

(a)

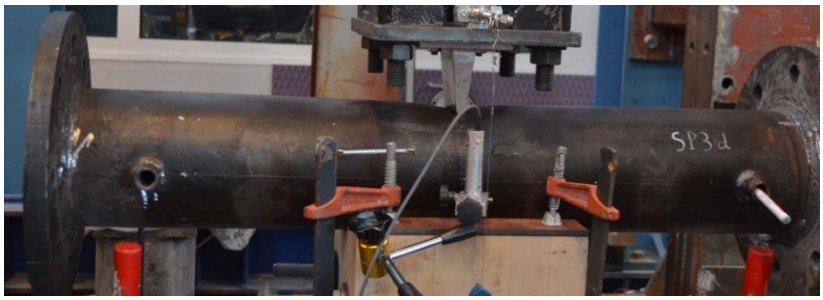

(b)

Figure 4-1: (a) General view of the finite element model, (b) the test set-up during denting

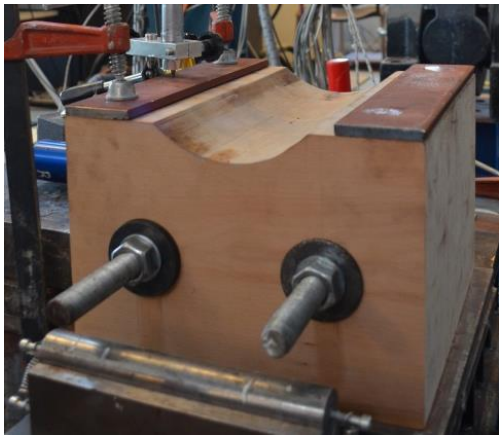

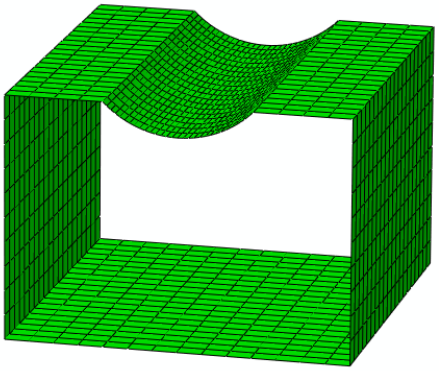

(a) (b)

Figure 4-2: The geometry of the wooden base from (a) the denting tests and (b) the finite element analysis

The pipe model rests on the support plate. During denting, the two pipe ends are non-restrained, resulting in a small uplifting of the pipe specimen. Following the experimental testing, the values of dent depth considered in this numerical study are 6 and 12% of the pipe diameter. These are the values of the residual dent size after removal of the denting tool and the corresponding elastic rebound. The deformed model and the von Mises stress distribution around the dent region, after elastic rebounding, are shown in Figure 4-3, and compare well with the dent profiles of the dented specimens; SP1d and SP5d (Figure 3-30). The dent profile of SP5d model is depicted along the longitudinal and hoop direction of the pipe is shown in Figure 4-4 after denting load removal. Additionally, as shown in Figure 4-5, force versus denting displacement curves of SP3d and SP6d are well compared with the experimental ones during denting and unloading. Nevertheless, the finite element model exhibits more

stiff behavior during unloading due to the fact that the the wooden base and the indenter were modeled as very stiff parts not similar to their actual material properties. The axial and hoop strain values at the ridges of the dent profile have, also, been obtained. Figure 4-6 shows the comparison of strain values obtained from test results (specimen SP5d) and numerical simulation, which is considered quite satisfactory.

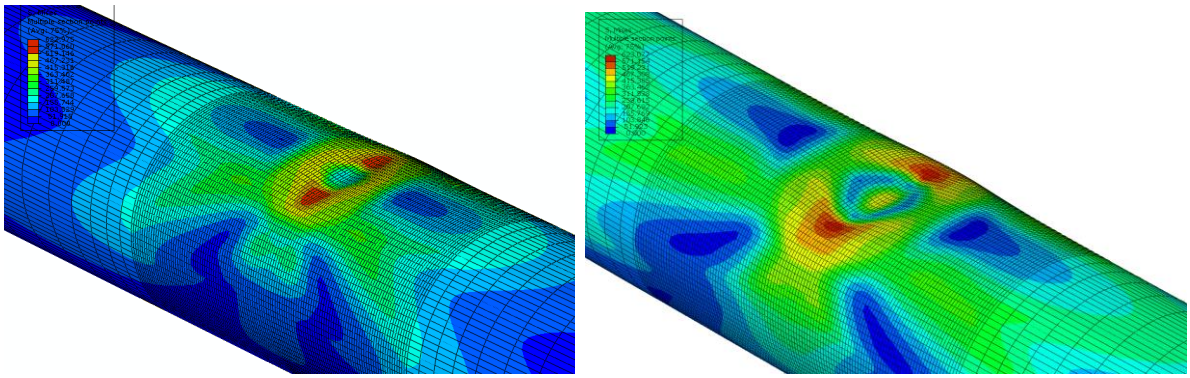

(a) (b)

Figure 4-3: Deformed geometry and Von Mises stress distribution after denting load removal; (a) SP1d (d/D=6%) and (b) SP5d models (d/D=12%)

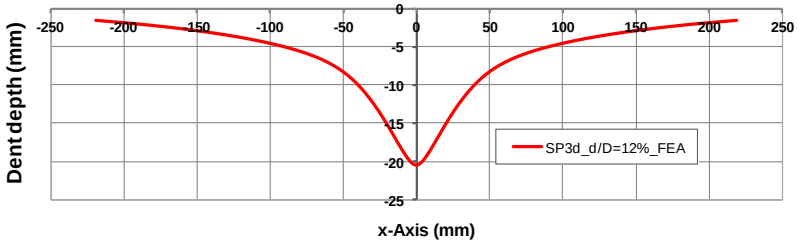

(a)

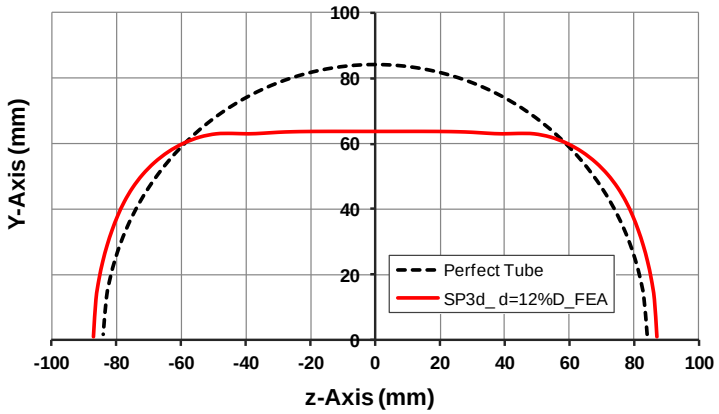

(b)

Figure 4-4: The dent profile at (a) the longitudinal direction parallel to the pipe axis and (b) the hoop direction, obtained from the finite element results

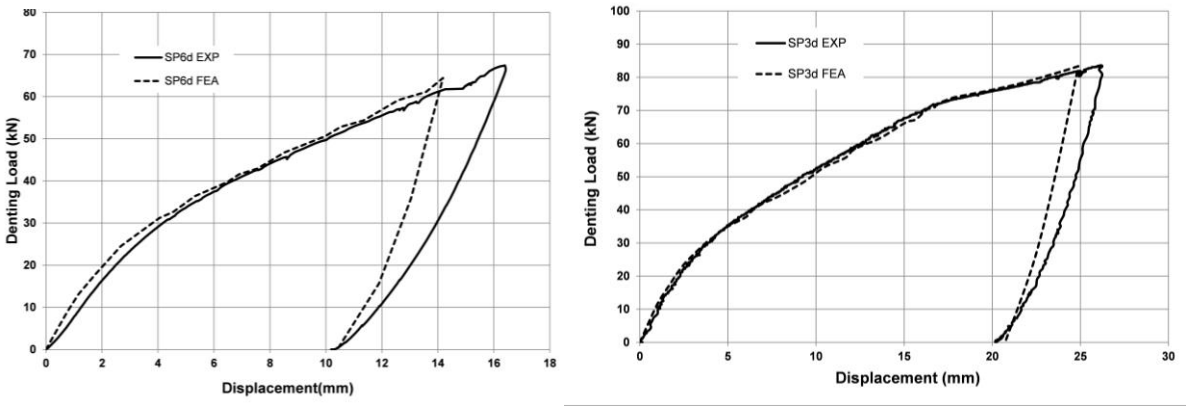

(a) (b)

Figure 4-5: Load vs displacement curves for (a) SP6d and (b) SP3d models during denting in comparison with experimental ones

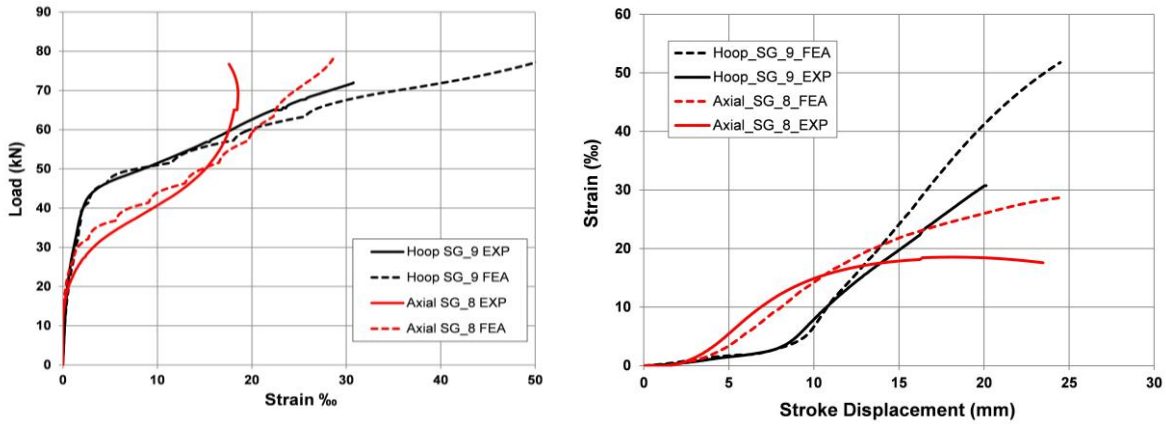

(a) (b)

Figure 4-6: Strain evolution in terms of (a) denting loading and (b) denting displacement, during the denting procedure for specimen SP5d.

Obtaining the dent profiles numerically, geometrical strain values were calculated at the dent region employing the local strain criterion method specified in ASME B31.8 [14] in order to determine whether the dents fall within the maximum acceptable strain limit of 6%.

The results shown in Table 10 indicated that the dents with d/D=12% exhibit slightly higher local geometric strain values than the ones with d/D=6% for both cases of D/t=35.2 and 55. It is, also shown that for specimens with D/t =35.2 the geometric strains appear to be lower than the case of specimens with D/t=55. This

difference is attributed to the fact that the dents produced in thinner specimens are considered shorter and sharper in comparison with the ones produced in specimens D/t=35.2. As a result, in the case of D/t=55, the local geometric axial and hoop dent curvature are found lower than the ones calculated for D/t=35.2 resulting in higher local geometric strains. It is, also, obvious from Table 10, that all dents fell far beyond the strain acceptability limits specified by ASME provisions; both geometrical strain values, ε_i and ε_0, were calculated higher than the strain limit of 6%. However, it is worth noticing that dented pipes with these specific local dents sustained numerous bending and pressure cycles before failure as described in Chapter 3 (see Table 4 and Table 7). From the above observations, it seems that this strain criterion could be considered rather conservative.

Table 10. Geometric strain calculations for dented models obtained from FE analysis

D_{nom}	t_{nom}	$(D/t)_{nom}$	d/D (%)	**Geometric Strain Calculations from FEA Results**	
				ε_i (%)	ε_o (%)
168.3	4.78	35.2	6.08	10.6	5.26
168.3	4.78	35.2	12	11.68	8.33
165	3	55	5.97	12.68	6.11
165	3	55	11.92	13.66	9.67

4.1.2 Simulation of Cyclic Bending of Dented Pipes

Following denting, cyclic bending loading of the dented pipes is simulated, similar to the experimental procedure. Loading is applied through transverse forces via displacement control conditions at two points of the beam elements, corresponding to the locations of wooden grips.

It is shown from Figure 4-7, Figure 4-8 and Figure 4-9 that the moment-curvature curves obtained from finite element analysis for SP1d, SP3d, SP5d and SP6d models compare fairly well with the experimental ones. The moment and curvature values are normalized with the values $M_0 = \sigma_y D_m^2 t$ and $k_0 = \frac{t}{D_m^2}$, respectively, where $\sigma_{y,}$ D_m and t refer to the yield stress of the material equal to 364 MPa, the mean diameter of

the pipes and the nominal thickness value, respectively. At the cyclic stages, a total of 10 cycles is applied numerically, and the corresponding range of maximum longitudinal axial local strains, $\Delta\varepsilon_x$ has been calculated and presented in Table 11 of Chapter 5. It is assumed that upon application of 10 cycles, stabilization of cyclic response is achieved.

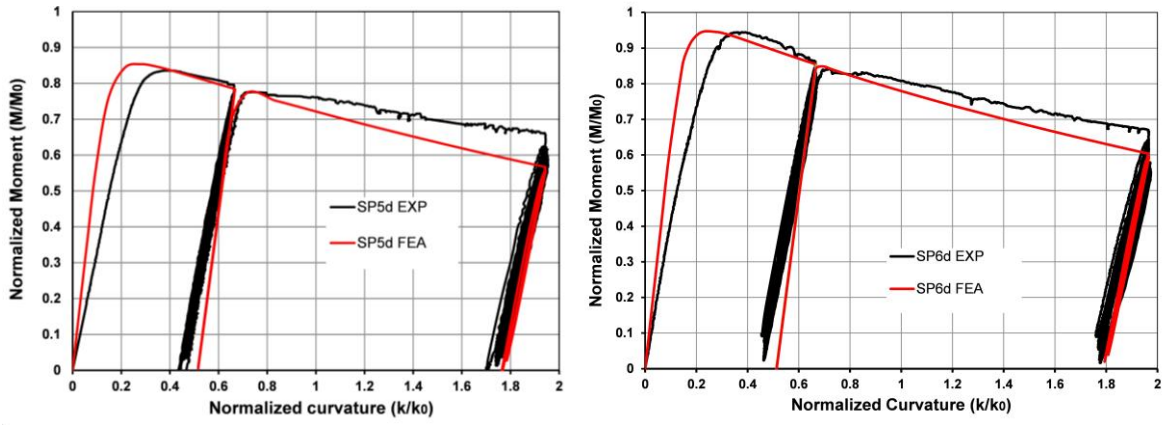

(a) (b)

Figure 4-7: Normalized moment-curvature curves; experimental and FEA results for (a) SP5d and (b) SP6d pipe specimens.

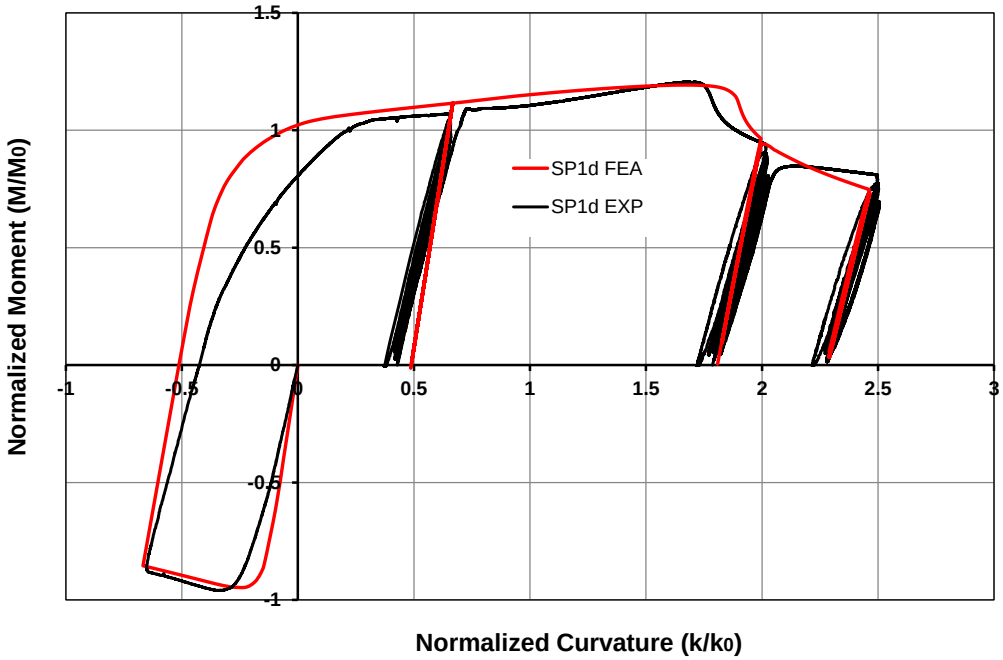

Figure 4-8: Normalized moment-curvature curves of specimen SP1d (including reverse and cyclic bending) during bending obtained from finite element analysis; comparison with experimental curve.

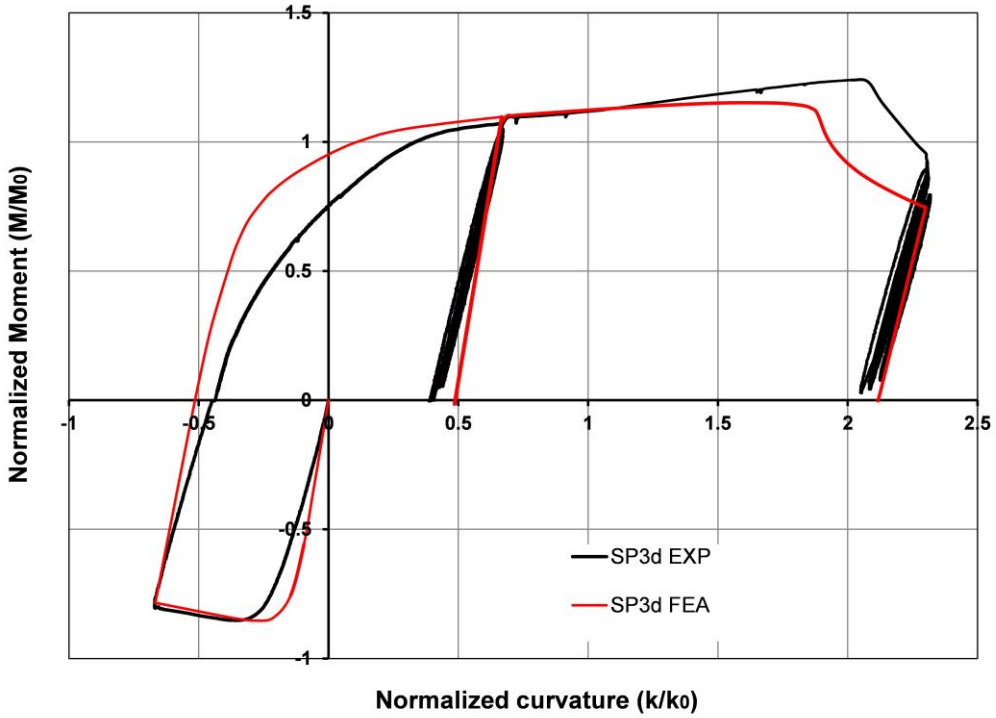

Figure 4-9: Normalized moment-curvature diagram during bending of specimen SP3d (including reverse and cyclic bending) obtained from finite element analysis; comparison with experimental curve.

The deformed shapes of the finite models (SP5d and SP3d), shown in Figure 4-10 and Figure 4-11, are well compared with the failure of the corresponding specimens (Figure 3-38 and Figure 3-42). In the deformed shape shown in Figure 4-11, one may observe the dented area at the top of the specimen SP3d, which is under tension, and the buckled area, developed due to reverse bending at the opposite side of the pipe wall due to excessive compression. The buckled area is the one that corresponds to the maximum longitudinal local strain range ($\mathbf{\Delta\varepsilon}_{max}$) (see also Table 11) and where fatigue crack, eventually, develops.

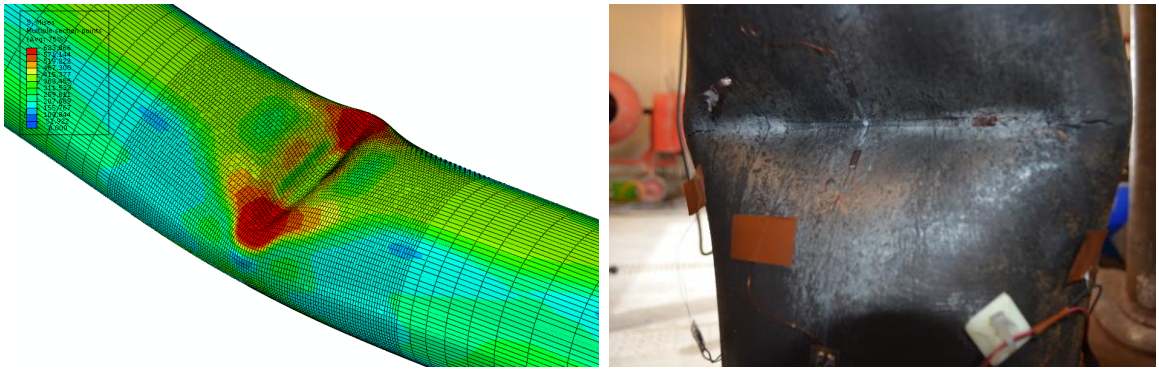

(a) (b)

Figure 4-10: Deformed shapes of the (a) finite element model and (b) SP5d specimen under cyclic bending conditions

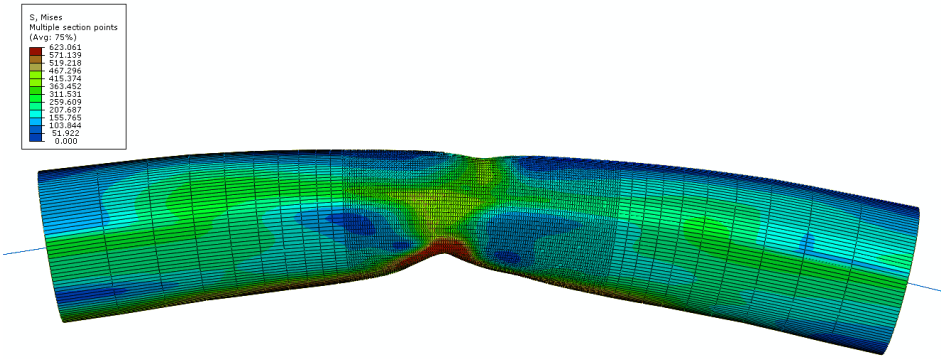

(a)

(b)

Figure 4-11: Deformed shapes of the (a) finite element model and (b) SP3d specimen under cyclic bending conditions

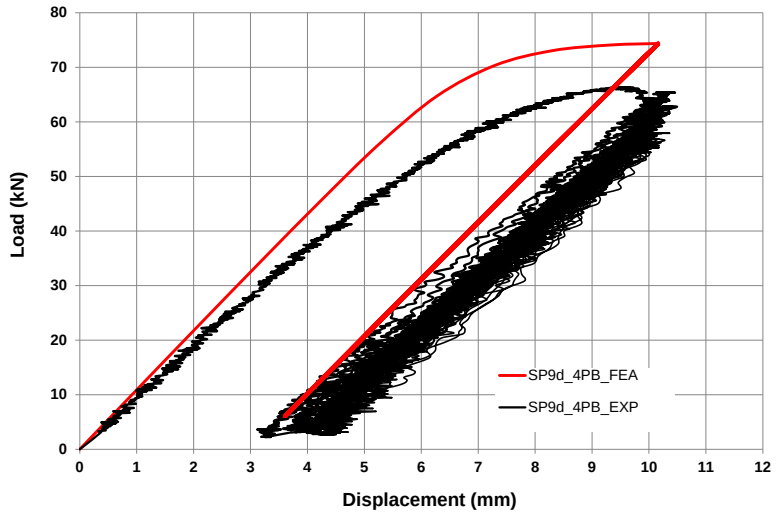

(a)

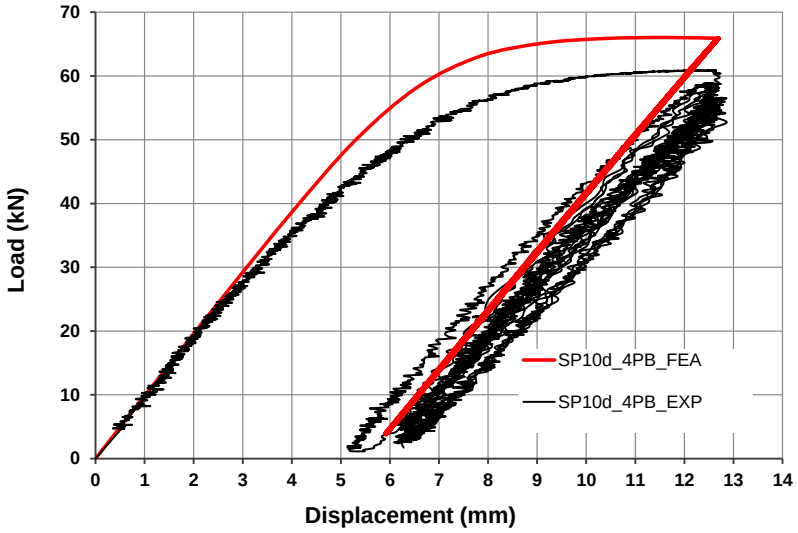

(b)

Figure 4-12: Experimental Load displacement curves compared with finite element results; specimens (a) SP9d and (b) SP10d.

The values of the so-called "strain concentration factor" (SNCF) have been also calculated at the critical region for the dented specimens under cyclic bending and depicted in Table 11. This SNCF factor is defined as follows:

$$SNCF = \frac{\Delta\varepsilon_{max}}{\Delta\varepsilon_{nom}} \tag{3.1}$$

The value $\Delta\varepsilon_{\max}$ is the maximum local strain range at the critical region, and $\Delta\varepsilon_{nom}$ is the nominal strain range due to the applied loading, calculated through

elementary mechanics of materials, considering the initial (intact) geometry of the tubular member.

4.2 Buckled Specimens

4.2.1 Simulation of Buckling

Finite element models with shell elements have been developed in order to simulate the development of a local buckle in the pipeline. Following the experimental procedure local buckling occurs under the application of 4-point bending loading via displacement control conditions. The loading is applied at two points of the stiff pipes, corresponding to the locations of wooden grips. The configuration of the finite element models is shown in Figure 4-13. As shown in this Figure, the central (machined) part of the pipe specimens (500mm-long) is simulated with four-node reduced-integration shell elements (S4R), while, the remaining part of the tube specimen is simulated with beam elements of appropriate cross-sectional and material properties.

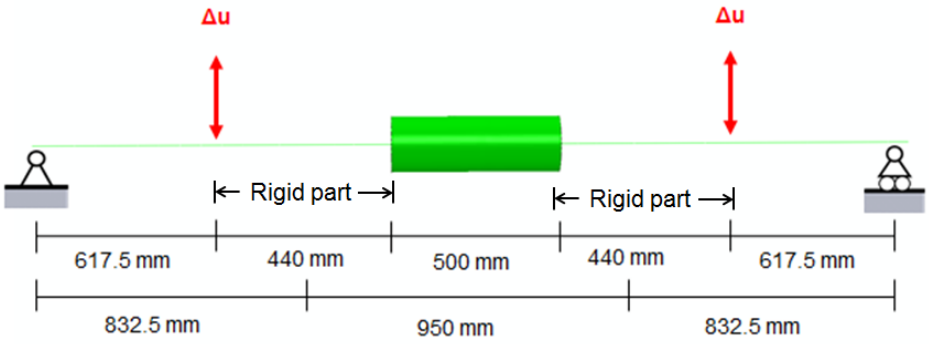

Figure 4-13: Side view of the finite element model configuration under 4-point bending

A uniform thickness value for each pipe model is taken into account equal to the corresponding mean thickness values of the specimens recorded prior testing.

For the optimization of the finite element model, a parametric study is conducted in order to investigate the sensitivity of the buckling response of pipes on the presence of initial imperfections.

The configuration of wrinkling imperfection is initially induced as a stress-free diamond-shape buckle consisting of one main buckle and two secondary minor

buckles on either side of the main buckle in a symmetric manner with respect to the pipe axis. This type of buckle is also similar to the one obtained in the experiments. The imperfection amplitude of wrinkling wave is reported in a non-dimensional form with respect to the pipe thickness (A/t), where "A" and t refer to the depth of the main buckle (depicted in Figure 4-15) and the pipe thickness, respectively. It is found the buckling response of pipes with D/t over 55 is extremely sensitive to the existence of the initial wrinkling imperfection; with the increase of initial imperfection, buckling occurs in earlier stages (Figure 4-15). Furthermore, the presence of initial imperfection may affect the shape of buckling. The buckling mode obtained numerically from the application of monotonic bending on a perfect pipe under monotonic bending is considered as a smooth buckle of symmetric configuration as shown in Figure 4-16. On the other hand, the final deformed geometry of a pipe, with a relatively negligible imperfection (A/t) equal to 0.0005, is similar to a diamond-shape buckle, which is consistent with the test results (Figure 4-16).

Therefore, in order to achieve effective finite element models for each case of test specimens, initial geometric imperfection in the form of a diamond-shape buckle of various yet small amplitudes (A/t) ranging from 0.0001 to 0.01 (obtained numerically) has been imposed on the pipe models.

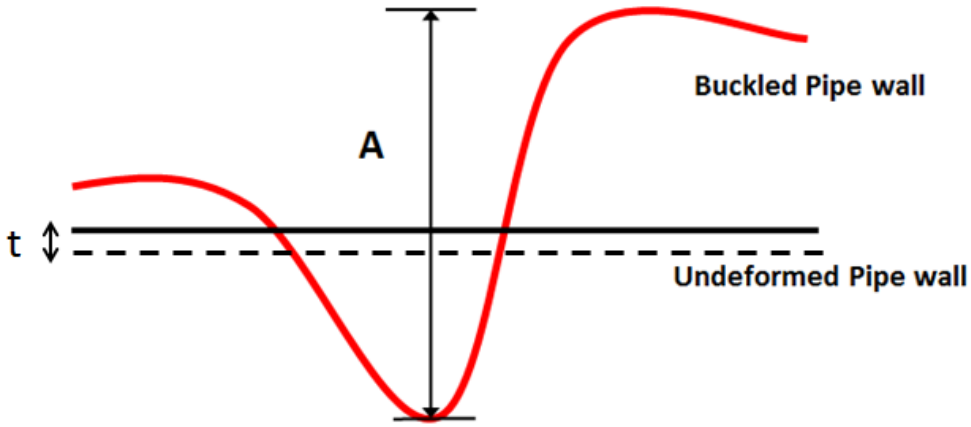

Figure 4-14: Schematic configuration of the buckle-type imperfection; Side view.

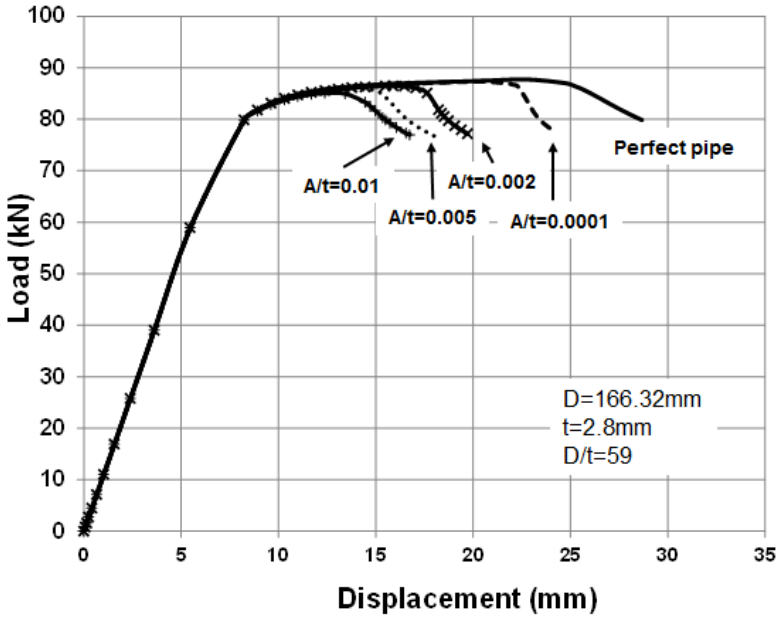

Figure 4-15: The effect of initial wrinkling imperfection on the buckling response of a pipe with D=166.32mm and t=2.8mm.

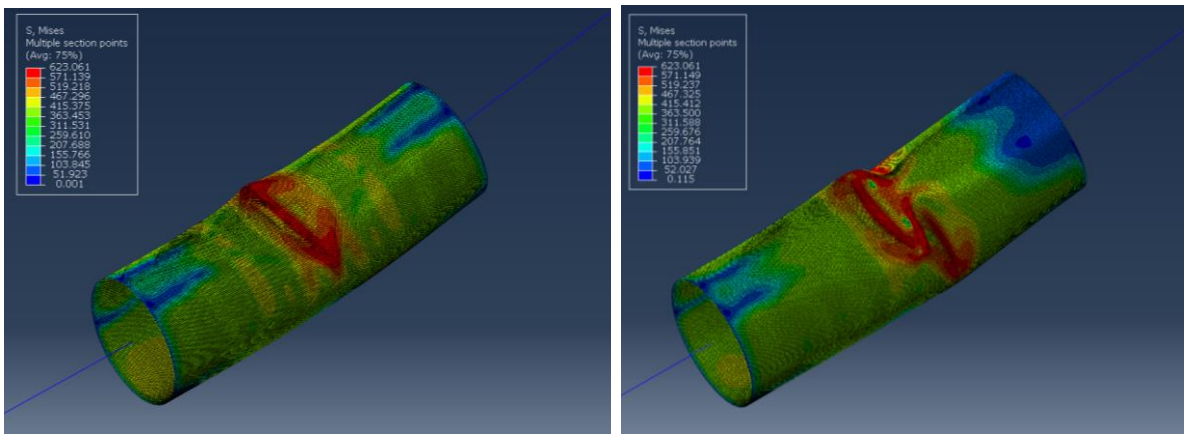

(a) (b)

Figure 4-16: Post-buckling failure modes of (a) perfect pipe and (b) pipe with initial wrinkling imperfection A/t=0.0001; diameter-to-thickness ratio D/t= 59.

Normalized moment-curvature diagrams have been obtained through finite element analysis and compare well with the experimental results, as shown in Figure 4-17 for SP4b, SP6b and SP7b specimens. An amplitude equal to 0.01, 0.005 and 0.0001 of the initial imperfection has been induced for the simulation of SP4b, SP6b and SP7b tested specimens, respectively.

Similar to the case of dented specimens, the displacement values corresponding to the average values recorded via the LVDTs. The buckled models after the application of monotonic bending are shown in Figure 4-18. As shown in Figure 4-19 and Figure 4-20, the buckled profiles of the pipe models compared well with the buckled shapes of the corresponding specimens.

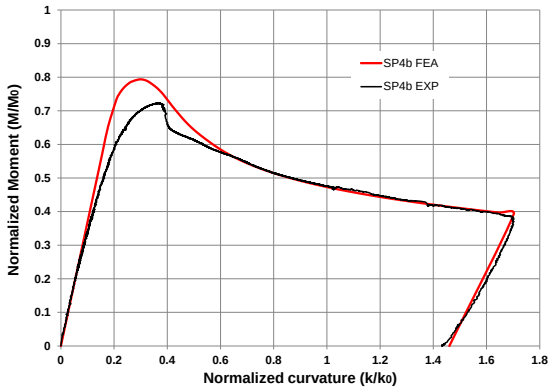

(a)

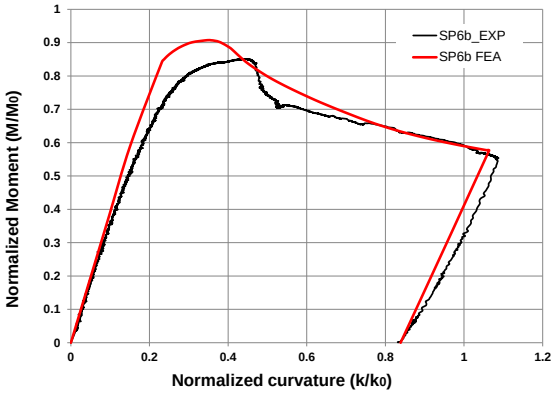

(b)

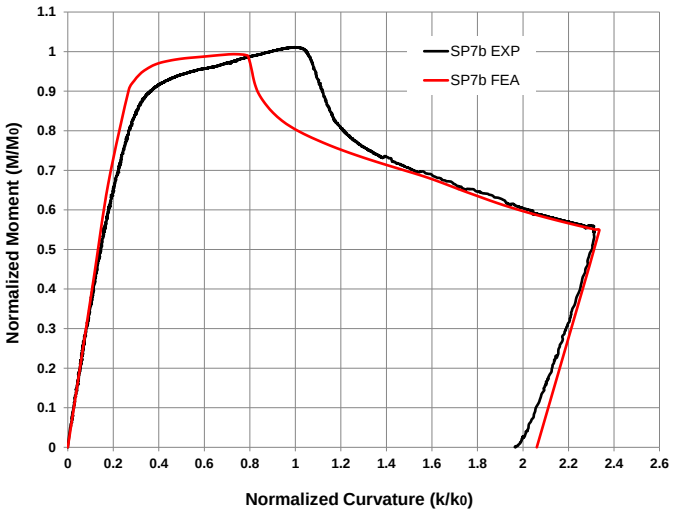

(c)

Figure 4-17: Normalized moment-Curvature diagrams for (a) SP4b, (b) SP6b and (c) SP7b under monotonic bending; experimental in comparison with finite element results.

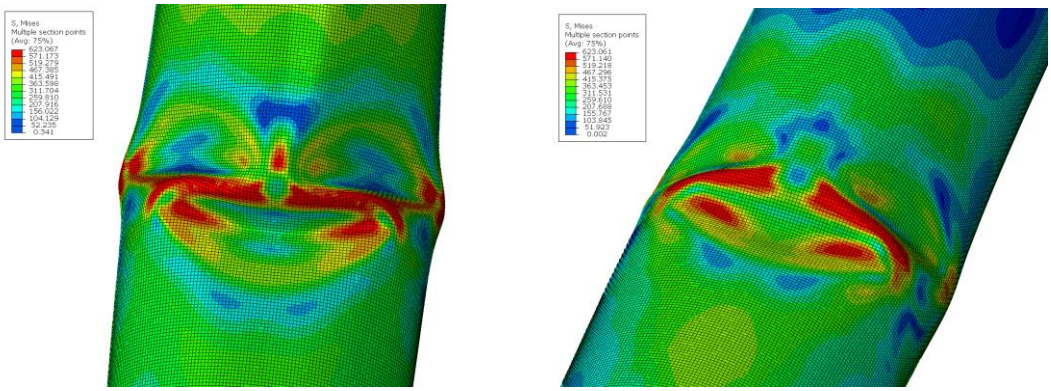

(a) (b)

Figure 4-18: Distribution of Von Mises stress at the buckle region of (a) SP4b and (b) SP6b model; general view of the deformed models.

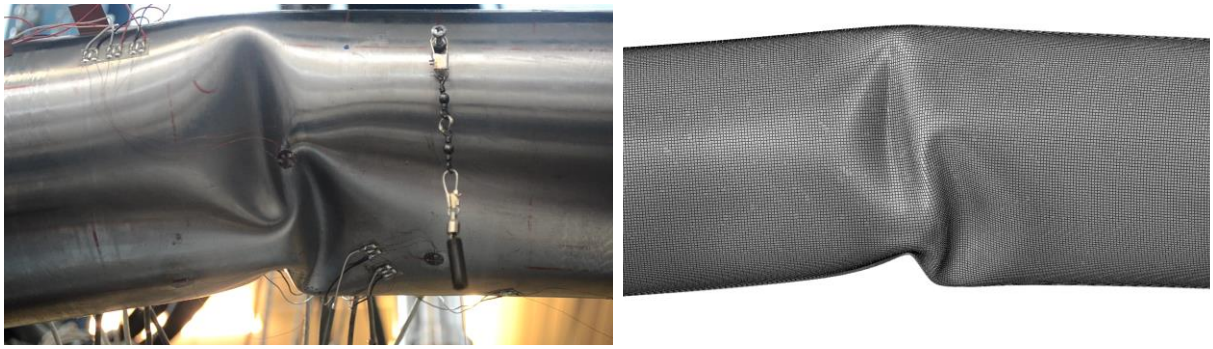

(a) *(b)*

Figure 4-19: (a) Buckle of SP4b specimen after monotonic bending and (b)the corresponding buckle obtained from finite element analysis.

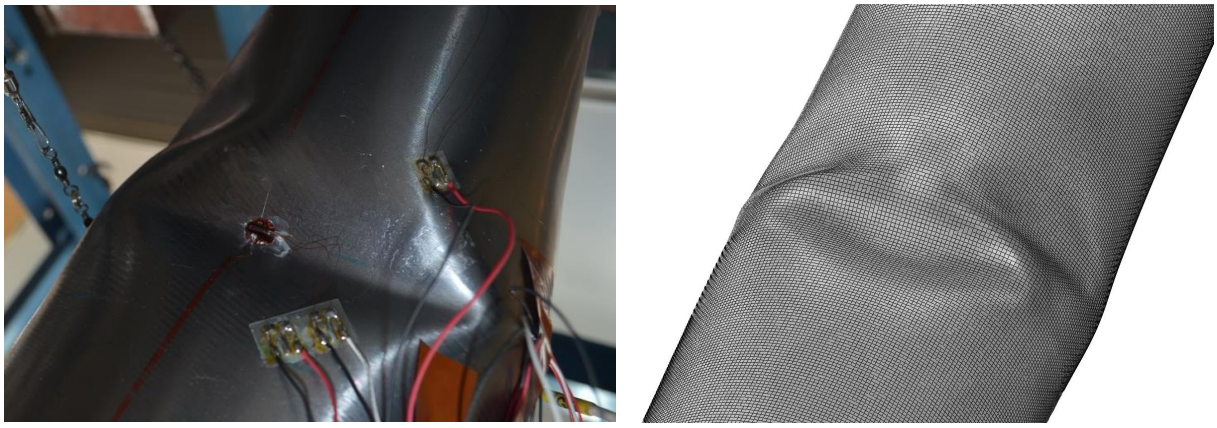

(a) *(b)*

Figure 4-20: (a) Buckle of SP6b specimen after monotonic bending and (b) the corresponding buckle obtained from finite element analysis.

4.2.2 Simulation of Cyclic Bending of Buckled pipes

Following buckling, cyclic bending of the buckled pipe is simulated, similar to the test procedure. During the numerical simulation, cyclic bending is performed following the experimental procedure as shown in Figure 4-21. Similar to the case of dented models, at the cyclic stages, a total of 10 cycles is performed numerically, and the corresponding range of maximum axial local strains, $\Delta\varepsilon_x$ has been calculated and presented in Table 12 of Chapter 5. It is assumed that upon application of 10 cycles, stabilization of cyclic response is achieved.

In addition, as described in following Chapter (Chapter 5) and presented in Table 12, the values of strain concentration factors (*SNCF*) have been calculated for the case of buckled specimens under cyclic bending.

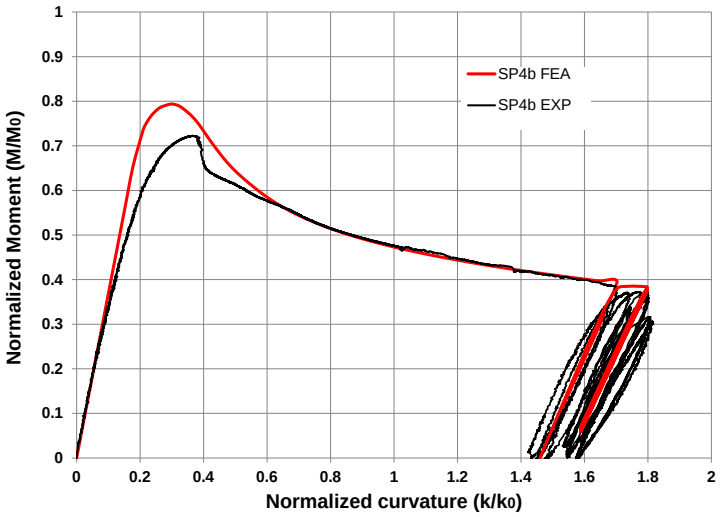

(a)

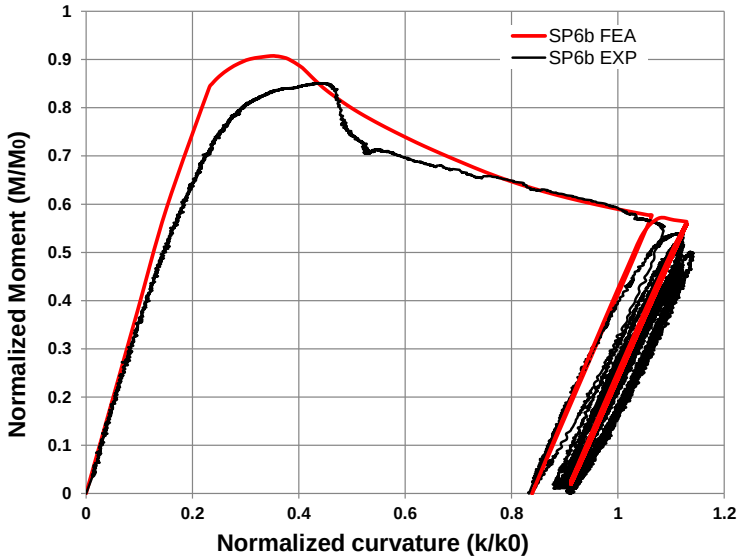

(b)

Figure 4-21: Normalized moment-curvature curves buckled specimens (a) SP6b and (b) SP4b under monotonic and cyclic bending; experimental in comparison with finite element results

4.3 Simulation of pressure loading

Internal pressure is applied in the numerical model of the dented or buckled specimens. The results show that with increasing pressure, the dented/buckled profile "smoothens" (Figure 4-22), the dent/buckle size decreases, and there is a tendency of gradual dent/buckle flattening, an observation also reported in [59].

Furthermore, for the range of cyclic pressure applied in dented pipes SP2d and SP4d (Δp=13.5 MPa, with a maximum value of 15 MPa), the corresponding strain concentration factor SNCF is small (also reported in Chapter 4). This can verify the fact that the dented pipe is capable of sustaining 5,000 pressure cycles without failure or other damage, as observed experimentally.

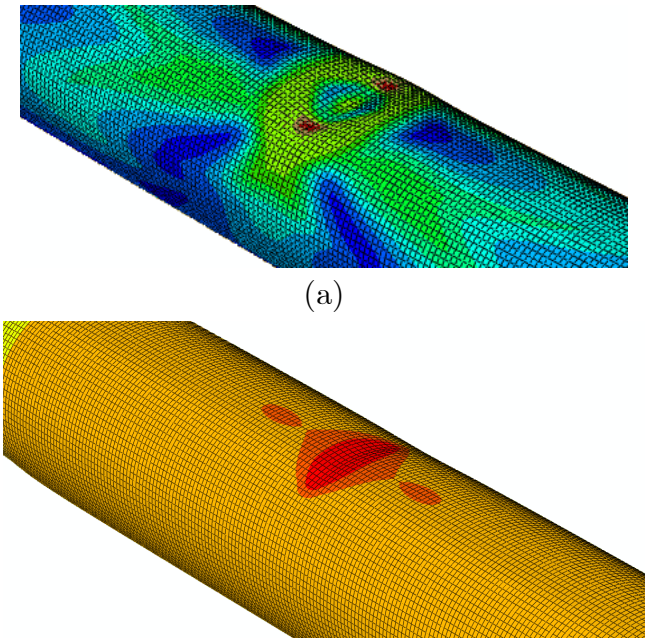

(a)

(b)

Figure 4-22: Dent geometry of SP4d model: (a) before pressure application for d/D = *6%; (b) after pressure application.*

The diagrams in Figure 4-23 present the response of the dented region of SP2d model upon monotonically increasing internal pressure. The increase of internal pressure results in a decrease of dent depth and the dent profile tends to flatten. The maximum sustained internal pressure obtained from the finite element analysis is equal to about P_{max}= 33 MPa until convergence of incremental solution has not been possible due to excessive plastification of pipe wall. This pressure load compares well with the burst pressure measured in the experiments.

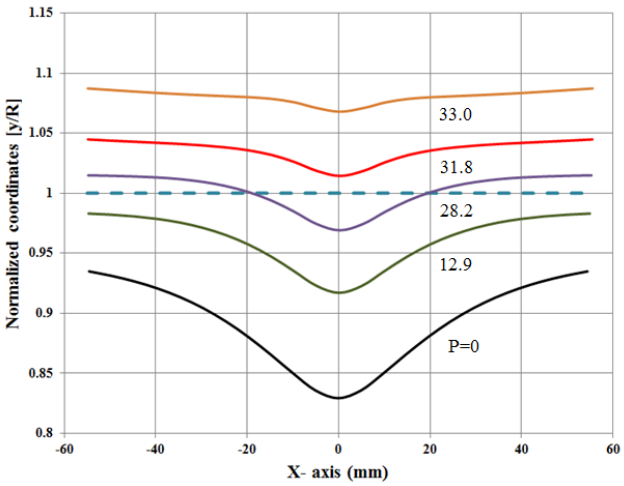

Figure 4-23: "Smoothening" of the dent profile with the increase of internal pressure

The coordinates in the vertical axis of Figure 4-23 refer to the configuration of the top outer wall generator for various pressure levels. The coordinates are normalized by pipe radius R. The results demonstrate the smoothening effect of internal pressure.

Cyclic internal pressure is applied in the numerical model of the buckled specimens SP7b and SP8b, following the test procedure followed for the two specimens. In particular, ten (10) pressure cycles of $\Delta p = 8.28$ MPa are applied, while for the SP8b specimen a combination of cyclic (10 pressure cycles) and monotonic pressure has been applied. It is assumed that upon application of 10 cycles, stabilization of cyclic response is achieved.

Local strain variations ($\Delta\varepsilon_{max}$) and the corresponding SNCF factors are calculated at critical locations and depicted in Table 13 of Chapter 4.

The results indicate that with increasing pressure, the buckled profile "smoothens" (Figure 4-24), the buckle depth decreases, and there is a tendency of gradual flattening of the buckled area.

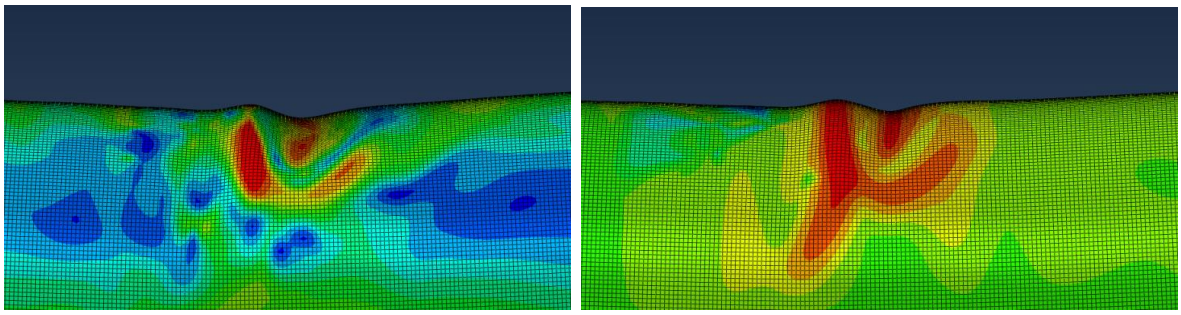

(a) (b)

Figure 4-24: Buckle geometry: (a) before pressure application for SP8b and (b) after pressure application.

The fatigue life for SP7b model and the burst pressure for SP8b specimen have also been estimated. Local strain ranges ($\Delta\varepsilon_x$) and the SNCF values have been computed for both SP7b and SP8b specimens under cyclic pressure as shown in Table 14 of Chapter 4.

4.4 Simulation of small-scale tests

After the completion of the eight (8) small-scale tests on bent strip specimens, finite element analysis has been conducted in order to simulate the experimental process. Nonlinear finite element tools have been employed to perform simulations on the monotonic bending and the lateral cyclic loading of the strips.

The model, shown in Figure 4-25a, is considered symmetric to the transverse axis in relation to the bending plane. At the 1st loading stage, according to the experimental procedure (reported in Chapter 2), the model consists of three (3) parts; the strip, the support cylinder (D=50mm) and the main central cylinder (D=16mm) all simulated with eight-node reduced-integration 3D solid elements (C3D8R). The two later parts remain inactive during the 2nd loading stage, where axial cyclic displacement is subjected with displacement range ratio (Δu) equal to 10, 15 & 20mm. The axial displacement is imposed through a fictitious node referred to as "reference node", allowing the rotation within the plane of bending simulating the pin-hinge connection gripped by the machine and bolted on the strip specimens. The representative nodes that correspond to the part of the strip specimen, which is connected to the end hinge, are coupled kinematically with the reference node.

Appropriate boundary conditions have also been implemented in order to simulate accurately the testing procedure.

For the material properties of the strip part, J_2 (von Mises) plasticity model with isotropic hardening has been employed similar with the one implemented for the simulation of full-scale tests. On the other hand, the two cylinders used in the stage of monotonic 3 point bending (shown in Figure 3-65) were considered undeformable with similar yield stress but larger value modulus of elasticity. The deformed geometry of the symmetric 90° – bent strip model at the end of the 1st loading stage (following monotonic bending) is indicatively shown in Figure 4-25b.

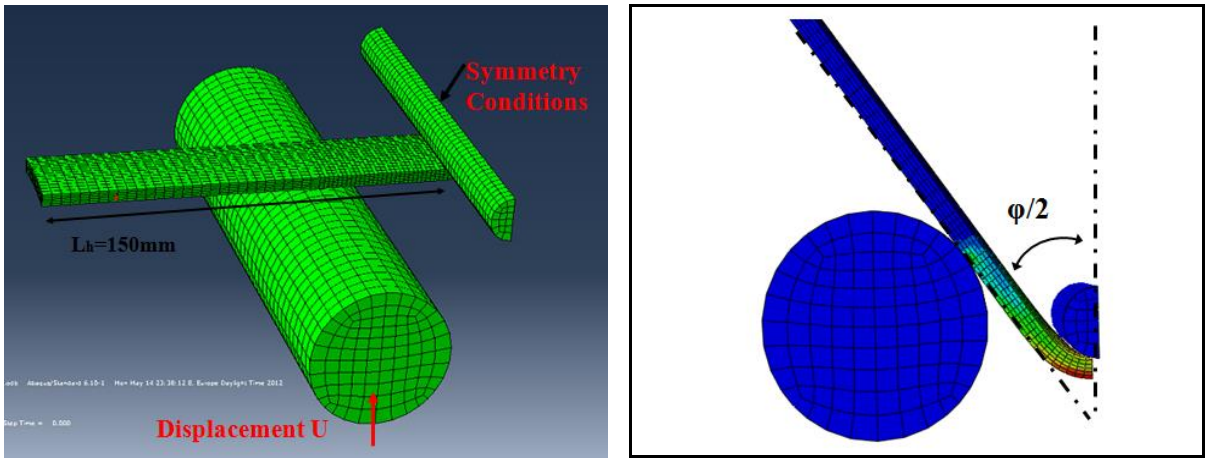

(a) (b)

Figure 4-25: (a) The symmetric model and (b) the deformed geometry after monotonic bending up to φ=90°

After monotonic bending, ten (10) cycles of axial displacement of various amplitudes (Δu=10, 15 and 20mm) have been applied to the 90° &120°-bent strip models. It is, also, assumed that upon application of ten (10) cycles, stabilization of cyclic response has been achieved.

The deformed strip configuration after the cyclic loading of Δu=10mm is shown in Figure 4-26. Moreover, for the S11 specimen, the load-displacement curve is well compared with the corresponding experimental curve as shown in Figure 4-27a, while for the S12 specimen, the finite element model exhibits lower compressive strength. It is also observed that for both cases, the finite element model is not capable of simulating the material strengthening during compression thus the finite element model exhibits a constant perfect plasticity at the compression branch of each loading cycle.

Furthermore, longitudinal strain distributions during the application of the 10 first loading cycles of Δu=10mm is obtained at the same locations where strain gauges have been attached in the strip specimen (inner and outer central part of the strip specimens) and presented in Figure 4-28. This figure shows that, regarding local strain reversals, a fairly good agreement between numerical and experimental results has been achieved. Unfortunately, the data acquisition system was not able to record strain values greater than 1%, thus limited data exist for the comparison of the finite element results with the test data. The fatigue analysis of those specimens will be reported in Chapter 5.

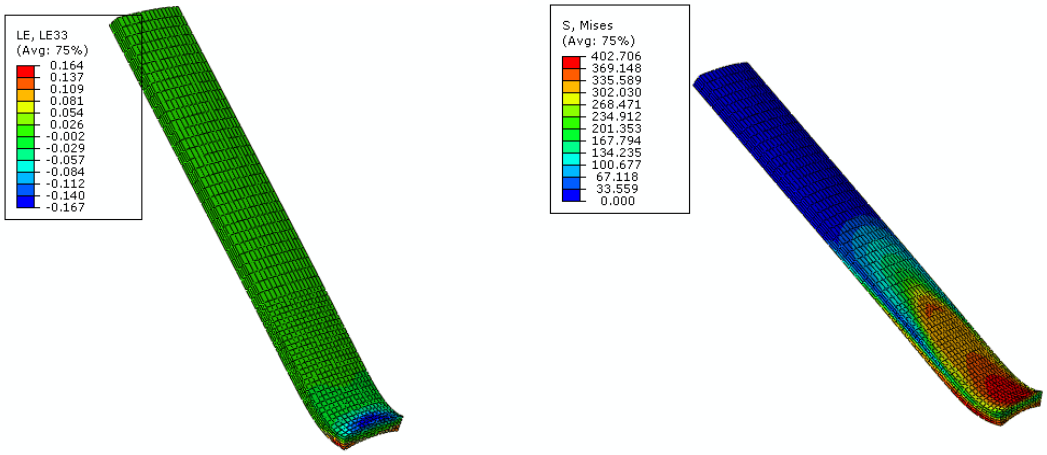

(a) (b)

Figure 4-26: (a) Longitudinal strain and (b) Von Mises stress distribution for the 90°-bent strip after 5 cycles of Δu=10mm

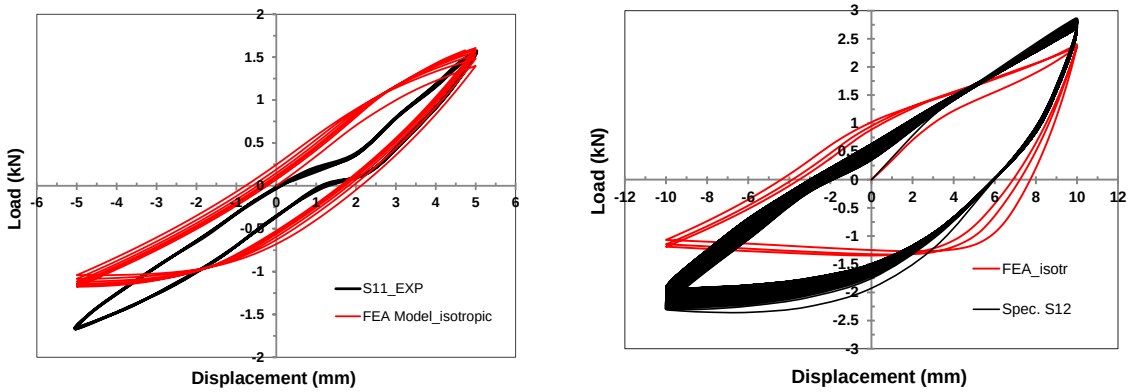

Figure 4-27: Comparison of experimental and finite element results in terms of load displacement curves for specimens (a) S11 and (b) S12.

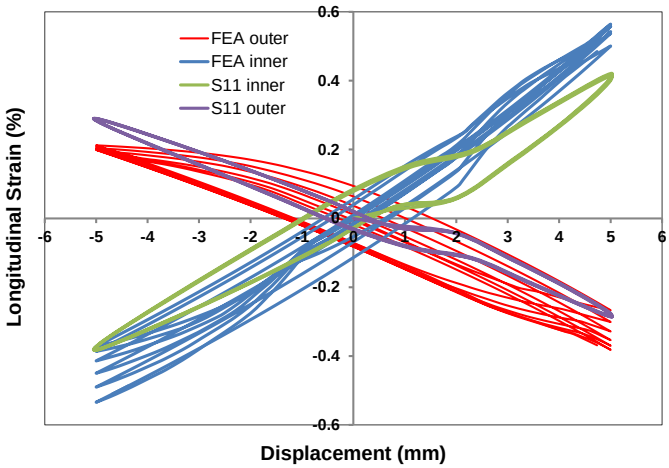

Figure 4-28: Comparison of experimental and finite element results in terms of longitudinal strain values during cyclic loading for specimen S11 (10 cycles of Δu=10mm)

Chapter 5 FATIGUE ASSESSMENT

5.1 Strain- life approach for fatigue life prediction

Using the numerical finite element model and the material fatigue curve, a simple and efficient strain- based fatigue assessment approach is proposed for the specimens under consideration. This approach denoted as "*Δε-N*" refers to a fatigue life prediction method initially introduced in a previous work by Dama et al. [59], and it is enhanced and validated in the course of the present research. As presented in [59], using this methodology, the structural condition of buckled pipes is assessed, subjected to both cyclic bending and cyclic internal pressure. In that early work, three full-scale 24-inch- diameter pipe specimens have been tested (buckled and cyclic tested) and analyzed using nonlinear finite element tools. As reported in [59], the maximum strain range from the finite element computations, and the "Δε-N approach" provided reasonable predictions for the number of cycles to failure observed in the tests. A similar (yet more elaborate) methodology on fatigue assessment has been proposed by API-579/ASME FFS-2007 "Fitness-for Service" [13] described in Annex B1, Section B1.5.4 of this standard.

To employ the "Δε- *N* approach", the values of local strain ranges $\Delta\varepsilon_{i\max}$ for each loading case (i) are obtained from numerical simulations on the dented or buckled specimens. These values of $\Delta\varepsilon_{i\max}$ are used as input to an appropriate fatigue curve of the pipe material to obtain the number of bending or pressure cycles to failure N_i (corresponding to $\Delta\varepsilon_i$). Combining the values of N_i for each loading case (i), a damage factor D_f is calculated which quantifies material damage due to low-cycle fatigue. Despite the fact that more sophisticated fatigue accumulation methodologies have been proposed in [73] and [74], in the present study the classical Miner's rule for variable amplitude loading expressed by the following equation (5.1) is adopted:

$$D_f = \sum_i \frac{n_i}{N_i} \tag{5.1}$$

In the above equation, N_i is the number of cycles corresponding to $\Delta\varepsilon_{i\max}$, obtained from an appropriate fatigue curve of the steel material and n_i is the number of real cycles applied corresponding to $\Delta\varepsilon_{i\max}$.

In the present case, the material curve, employed as "low-cycle" fatigue curve for calculation of the loading cycles to failure (N_i), has been presented in Chapter 2 and it is described as follows:

$$\Delta\varepsilon_{i\max} = 0.0104(2N)^{-0.1133} + 0.333(2N)^{-0.4807} \tag{5.2}$$

where $\Delta\varepsilon_{i\max}$ represents the maximum longitudinal local strain range ($\Delta\varepsilon_{xmax}$) at the dented area in dented pipes, computed numerically. In all cases examined, the ridge of the pipe has been identified as the most critical location. For the case of dented pipes under cyclic bending, the maximum strain range is obtained along the axial direction of the pipe ($\Delta\varepsilon_x$). For the case of buckled pipes the geometry is more complicated and, therefore, it is necessary to take into account the effects of hoop and shear-range strain components, denoted as $\Delta\varepsilon_x$ and $\Delta\varepsilon_\theta$ respectively, on the fatigue loading, considering the $\Delta\varepsilon_{i\max}$ value as the maximum equivalent local strain range
$(\Delta\varepsilon_{eq})_{\max}$ at the critical region of the buckle , given by the following expression:

$$\Delta\varepsilon_q = \sqrt{(\Delta\varepsilon_x)^2 + (\Delta\varepsilon_\theta)^2 - \Delta\varepsilon_x\Delta\varepsilon_\theta + 3(\Delta\varepsilon_{x\theta})^2} \tag{5.3}$$

In Figure 5-1, the critical region is located at the dent or buckle "ridge" and the maximum local strain ranges $\Delta\varepsilon_{i\max}$ are calculated from finite element analysis using a J_2 flow theory. It is also observed that for both dented and buckled pipes, fatigue cracking initiated during the cyclic tests at the location where maximum local strain ranges has been calculated in the finite element analysis (Figure 5-1).

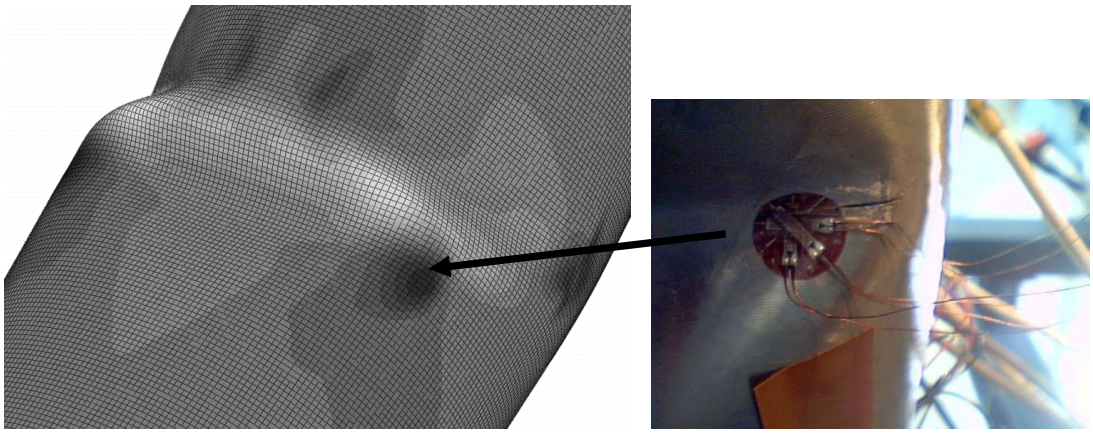

Figure 5-1: The location crack initiation of SP6b specimen coincides with the location of the maximum local strain ranges measured from finite element analysis.

Following the practice proposed in previous fatigue assessment methodologies, the so-called- Strain Concentration factor (*SNCF*) has been calculated using the finite element analysis tools of the pipe specimens under consideration. In particular, during the application of ten (10) loading cycles as follows:

$$\Delta\varepsilon_{i\max} = (SNCF)\Delta\varepsilon_{nom} \tag{5.4}$$

where the value $\Delta\varepsilon_{nom}$ represents the nominal strain range due to the applied loading, calculated through elementary mechanics of materials, considering the initial (intact) geometry of the pipe.

In the case of four-point bending, $\Delta\varepsilon_{nom}$ is calculated in the longitudinal direction of the pipe as follows:

$$\Delta\varepsilon_{nom} = \frac{2\alpha\Delta F}{E\pi D^2 t} \tag{5.5}$$

where ΔF is the range of total transverse load range applied on the specimen, and α is the distance between the hinge support and the location of load application.

From the finite element analysis described previously and the simplified assessment methodology, the values of damage factor and the corresponding SNCF value have been calculated for the specimens under consideration and shown in Table 11 and Table 12. The values of damage factor under cyclic bending are quite close to 1, indicating a good correlation between test results and numerical analysis. Despite the fact that a classical J_2 flow plasticity model has been obtained in the finite element simulations. It is expected that the predictions would improve if a more

elaborate cyclic plasticity model is used. Nevertheless, the correlation between experimental and numerical results is considered satisfactory.

The *SNCF* values, regarding the buckled specimens and the last cyclic stage of the dented specimens, can be considered rather significant, corresponding to severe local deformation of the pipe at the buckled area. This is attributed to the fact that in that area, the pipe wall is quite distorted, and the cyclic loading is associated with severe folding/unfolding of the pipe wall. The calculated values of *SNCF* are also consistent with those reported by Dama et al. [59] for locally buckled large-diameter pipes.

Table 11: Fatigue analysis for dented specimens under cyclic bending

Specimen	**Cycles Applied N_i**	**$\Delta\varepsilon_{max}$(%)**	**D_f**	***SNCF***
SP1d	500	0.154	1.05	0.65663
	500	0.593		3.35546
	400	1.834		**11.224**
SP3d	500	0.181	1.24	0.83118
	1000	1.404		**8.3415**
SP5d	500	0.508	1.9	2.96545
	450	2.232		**19.698**
SP6d	500	0.628	0.98	3.68748
	600	1.307		**8.7569**

Table 12: Fatigue analysis for buckled specimens under cyclic bending

Specimen	**Cycles Applied N_i**	**$\Delta\varepsilon_{max}$(%)**	**D_f**	***SNCF***
SP4b	550	1.780	1.80	**16.13**
SP5b	920	1.420	1.19	**8.63**
SP6b	200	2.711	1.35	**22.459**

In the case of cyclic internal pressure loading, the value of strain concentration factor (SNCF) is computed as the ratio of the maximum local strain range in the hoop direction obtained numerically over the value of the corresponding nominal strain is computed (similar to the case of bending), from elementary mechanics of materials as follows:

$$\Delta\varepsilon_{nom} = \frac{D}{2t}\frac{\left(1-v^2\right)}{E}\Delta p \tag{5.6}$$

where D and t are outer diameter and thickness of the pipe, respectively. In the above equation, E and v are Young's modulus of pipe material and Poisson's ratio, respectively, while Δp is the range of the applied pressure, which is constant at every pressure cycle.

For the range of cyclic pressure Δp applied during the tests on the buckled specimens SP2d and SP4d (Δp=13.5MPa, with a maximum value of 15 MPa), the corresponding strain concentration factor *SNCF* is computed numerically equal to about 3.2 for both specimens corresponding to a local strain variation equal to 0.25%. Using this value, the fatigue life of SP2d specimen is estimated equal to 500,000 cycles (Table 13). This verifies the fact that SP2d and SP4d specimens are capable of sustaining 5,000 pressure cycles without failure or other damage, as observed experimentally. Furthermore, the fact that the SNCF value of SP2d is quite similar to SP4d, shows that the existence of a dent does not have a significant effect on the fatigue life of these specimens. Similarly, the value of strain concentration factor (SNCF) computed numerically for the SP7d specimen is also found quite similar when compared with the one calculated for SP8d as shown in Table 13. Despite the fact that the SP8d failed after 2500 pressure cycles and SP7d survived 5000 cycles without damage, the fatigue life for both specimens was estimated over 1,000,000 pressure cycles using the "$\Delta\varepsilon$-N" approach. Therefore based on the results of cyclic response of thin dented pipe specimen SP7d one may conclude that the presence of smooth dents may not affect the fatigue life of pipes. Based on the results of specimen SP8d that failed after a significant number of cycles, one may conclude that the fatigue crack was developed due to the fact that the local thickness values close to the dent were recorded about 1.8 mm which is lower than the mean pipe thickness thickness (equal to 3mm). In addition, the maximum pressure loading obtained from the numerical analysis equal to about 20 MPa, until convergence of solution is not

possible due to excessive plastification of pipe wall. This value close to the analytical expression used for perfect pipes verifying the fact that the burst pressure is not affected by the presence of smooth dents.

Furthermore, for the range of cyclic pressure applied during the test on the buckled specimen SP8b (Δp=8.3 MPa, with a maximum value of 9.2 MPa), the corresponding strain concentration factor *SNCF* is computed numerically equal to 7.41, corresponding to a local strain variation equal to 0.59% and the fatigue life of specimen SP8b was estimated by Eq (4.2) about 11,000 cycles (Table 14). This implies that specimen SP8b should be capable of sustaining 5,000 pressure cycles without failure or other damage and this is compatible with the behavior observed experimentally. The maximum internal pressure obtained from the finite element analysis is equal to about P_{burst}= 20 MPa until convergence of solution is not possible due to excessive plastification of pipe wall. This pressure level is close to the analytical solution but greater than the burst pressure measured in the pressure test of SP8b. This is attributed to the fact that, around the region of rupture, pipe thickness value has been recorded equal to 2.2mm which is quite lower than the average value of 2.8mm. Concerning SP7b specimen, the SNCF computed numerically is quite lower than the one calculated in the case of SP8b. The corresponding strain concentration factor *SNCF* is computed equal to 6.89 while corresponding local strain variation is obtained equal to about 0.55%. The fatigue life of SP7b specimen was estimated by Eq (4.2) about 16,000 cycles (Table 14).Although SP7b was buckled excessively, the SNCF factor obtained numerically, during cyclic loading, is estimated very close to the SNCF value of SP8b. This could be attributed to the fact that with the increasing internal pressure, the buckles tend to flatten and the pipe resistance to rupture becomes independent of the existence of buckle. However, SP7b ruptured at 570 cycles, due to the fact that the thickness values recorded prior to testing at the region where tha buckle occured were equal to 2.1 mm which is significantly lower than the nominal thickness value of the pipe (3mm). The maximum internal pressure obtained from the finite element analysis is equal to about P_{burst}= 20 MPa which is equal to the analytical expression of burst pressure of a perfect pipe.

Table 13: Fatigue analysis for dented specimens under cyclic pressure

Specimen	**Cycles Applied n_i**	**$\Delta\varepsilon_{max}$(%)**	***SNCF***
SP2d	5000 no rupture	0.259	**3.11**
SP4d	5000 no rupture	0.252	**3.03**
SP7d	5000 no rupture	0.18	**2.26**
SP8d	2500 to rupture	0.203	**2.54**

Table 14: Fatigue analysis for buckled specimens under cyclic pressure

Specimen	**Cycles Applied n_i**	**$\Delta\varepsilon_{max}$(%)**	***SNCF***
SP7b	570 to rupture	0.592	**7.41**
SP8b	5000 no rupture	0.548	**6.89**

5.2 API 579/ASME FFS-1 fatigue life predictions compared with Strain– Life Approach for specimens under cyclic pressure

API 579 first published in 2000 [70], constitutes a major advancement in specifying methods for assessing severity of cracks, mechanical damage and corrosion. Although API 579 emphasized mainly on welded vessels and piping, the assessment procedures can be used for non-welded components or structures [71]. API 579 was evolved to determine rules for investigating whether fabrication flaws should be repaired or not, replacing arbitrary "workmanship" rules. API 579/ASME FFS-1[13] [72], published in 2007 by the joint API/ASME committee, specified a modern approach to flaw assessment and was adopted by the offshore industry.

More specifically, the assessment levels specified by API 579/ASME FFS-1[13] [72] for the evaluation of the effect of a dent on pipeline structural integrity under pressure fluctuations is provided below:

a) Level 1 Assessment is limited to smooth dents in carbon steel cylindrical shells located away from structural discontinuities. The acceptability criterion is based on limiting the maximum dent depth in a pressurized pipe (d_{dp}) equal to 7% of the outside pipe diameter (D_{nom}).

b) Level 2 Assessment is similar to the Level 1 Assessment. In addition, a fatigue assessment to evaluate the maximum allowable cycles of a pipe under cyclic pressure loading is provided.

c) Level 3 Assessment specifications aim at the evaluation of dents in complex geometries subjected to general loading conditions. A Level 3 Assessment is also required for materials other than carbon steel. Numerical stress analysis techniques are utilized in a Level 3 assessment (as described in the APPENDIX).

According to API 579/FFS-1 provisions for smooth (non-gouged) dents, the maximum allowable number of pressure cycles has been calculated for specimens tested under pressure named as SP2d, SP4d, SP7d and SP8d.

Following the procedure described in Chapter 12 for Level 2 assessment specified in [72], the maximum number of pressure cycles is calculated for each specimen, as shown in Table 15. These values are significantly lower than both analytical and experimental results. Moreover, the dents developed on SP2d and SP8d specimens are considered not acceptable for Level 1 assessment, as the dent depth on the pressurized specimens (d_{dp}) is found greater than 7% of the nominal diameter (D_{nom}). Figure 5-2, shows the fatigue curve specified by API 579/FFS-1 in comparison with the material fatigue curve of X52, obtained experimentally as described in Chapter 2. With the use of this specific material curve, the assessment methodology recommended by API 579/FFS-1 becomes significantly conservative, predicting the number of cycles that a smooth (non-gouged) dent could withstand under cyclic pressure. This conservativeness could be attributed to the fact that API 579/FFS-1 methodology accounts indirectly for aging of the pipe material due to service cyclic loadings applied through the pipe operational life. On the contrary, the pipe specimens used in this experimental procedure, were recently fabricated without any prior loading or aging, i.e. without initial material degradation.

Table 15: Results of prediction of fatigue pressure cycles;

Specimen	Cycles Applied Experimentally n_i	API 579/ASME FFS-1 Max Allowable Pressure Cycles
SP2d	5000 no rupture	14
SP4d	5000 no rupture	764
SP7d	570 to rupture	197
SP8d	5000 no rupture	34

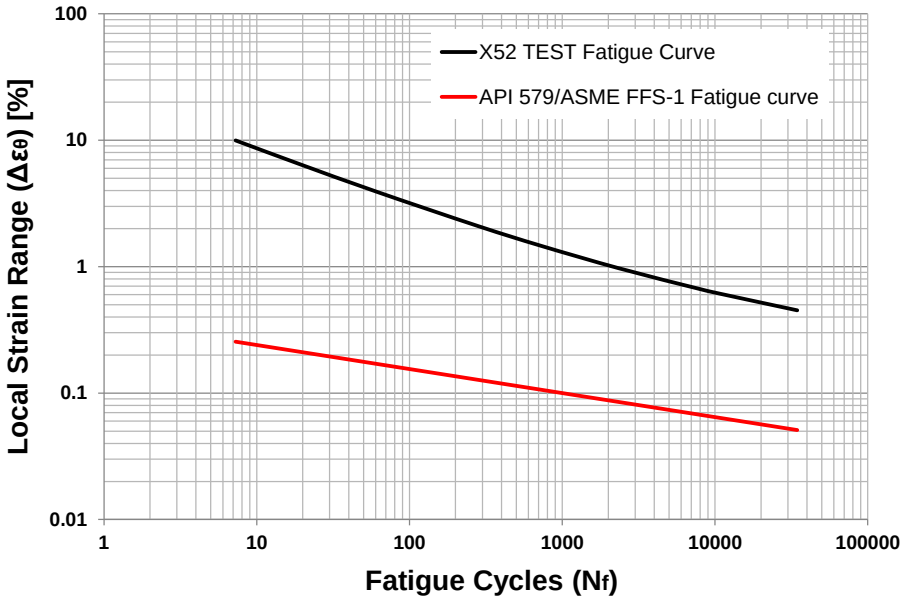

Figure 5-2: Comparison of API 579 fatigue curve vs X52 fatigue curve.

5.3 Correlation of small- scale tests with material fatigue curve

The *"Δε-N"* simplified assessment approach employed in the previous fatigue assessment methodology is also employed for the prediction of the fatigue life of the longitudinal strips under cyclic loading (small-scale tests) as shown in Figure 5-3. In particular, following the fatigue analysis proposed in Chapter 5.1, the values of longitudinal local strain ranges $\mathbf{\Delta\varepsilon}_{xmax}$ are obtained numerically at the outer surface of the strip models at the end of the tenth (10^{th}) loading cycle (Table 16), assuming that upon application of then (10) cycles, stabilization of cyclic response is achieved. Using these strain values and employing the fatigue curve of the material, represented in Eq

(5.2), the number of fatigue cycles to failure is computed for each case of strip specimen test.

As shown in Figure 5-4, the fatigue life estimated through the above simplified fatigue approach compares well with the fatigue cycles obtained from the experiments. This shows that a fatigue assessment based on finite element analysis of the dented/buckled pipe together with an appropriate material curve may constitute a reliable tool for predicting the fatigue life of pipes with local wall distortions.

Figure 5-3: Loading and test configuration of strip specimens

Table 16: FEA and Experimental Results-Longitudinal strains

Δu(mm)	**Specimen**	**N_f**	**$\Delta\varepsilon_{xmax}$(%)**	
			Fatigue Curve	**FEA Model**
10 (±5)	**S15**	9222	0.638	0.590
15 (±7.5)	**S13**	1889	1.044	1.151
20 (±10)	**S12**	515	1.661	1.633
10 (±5)	**S22**	585	1.583	1.269
15 (±7.5)	**S23**	267	2.137	1.830
20 (±10)	**S26**	147	2.714	2.805

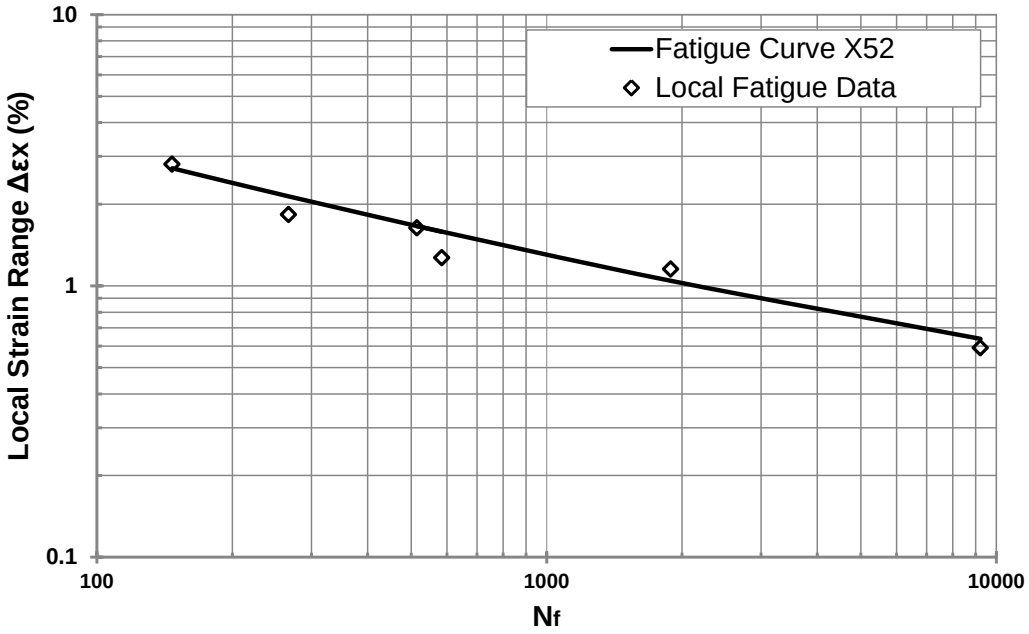

Figure 5-4: Comparison of Small-scale tests and FEA results with the fatigue curve of X52

Chapter 6 SUMMARY AND CONCLUSIONS

In the first part of the dissertation, an extensive literature survey is conducted on previous experimental and numerical work related to the structural response of dented and buckled steel pipes. The literature review and the evaluation of current pipeline assessment guidelines indicated that significant information exists on dented steel pipes, but limited research has been conducted on the structural assessment of buckled pipes. Furthermore, the review indicates that the structural response of both buckled and dented steel pipes under cyclic structural loading (e.g. bending) is an open issue.

Tensile and cyclic fatigue tests on coupon specimens have been performed by University of Porto (FEUP), in order to obtain the monotonic stress-strain curve and the fatigue curve for the X52 steel of the pipe specimens used in the experimental work.

The experimental program performed in the present work consisted of full-scale and small-scale tests. The main experimental full-scale work consisted of sixteen (16) tests on 6-inch-diameter steel pipe specimens. The nominal specimen thickness is either t=4.78mm (nominal D/t ratio equal to 35.2) or t=3mm, (D/t ratio equal to 55). The latter specimens have been machined, so that the reduced thickness is obtained.

Following material characterization, initial measurements and instrumentation, the specimens were either dented or buckled. More specifically, the first group of six (6) specimens (D/t=35.2) were dented via a steel special-purpose steel wedge-form denting tool. The pipes were subjected to dent depths equal to (a) 6% of the pipe diameter and (b) 12% of the pipe diameter. Subsequently, four (4) of the dented specimens were subjected to cyclic bending, whereas the other two (2) specimens

were tested under internal cyclic pressure. All six specimens have failed due to fatigue cracking.

The mechanical behavior of the thinner (machined) 3-mm-thick pipes was also examined. Four (4) 6-inch-diameter thin-walled were also dented and subsequently subjected to either cyclic four point bending (2 specimens) or cyclic pressure (2 specimens). Moreover, six (6) additional thin-walled specimens were buckled and subjected to either cyclic four point bending (4 specimens) or cyclic and monotonic pressure until burst (2 specimens). Global load-displacement curves, and local strains have been obtained from the full-scale tests in each loading stage (denting/buckling process and cyclic bending).

In addition, the number of cycles to failure for the case of four (4) dented pipes with D/t=35.2 under cyclic bending recorded was at the range of 950 to 1400 cycles. The other two dented pipes with D/t=55 failed after the application of 125 and 2300 bending cycles. Furthermore, the number of bending cycles to failure (crack initiation) referring to the four (4) buckled specimens with D/t=55, have been recorded ranging from 200 to 920. Fatigue cracks were observed at the ridge of the dent at the hoop direction of the pipes.

The additional four (4) dented specimens with D/t=35.2 (2 specimens) and D/t=55 (2 specimens) sustained 5000 pressure cycles with no damage detected except for the case of specimen SP8d, which failed due to fatigue cracking at the buckle ridges after 2500 cycles. Unlike the case of SP8d specimen, it was observed that the burst capacity of the rest three specimens was not affected by the application of 5000 pressure cycles or the presence of the dent. This was derived from the fact that the maximum pressure obtained from the burst tests was equal to the analytical prediction of burst of a perfect pipe and rupture occurred at a location away from the dent.

Furthermore, it was shown that, although, dents of d/D=12% did not fall within the local strain acceptability limits (e_i and $e_0 > 6\%$) specified by ASME B31.3, sustained numerous pressure or bending cycles before cracking during the experimental procedure. It could be derived that the specific acceptable strain limits referring to plain (non-gouged) dents on pipes with D/t values lower than 55 could be considered rather conservative.

Regarding the two buckled specimens under cyclic and monotonic pressure, specimen SP7b failed due to fatigue cracking after 570 pressure cycles in contrast with SP8b which sustained 5000 pressure cycles with no damage detected. Furthermore, after the application of 5000 pressure cycles, SP8b specimen ruptured under monotonically increasing pressure at a location away from the buckled region.

Small-scale tests have also been performed on ten (10) 300-mm-long and 40-mm-wide strip specimens have been extracted longitudinally from the X52 6-inch-diameter pipe specimens (D/t=33.5). First, the longitudinal strips are bent monotonically at mid-length at 90 and 120 degrees, representing the shape of a dented pipe generator at the compression side, as obtained in the full-scale tests at the critical region of the dent. Subsequently, cyclic load is applied through a special set-up until fatigue crack failure, simulating the local conditions in a dented or buckled region of a pipe subjected to cyclic bending, as in the case of the full scale tests. Limited local strain values were recorded at the crest of the strip. Nevertheless, the predicted values of local strain obtained from finite element analysis have been correlated very well with the X52 steel material fatigue data.

Moreover, detailed finite element models were developed in ABAQUS/Standard using reduced-integration four-node shell elements (S4R), and material behavior was simulated through a von Mises (J_2) plasticity model. In addition, for the simulation of buckling, initial stress-free buckle-type imperfection of various amplitudes was induced on the finite element pipe model. The load displacement curves for both dented/buckled pipes under monotonic or cyclic bending were found in good agreement with the experimental results.

Furthermore, the small-scale tests were also simulated numerically in ABAQUS/Standard using eight-node reduced integration solid elements (C3D8R) and J_2 flow plasticity model with isotropic hardening for the material inelastic behavior. Global load-displacement curves were also obtained and were found to compare well with the experimental data.

Using the finite element simulations, the maximum local strain variation ($\Delta\varepsilon_{max}$) developed at the critical region of both full-scale and small-scale experiments subjected to cyclic loading was calculated. The value of this local strain was also compared with the "nominal" $\Delta\varepsilon_{nom}$ value, which can be readily computed from

elementary Mechanics of Materials. Having obtained the local strain variation, a simplified fatigue assessment methodology is proposed for the prediction of the fatigue life of dented and buckled pipes. This strain–life fatigue approach could be considered as a simplified method similar to the one specified by API 579/ASME FFS-1 Level 3: Assessment of dented components. This "$\Delta\varepsilon$-N" methodology provides the fatigue life of a cyclic-loaded dent/buckled specimen, employing (a) the so-called damage factor D, which is based on Miner's rule for fatigue damage accumulation under variable cyclic loading conditions, and (b) a strain-based fatigue curve for the parent material.

The calculated values of the damage factor for the specimens under cyclic bending are quite close to 1, showing a good correlation between material fatigue testing, full-scale experiments and numerical simulations. This good correlation is notable, given the fact that a simple rule of fatigue damage accumulation is adopted (Miner's rule) and a standard J_2 flow plasticity model is employed in the finite element calculations.

For the case of cyclic pressure the fatigue life of dented and buckled pipes under cyclic pressure (SP1d, SP4d, SP7d, SP8d, SP7b and SP8b), predicted by the simplified approach "$\Delta\varepsilon$-N", ranged from 10,000 to 1,000,000 cycles. On the other hand, the maximum allowable pressure cycles predicted as specified in API 579/FFS-1 provisions, were calculated within a range of values from 14 to 764, which is considered significantly conservative in comparison with the fatigue assessment methodology "$\Delta\varepsilon$-N" and the experimental results. This conservativeness could be attributed to the fact that API 579/FFS-1 methodology takes into account the aging of the pipe material through its operational life. In the present case, the tested pipe specimens were recently produced and manufactured without being subjected to cyclic loadings, thus no initial material degradation has been considered prior to testing.

The good correlation found between the numerical and experimental results has motivated the proposal of a simple and efficient assessment methodology. It is believed that, towards efficient pipeline operational management and safeguarding the unhindered flow of energy (hydrocarbon) resources, this methodology can be considered as a reliable tool for the fatigue life prediction of damaged pipelines with local wall distortions. Throughout this research effort, three (3) technical papers have

been presented in conferences as reported in [75], [76] and [77] related to the experimental and numerical work performed through the collaboration of the Department of Mechanical Engineering and the Laboratory of "Reinforced Concrete Technology and Structures" of the Department of Civil Engineering at the University of Thessaly, both located in Volos, Greece.

For better understanding of the residual capacity of pipes with local wall distortions, additional tests could be conducted, accounting for various geometrical characteristics, pipe wall flaws, especially for the case of cyclic bending loading in the presence of high- internal pressure extending the present work. Furthermore the case of gouged (with surface cracking) local distortions (mainly gouged dents) should be considered. The structural capacity of a damaged pipe including aging effects would be of particular importance for the piping/ pipeline industry; in such case tests under sour environmental conditions or tests on aged pipe specimens should be performed. Finally, enhanced material numerical models should be implemented more suitable in describing on cyclic-plasticity phenomena and adopting more elaborate low-cycle fatigue damage accumulation methodologies in order to simulate accurately the response of pipe material.

Chapter 7 ACKNOWLEDGEMENTS

This research has been co-financed by the European Union (European Social Fund – ESF) and Greek national funds through the Operational Program "Education and Lifelong Learning" of the National Strategic Reference Framework (NSRF) - Research Funding Program: Heracleitus II, investing in knowledge society through the European Social Fund.

Chapter 8 REFERENCES

[1] Hopkins P., "The Structural Integrity of Oil and Gas Transmission Pipelines," Penspen Ltd., Newcastle upon Tyne, UK

[2] Doglione, R., and Firrao, D., 1998, "Structural Collapse Calculations of Old Pipelines," *International Journal of Fatigue*, **20** (2), pp. 161–168.

[3] Netto, T. A., Ferraz, U. S., and Estefen, S. F., 2005, "The Effect of Corrosion Defects on the Burst Pressure of Pipelines," *Journal of Constructional Steel Research*, **61** (8), pp. 1185–1204.

[4] National Transportation Safety Board, "Natural gas pipeline rupture and fire," Pipeline Accident Report NTIS No. PB2003-916501, D.C. 20594, Near Carlsbad, New Mexico, 2000, pp. 1-14.

[5] National Transportation Safety Board, "Texas Eastern Gas Pipeline Explosion", Pipeline Accident Report NTSB number PAR-95-01, D.C. 20594, Edison NJ, 1994, pp. 1-8.

[6] "Pipeline Performance in Alberta, 1990-2005," Alberta Energy and Utilities Board, Report, 2007.

[7] A. Cosham and Phil Hopkins. "A new industry document detailing best practices in pipeline defect assessment," Penspen Integrity (APA), Newcastle Upon Tyne, NE6, 2001, UK, pp. 1-43.

[8] A. Cosham, M. Kirkwood, "Best practice in pipeline defect assessment", in 'Proc. of the International Pipeline Conf.', IPC2000-0205, Alberta, Canada, (ed.), M. Mohitpour, ASME, NY, Vol. 1, 2000, pp. 1-11.

[9] A. Cosham, P. Hopkins, "The pipeline defect assessment manual", in 'Proc. of the 4th International Pipeline Conf.', IPC2002-27067, Alberta, Canada, (ed.), AL Edgeworth, Part B, ASME, NY, Vol. 2, 2002, pp. 1565-1581.

[10] A. Cosham, P. Hopkins, "The effect of dents in pipelines-guildance in the pipeline defect assessment manual", in 'Proc. of the Tenth International Conf. on Pressure Vessel Technology', ICPVT-10, Vienna, Austria, (ed.), J. L. Zeman, ¨OGS, Austria, Vol. 1, 2003, pp. 111-119, (ISBN: 3-9501528-1-4).

[11] "Recommendations on transmission and distribution practice", IGE/TD/1, Edition 3-Steel Pipeline for High Pressure Gas Transmission, Inst. Gas Engineers, 1993, pp. 1-163.

[12] T. E. Zimmerman, P. Hopkins, N. Sanderson, "Can limit state design be used to design a pipeline above 80% SMYS?, in 'Proc. of the 17th International Conf. Offshore Mechanics and Arctic Engineering, OMAE98, Lisbon, Portugal,(ed.), C.G. Soares, ASME, NY, Vol. 1, 1998, pp. 1-20, (CD-ROM ISBN: 0791819523).

[13] API 579/ASME FFS-1, "Fitness-for-Service," 2007

[14] ASME B31.8, 2007, Gas transmission and distribution piping systems. 2007 ed. ASME.

[15] Iflefel, I. B., "The influence of Dents and Gouges on the Load Carrying Capacity of Transmission Pipelines," University of Liverpool, March 2006.

[16] Jones D. G., "The significance of mechanical damage in pipelines," *3R International*, Vol. 21, No. 7, July 1982.

[17] S. P. Belonos, R. S. Ryan, "Dents in pipeline", Oil & Gas Journal, Vol. 36, 1958, 155-161.

[18] C. R. Alexander, "Analysis of dented pipelines considering constrained and unconstrained dent configrations", in 'Proc. of the 1999 Energy Sources Technology 227 Conf.', ASME-99, Texas, USA, ASME, NY, 1999, pp. 1-13.

[19] C. R. Alexander, L. M. Connelly, "Analytical recreation of a dent profile considering varied soil, operating, and boundary conditions", in 'Proc. of the 1998 Energy Sources Technology Conf.', ASME-98, Texas, USA, Vol. 1, 1998, pp. 1-7.

[20] B. N. Leis, R. B. Francini, R. Mohan, D. L. Rudland, R. J. Olson, "Pressure displacement behaviour of transmission pipelines under outside forces–towards a serviceability criterion for mechanical damage", in 'Proc. of the Eighth Int.

Offshore and Polar Engineering Conf.', Montreal, Canada, (ed.), J.S. Chung, J. Wardenier, R.M.W. Frederking, W. Koterayama, ISOPE, CA, Vol. 2, 1998, pp. 60-67.

[21] D. C. Brooker, "Denting of pressurized pipelines under localized radial loading", International Journal of Mechanical Sciences, Vol. 46, 2004, 1783-1805.

[22] O. L. Seng, "Derivation of stresses associated with a long axial dent in a pressurized cylinder", International Journal of Mechanical Sciences, Vol. 33, 1991, 115-123.

[23] Gresnigt, A. M., Karamanos, S. A., Andreadakis K. P., "Lateral Loading of Internally Pressurized Steel Pipes," *Journal of Pressure Vessel Technology*, Vol. 129, pp. 630-638, November 2007.

[24] Gresnigt, A. M., 1984, "Handrekenmodel en Proeven Indeukdiepte/ Rekenmetingen Gastransportbuizen _Analytical Model and Indentation Tests/ Strain Measurements in Gas Pipelines_," Research Report B-84-425/ 63.6.0900.

[25] Pacheco L. A., Durkin S., "Denting and Collapse of Tubular Members-A Numerical and Experimental Study," *International Journal of Mechanical Sciences*, Vol. 30, No. 5, pp. 317-331, 1988.

[26] Spiekhout J., Gresnigt A. M., Koning C., Wildschut H., "The influence of Pipe wall Thickness on Resistance to Damage of Gas Transmission Pipelines," *3R International*, Vol. 25, pp. 198-203, April 1986

[27] Jones D. J., "The significance of mechanical damage in pipeline,"3R International, Vol. 21, Issue 7, 1982, pp. 347-354.

[28] A. J. Rinehart, P. B. Keating, "Length effects on fatigue behavior of longitudinal pipeline dents", in 'Proc. of the 4th International Pipeline Conference', IPC02- 27244, Calgary, Canada, (ed.), AL Edgeworth, ASME, NY, Part-B, 2002, pp. 1849-1858.

[29] M. Beller, C. Mattheck, J. Zimmermann, "Stress concentrations in pipelines due to presence of dents", in 'Proc. of the 1st International Offshore and Polar Engineering Conf.', UK, (ed.), J.S. Chung, J. Wardenier, R.M.W. Frederking, W. Koterayama, ISOPE, CA, Vol. 2, 1991, pp. 421-424.

[30] Hopkins P., Jones D. G., Clyne A. J., "The significance of dents and defects in transmission pipelines", Journal of the IMech, Part E, 1989, 137-145.

[31] Ong, L. S. 1991, "Derivation of Stress Associated with a Long Axial Dent in a Pressurized Cylinder," Int. J. Mech. Sci., 33 (2), pp. 115–123.

[32] Ong L. S., Soh A. K., Ong J. H., "Experimental and finite element investigation of a local dent on a pressurized pipe", Journal of Strain Analysis, Vol. 27, 1992, pp. 177-185.

[33] E. R. Lancaster, S. C. Palmer, "Experimental study of strains caused by pressurization of pipes with dents", in 'Proc. of the 4th International Offshore and Polar Engineering. Conf.', ISOPE-94, (eds) J.S. Chung, Maeda Hisaaki, Naito Shigeru, Ikeda Yoshiho, Osaka, Japan, ISOPE, Colorado, Vol. 2, 1994, pp. 110-117.

[34] T. D. Park, S. Kyriakides, "On the collapse of dented cylinders under external pressure", International Journal of Mechanical Sciences, Vol. 38, 1996, pp. 557-578.

[35] M. J. Rosenfeld, "Investigations of dent rerounding behaviour", in 'Proc. of the International Pipeline Conf.', Calgary, Canada, ASME, NY, Vol. 1, 1998, pp. 299-307.

[36] Fowler, J. R., 1993, "Criteria for Dent Acceptability in Offshore Pipelines," Offshore Technology Conference, OTC 7311, Houston, pp. 481–493.

[37] Buitrago, J., and Hsu, T. M., 1996, "Stress Concentration Factors for Dented Tubular Members," Offshore Mechanics & Artic Engineering Conference, OMAE, Vol. I, pp. 291–296.

[38] Pinheiro B., Pasqualino, I. P., "Fatigue analysis of damaged steel pipelines under cyclic internal pressure," International Journal of Fatigue, Vol. 31, pp. 962–973, 2008.

[39] Limam A., Lee L.-H., Kyriakides S., "On the Collapse of Dented Tubes under Combined Bending and Internal Pressure," *International Journal of Mechanical Sciences,* 2011.

[40] Pournara, A. E. and Karamanos, S. A., 2012, "Structural integrity of steel hydrocarbon pipelines with local wall distortions", *Pressure Vessel and Piping Conference*, ASME, PVP2012-78131, Toronto, Canada.

[41] Yablonskikh Y., 2007, “Assessment and analysis of pipeline buckles,” GE Oil and Gas PII Pipeline Solutions, Aberdeen.

[42] Noronha Jr. D. B., Martins R. R., Breno Pinheiro Jacob, Eduardo de Souza, “Procedures for the strain based assessment of pipeline dents,” International Journal of Pressure Vessels and Piping, March 2010, Vol. 87, pp. 254- 265.

[43] Baker M., 2004, Pipe Dent Study, Final Report to Department of Transportation, Research and Special Programs Administration Office of Pipeline Safety, OPS TT011.

[44] BS 7910:2005, “Guide to methods for assessing the acceptability of flaws in metallic structures,” British Standards Institute, London, UK, 2005.

[45] P. Roovers, R. Bood, M. Galli, U. Marewski, M. Steiner, M. Zarea, “EPRG methods for assessing the tolerance and resistance of pipelines to external damage”, Pipeline Technology Conference, Brugge, Belgium, (ed.), R. M. Denys, ASME, NY, Vol. 2, 2000, pp. 405-425, (ISBN: 0-444-502718).

[46] L. G. Brazier, “On the Flexure of Thin Cylindrical Shells and Other Thin Sections,” Proceedings of the Royal Society, series A, vol. 116, pp. 104-114, 1927.

[47] R. L. Moore and J. W. Clark, “Torsion, compression, and bending tests of tubular sections machined from 75S-T6 rolled round rod,” National advisory committee for aeronautics, Washington, USA, 1952.

[48] J. C. Wilhoit and J. E. Merwin, "Critical Plastic Buckling Parameters for Tubing in Bending Under Axial Tension," in Offshore Technology Conference, Dallas, USA, 1973.

[49] T. G. Johns, R. E. W. R. Mesloh and J. E. Sorenson, "Inelastic Buckling of Pipelines under Combined Loads," in Offshore Technology Conference, Dallas, USA, 1975.

[50] P. Tugcu and J. Schroeder, “Plastic deformation and stability of pipes exposed to external couples,” Int. J. of Solids and Structures, vol. 15, pp. 643-658, 1979.

[51] B. D. Reddy, “An epxerimental study of the plastic buckling of circular cylinders in pure bending,” Int. J. of Solids and Structures, vol. 15, pp. 669-683, 1979.

[52] A. A. van Douwen, A. M. Gresnigt and J. W. B. Stark, "Plastic design of buried steel pipelines for transport of oil, gas or water, verified by tests on scale models," TNO-IBBC, Rijswijk, The Netherlands, 1974.

[53] S. Kyriakides and P. K. Shaw, "Inelastic Buckling of Tubes Under Cyclic Bending," Journal of Pressure Vessel Technology, vol. 109, pp. 169-178, 1987.

[54] S. Kyriakides and G. T. Ju, "Bifurcation and localization instabilities in cylindrical shells under bending - Part I: Experiments," Int. J. of Solids and Sructures, vol. 29, no. 9, pp. 1117-1142, 1992.

[55] G. T. Ju and S. Kyriakides, "Bifurcation and localization instabilities in cylindrical shells under bending - Part II: Predictions (EMRL Report No. 90/10)," Int. J. of Solids and Structures, vol. 29, no. 9, pp. 1143-1171, 1992.

[56] Das, S., Cheng, J. J. R., Murray, D. W. "Prediction of Fracture in Wrinkled Energy Pipelines Subjected to Cyclic Deformations"

[57] Das, S., Cheng, J. J. R., Murray, D. W., 2007, "Prediction of the fracture life of a wrinkled steel pipe subject to low cycle fatigue load", Canadian Journal of Civil Engineering, 34 (9), pp. 1131-1139.

[58] Zhang, Y., Das, S., "Failure of X52 Wrinkled Pipelines Subjected to Monotonic Axial Deformation" Journal of Pressure Vessel Technology, Vol. 130, May 2008.

[59] Dama, E., Karamanos, S. A. and Gresnigt, A. M., 2007, "Failure of Locally Buckled Pipelines.", ASME Journal of Pressure Vessel Technology, 129, pp. 272-279.

[60] PD 8010-2:2004, "Code of practice for pipelines. Subsea pipelines,"

[61] DNV-OS- F101, "Submarine pipelines," Det Norske Veritas AS, October 2013

[62] AZ 662, "Oil and Gas pipeline systems," CSA Standard, 2007.

[63] M. J. Rosenfeld, James D. Hart, Nasir Zulfiqar and Richard W. Gailing, "Development of Acceptance Criteria for Mild Ripples in Pipeline Field Bends" 4th International Pipeline Conference, Sept. 29–Oct. 3, Calgary, Alberta, Canada, 2002.

[64] Baker M., 2004, Pipe Wrinkle Study, Final Report to Department of Transportation, Research and Special Programs Administration Office of Pipeline Safety, OPS TT011.

[65] ASME B31.4, "Pipeline Transportation Systems for Liquid Hydrocarbons and Other Liquids" by ASME, 2004.

[66] Alexander C., Kulkarni S., "Evaluating the Effects of Wrinkle Bends on Pipeline Integrity," Proceedings of IPC2008, 7th International Pipeline Conference, Sept. 29 – Oct. 3, 2008, Calgary, Alberta, Canada

[67] American Petroleum Institute, *Specification for Line Pipe*, API-5L, 43th edition, 2004.

[68] Fernandes A. A. (coordinator), Ultra Low Cycle Fatigue of steel under high-strain loading conditions, 3rd Annual Progress Report of ULCF-RFCS Project, Porto, 2013.

[69] ABAQUS Standard v.6.10

[70] API 579 2000," Fitness-For-Service Engineering Assessment Procedure", March 2000.

[71] Bennett, D. C., Mixon N., "API 579-2/ASME FFS-2 2009, "Fitness-For-Service- Post-construction Code for pressure Equipment with Flaws and Corrosion Damage,"2001.

[72] API 579-2/ASME FFS-2 2009, "Fitness-For-Service Example Problem Manual", 11 August, 2009.

[73] Bousaa, Dj., Dang Van, K., Labee, P., Tang, H. T., " Fatigue- Seismic Ratcheting Interactions in Pressurized Elbows," Journal of Pressure Vessel and Technology, Vol. 116, p.p. 396-402, November 1994.

[74] Dang Van, K., Moumni, Z., "Evaluation of fatigue-ratcheting damage of a pressurized elbow undergoing damage seismic inputs," Journal of Nuclear Engineering and Design, Vol. 196, p.p. 41-50, 2000.

[75] Pournara, A. E. and Karamanos, S. A., 2012, "Structural integrity of steel hydrocarbon pipelines with local wall distortions", Pressure Vessel and Piping Conference, ASME, PVP2012-78131, Toronto, Canada.

[76] Pournara, A. E., Karamanos, S. A., Papatheocharis, T. and Perdikaris, P. C., "Structural integrity of steel hydrocarbon pipelines with local wall distortions", 10th International Pipeline Conference, ASME, IPC2014-33210, Calgary, Canada, 2014.

[77] Pournara, A. E., Karamanos, S. A., Perdikaris, P. C., Papatheocharis T., "Structural Integrity of Buckled Steel Pipes" Proceedings of ASME 34th International Conference on Ocean, Offshore and Arctic Engineering, OMAE 2015, May 31- June 5, St. John's, NL, CANADA.

Chapter 9 APPENDIX

API 579-1/ASME FFS-1 STANDARD

The assessment levels specified by API 579/ASME FFS-1[72] for the evaluation of a dent is provided below:

a) Level 1 Assessment is limited to dents in carbon steel cylindrical shells located away from structural discontinuities. The acceptability criterion is based on limiting the maximum dent depth in a pipe to a percentage of the pipe outside diameter.

b) Level 2 Assessment is similar to the Level 1 Assessment. In addition, a fatigue assessment to evaluate the maximum allowable cycles of a pipe under cyclic pressure loading is provided.

c) Level 3 Assessment aims at the evaluation of dents in complex geometries subjected to general loading conditions. A Level 3 Assessment is also required for materials other than carbon steel. Numerical stress analysis techniques are also utilized as described below.

A1. Data Requirements

As described in Part 12, paragraph 3 of API 579/ASME FFS-1, to initiate assessment procedure of a dented pipe, maintenance and operational history data is required as specified in paragraph 2.3.2 of Part 2. Further required data and measurements for assessment of a dent are listed below:

a) *Dent Depth in the Pressurized Condition,* d_{dp} *, and Unpressurized Condition,* d_0 – The maximum depth of the dent in the pressurized and the unpressurized condition shall be determined. These values may be measured directly. The Owner-User should consider the risk before increasing the pressure from the current level to measure the depth of the dent in the pressurized condition. Alternatively, if the operating pressure is greater than or equal to 70% of the maximum allowable pressure ($MAWP$), then the relationship between the dent depth in the pressurized condition (d_{dp}) and the

dent depth in the unpressurized condition (d_0) is given by Equation (12.5) according paragraph 3.3.1 of Part 12.

$$d_{dp} = 0.70\ d_0 \qquad (12.5)$$

Otherwise, the dent depth in the pressurized condition shall be assumed to be equal to the dent depth in the unpressurized condition, or $d_{dp} = d_0$.

b) *Minimum Specified Ultimate Tensile Strength*, σ_{uts} – The minimum specified ultimate tensile strength may be determined based on the material specification. If the material specification is unknown, then σ_{uts} =414 *MPa* (60) *ksi* may be used in the assessment. This information is required for a Level 2 Assessment, and may be required for a Level 3 Assessment.

c) *Cyclic Pressure Components*, P_{max} and P_{min} – If the component is in cyclic pressure service that can be represented by a maximum and minimum pressure, the maximum and minimum pressures of the cycle shall be determined. This information is required for a Level 2 Assessment, and may be required for a Level 3 Assessment.

d) *Dent Spacing to Weld Joints,* L_w – *M*easurements should be made to determine the spacing between the edge of the dent and the nearest weld joint. This information should be detailed and provided on an inspection sketch.

e) *Dent Spacing to Major Structural Discontinuities,* L_{msd} – *M*easurements should be made to determine the spacing between the edge of the dent and the nearest major

A2. Level 1 Assessment- Dent Assessment Procedure

The Level 1 Assessment procedure for determining the acceptability of a dent specified by API 579/ASME FFS-1 is described in Part 12, paragraph 4.2 as follows:

a) STEP 1 – Determine the pipe diameter the future corrosion allowance, the measured wall thickness and the future wall thickness named as D, FCA, t_{rd} , respectively.

b) STEP 2 – Determine the wall thickness t_c to be used in the assessment using Equation (12.7)

$$t_c = t_{rd} - FCA \qquad (12.7)$$

c) STEP 3 – If Equations (12.8) and (12.9) are satisfied, proceed to STEP 4. Otherwise, the Level 1 Assessment is not satisfied.

$$L_{msd} \geq 1.8\ \sqrt{D t_c} \qquad (12.8)$$

$$L_w \geq \max[2t_c,\ 25\ mm] \qquad (12.9)$$

d) STEP 4 – If the component is not in cyclic service and Equation (12.10) is satisfied, proceed to STEP 5.
Otherwise, the Level 1 Assessment is not satisfied.

$$d_{dp} \leq 0.07\ D \qquad (12.10)$$

e) STEP 5 – Determine the $MAWP$ for the component employing Equation (A.289) of Annex A, paragraph A.2) using the thickness from STEP 2.
If the value of $MAWP$ is greater than or equal to the current design condition, then the component is acceptable for continued operation. Otherwise, the Level 1 Assessment is not satisfied.

If the dented pipe does not meet the Level 1 Assessment requirements, then the following, or combinations of the following, shall be considered:
a) Repair, replace, or retire the component.
b) Adjust the FCA by applying remediation techniques (see Part 4 paragraph 4.6).
c) Conduct Level 2 or Level 3 Assessment.

A3. Level 2 Assessment- Dent Assessment Procedure.

The Level 2 Assessment procedure for determining the acceptability of a dent specified in paragraph 4.3 of Part 12 is described as follows:
a) STEP 1 – Determine the parameters D, FCA, t_{rd} similar with paragraph 4.2
b) STEP 2 – Determine the wall thickness t_c to be used in the assessment using Equation (12.6)
c) STEP 3 – If the requirements in paragraph 1 are satisfied, then proceed to STEP 4. Otherwise, the Level 2 Assessment is not satisfied.
d) STEP 4 – If Equation (12.10) is satisfied, proceed to STEP 5. Otherwise, the Level 2 Assessment is not satisfied.
e) STEP 5 – Determine the $MAWP$ for the component (see Annex A, paragraph A.2 Eq A.289) using the thickness from STEP 2. If the $MAWP$ is greater than or equal to the current design condition, proceed to STEP 6.
Otherwise, the Level 2 Assessment is not satisfied.
f) STEP 6 –If the component is subject to pressure cycles, then determine the acceptable number of cycles as shown below.
1) STEP 6.1 – Determine the circumferential stresses,

$\sigma^{c}_{m,max}$ and $\sigma^{c}_{m,min}$, based on P_{max} and P_{min}, respectively, for the component (see Annex A, paragraph A.2) using the thickness from STEP 2.

2) STEP 6.2 – Determine the acceptable number of cycles using Equations (12.15)-(12.21) of Part 12, paragraph 4.3.1.

If the acceptable number of cycles is greater than or equal to the sum of the past and future anticipated number of cycles, then the component is acceptable to continue to operate under the specified conditions. Otherwise, the Level 2 Assessment is not satisfied.

A4. Level 3 Assessment -Cyclic loading

A4.2 Fatigue Assessment – Elastic-Plastic Stress Analysis and Equivalent Strain

As specified by API 579/ASME FFS-1 in Annex B, paragraph B1.5.4, the following procedure can be used to evaluate protection against failure due to cyclic loading using elastic-plastic stress analysis.

a) STEP 1 – Determine a load history based on the information in paragraph B1.1.1.3 and the methods described in Annex B2. The load history should include all significant operating loads and events that are applied to the component.

b) STEP 2 – For a location of the component subject to fatigue loading, determine the individual stress strain cycles using the cycle counting methods in Annex B2. Define the total number of cyclic stress ranges in the histogram as M.

c) STEP 3 – Determine loading at the start and the end of the k^{th} cycle counted in STEP 2. Using these data, determine the loading range (differences between the loadings at the start and end of the cycle).

d) STEP 4 – Perform elastic-plastic stress analysis for the k^{th} cycle (see paragraph B1.5.4.1.c).

For the Twice Yield Method, the loading at the start point of the cycle is zero and the loading at the end point is the loading range determined in STEP 3. The cyclic stress range-strain range curve or hysteresis loop stress-strain curve (see Annex F, paragraph F.2.4) is used in the analysis. For thermal loading, the loading range in Twice-Yield Method may be applied by specifying the temperature field at the start point for the cycle as an initial condition, and applying the temperature field at the end point for the cycle in a single loading step.

e) STEP 5 – Calculate the effective strain range $\Delta_{\varepsilon ff,k}$ and $\Delta_{peq,k}$ for the kth cycle using Equations (B1.41) and (B1.42) where, the stress range $\Delta S_{P,k}$ is given by Equation (B1.29).

f) STEP 6 – Determine the effective alternating equivalent stress $S_{alt,k}$ for the k^{th} cycle by Equation (B1.43)

g) STEP 7 – Determine the permissible number of cycles, N_k, for the alternating equivalent stress computed in STEP 6. Fatigue curves based on the materials of construction are provided in Annex F.

h) STEP 8 – Determine the fatigue damage $D_{f,k}$ for the k^{th} cycle using Equation (B1.44)

$$D_{f,k} = \frac{n_k}{N_k} \qquad \text{(B1.44)}$$

i) STEP 9 – Repeat STEPs 3 through 8 for all stress ranges, M, identified in the cycle counting process in STEP 2.

j) STEP 10 – Compute the accumulated fatigue damage using the following equation (B1.45). The location in the component is acceptable for continued operation if this equation is satisfied.

$$\sum_{k=1}^{M} D_{f,k} \leq 1 \qquad \text{(B1.45)}$$

k) STEP 11 – Repeat STEPs 2 through 10 for each point in the component subject to a fatigue evaluation.